Title
LONGITUDINAL DISPERSION IN PACKED EXTRACTION COLUMNS

Authors
Hennico, Alphonse
Jacques, Gabriel
Vermeulen, Theodore.

Publication Date
1963-03-18

UCRL-10696

University of California

Ernest O. Lawrence Radiation Laboratory

LONGITUDINAL DISPERSION IN PACKED EXTRACTION COLUMNS

DISCLAIMER

UCRL-10696
UC-4 Chemistry
TID-4500 (19th Ed.)

Research and Development

UNIVERSITY OF CALIFORNIA

Lawrence Radiation Laboratory
Berkeley, California

Contract No. W-7405-eng-48

LONGITUDINAL DISPERSION IN PACKED EXTRACTION COLUMNS

Alphonse Hennico, Gabriel Jacques, and
Theodore Vermeulen

March 18, 1963

Printed in USA. Price $2.75. Available from the
Office of Technical Services
U. S. Department of Commerce
Washington 25, D.C.

LONGITUDINAL DISPERSION IN PACKED EXTRACTION COLUMNS

Contents

LONGITUDINAL DISPERSION IN PACKED EXTRACTION COLUMNS

Alphonse Hennico, Gabriel Jacques, and Theodore Vermeulen

Lawrence Radiation Laboratory
University of California
Berkeley, California

March 18, 1963

ABSTRACT

In this study, axial dispersion in packed beds has been investigated with particular reference to extraction-tower design.

A new model for dispersion behavior, based upon "segmented laminar flow", is derived for analysis of breakthrough curves at low flowrates; its applicability is discussed in comparison with other theoretical models of mixing.

Axial dispersion coefficients in single-phase flow were measured by a step-input method over a wide range of Reynolds numbers (3 to 2000). Nine different types of packings were used, involving regular and random arrangements of spheres, and random arrangements of Raschig rings, Berl saddles, and Intalox saddles. Different constant values of axial Péclet number are found in the turbulent range and the laminar range, which are separated by a fairly sharp transition region. Viscosity is found to have a large effect upon axial dispersion; for two solutions of different viscosity, the Péclet-number values are identical at the same Reynolds number. The axial Péclet number is found to vary inversely with bed porosity. No effect of packing arrangement is observed.

For two-phase countercurrent flow of water and kerosene, axial-dispersion coefficients were measured for the continuous phase; they were also measured for the dispersed phase, both where the current

does and does not wet the packing material. The continuous-phase Péclet number appears to increase with decreasing continuous-phase Reynolds number, and also with an increasing ratio of dispersed-phase flow rate to continuous-phase flowrate. For a nonwetting dispersed phase, the Péclet number remains practically constant, whereas for a wetting discontinuous phase it decreases somewhat with an increasing ratio of discontinuous-phase flowrate to continuous-phase flowrate. On the basis of typical calculations of mass-transfer rates from experimental extraction data, we conclude that longitudinal dispersion is an important effect and should be calculated as an independent factor in extraction column design.

GENERAL INTRODUCTION

The development of rational design methods for fixed-bed extraction columns, absorption columns and chemical reactors requires a knowledge of the extent of mass transport in the direction of flow. This phenomenon, called "longitudinal dispersion" or "axial mixing," tends to decrease the driving forces for transport processes or chemical reaction and thus limits the separations or conversions obtainable.

Longitudinal dispersion is the result of three effects. The first is true molecular diffusion in the axial direction. The second is turbulent fluid-phase mixing which occurs in the spaces between the packing. The third, additional axial mixing, is caused by nonuniform velocity and subsequent transverse diffusion; this is sometimes called Taylor diffusion, from G. I. Taylor's analysis of molecular diffusion effects during laminar flow in pipes. These mechanisms, whether acting separately or in combination, are known to produce essentially similar integral effects and hence are all describable approximately in terms of solutions to the diffusion equation. The numerical value of the diffusion coefficient that results from applying these solutions to experimental data is known as an "effective axial-dispersion coefficient."

This investigation is intended as a step in the direction of developing extraction-column design methods that take longitudinal dispersion into account. This study consists of three parts.

In Part I we propose a new model called "segmented laminar flow" for describing the longitudinal mixing process at low flowrates; for comparison, the most common theoretical models used for analyzing axial-dispersion experiments are also reviewed.

In Part II we report new experimental results on axial dispersion for liquid flow through fixed beds of different packing, with interpretation and correlation of these results.

In Part III we make an experimental study of axial dispersion in two-phase flow. The two liquids used were water and kerosene. The columns were packed with 3/4-in. ceramic Raschig rings, 3/4-in.

carbon Raschig rings, and 1-in. Berl saddles. The carbon rings were used to investigate the influence of "wetability" upon axial dispersion in the dispersed phase.

PART I. THEORETICAL MODELS FOR LONGITUDINAL DISPERSION

The subject of lengthwise fluid mixing in continuous-flow packed-column systems has received much attention during the past decade. A number of studies have shown that longitudinal dispersion (or "axial mixing") can exert a significant effect in reducing the mass-transfer performance of columns below that predicted from true mass-transfer coefficients alone, and hence, that this effect should be accounted for separately.[24, 34, 38] Several mixing models have been proposed for explaining experimental breakthrough (concentration vs time) data for the outflow. The problem of these models is essentially that of predicting the behavior of an initially sharp interface between two miscible fluids.

The most widely used approach to axial dispersion is the diffusion model. In this model the dispersion process is characterized by a diffusion equation, with an axial-dispersion coefficient in place of the usual molecular diffusivity. A simple solution to the diffusion model, assuming infinite boundary conditions, was first obtained by Danckwerts.[10] The main features of the simple diffusion model were further discussed by several other investigators,[1, 7, 13, 31, 33, 39] but this model does not give an adequate description of axial dispersion in "shallow" beds. An exact analytic solution to the diffusion model, for miscible fluid displacement in beds of finite length, was first presented by Yagi and Miyauchi.[42] Extensive numerical results, based on an asymptotic approximation to this solution, were reported by Brenner.[3]

A second model for axial dispersion, the perfect-mixing cell model, in which each of the interstices of a packed bed acts as a mixing stage, was proposed by Kramers and Alberta.[29] When the series-mixer model was applied to experimental data, it was often found that fewer than ten mixers were needed to reproduce the observed data. Since the beds involved were more than ten packing-particle diameters in length, Carberry suggested that incomplete mixing in the individual

void cells would reduce the calculated number of mixers, relative to the actual number of void cells as indicated by the number of layers of packing.[6] Accordingly, he introduced a mixing-efficiency factor for the series-mixer model, which constituted a free parameter for fitting the model to the experimental data. For "deep" beds (those having 20 or more perfect mixers in series), it has been shown that the diffusion and series-mixer models predict essentially identical residence-time distributions and breakthrough curves.[1]

A random-walk model, developed by Einstein[15] for the stream transport of suspended solid particles, has been extended by Jacques and Vermeulen[24] and Cairns and Prausnitz[5] to the problem of longitudinal dispersion in packed beds. This model, describing the random path of tracer molecules by statistical considerations, also approaches the simple diffusion model at high flowrates. Here we show that, for practical purposes, the random-walk model is numerically equivalent to the diffusion model with finite boundary conditions. One should keep in mind that the longitudinal dispersion coefficients, obtained by using the random-walk model, are defined by comparison with the diffusion model.

A different statistical model has been investigated by de Josselin de Jong,[26] and analyzed more completely by Saffman.[37] In this model the porous medium is considered as an assembly of randomly oriented straight circular-bore capillary tubes of equal length. The slope of the breakthrough curve, predicted by Saffman's derivation, for "deep" beds is

$$\frac{U_0}{h}\frac{d(c/c_0)}{dt} = \left(\frac{U_0 h}{4\pi E_s}\right)^{1/2} \frac{\ln(54\ h/\ell)}{\sqrt{96}} \quad ,$$

whereas, in the simple diffusion model,

$$\frac{U_0}{h}\frac{d(c/c_0)}{dt} = \left(\frac{U_0 h}{4\pi E_D}\right)^{1/2} .$$

In these equations U_0 is the superficial velocity, h is the height of bed, ℓ is length of capillary, t is time, c is concentration, and E is the dispersion coefficient. If the capillary-flow model is correct, the ℓ and E ($=E_s$) its uses would be constant; then, by comparison, the E ($=E_D$) given by simple diffusion would decrease with increasing h. Conversely, if the diffusion model is correct, E_D would be constant, and E_s would increase with increasing h. The capillary model seems to have two basic defects:[9] A packing of spherical particles has an open-pore structure seemingly not analogous to a capillary structure except perhaps during laminar flow; further, a streamline through the packing does not point in every direction with equal probability, but is strongly weighted toward the average direction of flow.

A number of other models of lesser importance have been proposed in which parallel and series-parallel communication of void cells[14] or material exchange between flowing channels and stagnant pockets of fluid[14, 19, 28] are used to describe dispersion in packed beds. These models usually include a sufficient number of parameters to allow fitting the model to the available data; they introduce assumptions regarding the frequency of communication of neighboring cells and the relative importance of participating transport mechanisms, which are not usually verifiable by independent laboratory measurements.

Experimental studies conducted as part of the present investigation indicate that the random-walk and exact diffusion treatments give an excellent fit to the concentration vs time curves obtained at higher flow rates, but give a relatively imperfect fit to those for lower flow rates. As shown in the next section, the higher flow rates can be identified with a turbulent flow regime, and the lower rates with a laminar regime. To meet a need for more detailed study of the laminar regime, a new model is introduced which is statistical in its concept but explicit in its mathematical behavior, being patterned after G. I. Taylor's study of the dispersion effect that results from velocity distribution in laminar flow through cylindrical tubes.[40]

For comparison with this new model, the main features of the diffusion, random-walk, and void-cell mixing models are reviewed here and their applicability to laminar-flow conditions discussed. It is seen that the use of one or another of these models can lead to axial-dispersion coefficients differing by a factor of two in "shallow" beds.

A. Segmented-Laminar-Flow Model

1. Nature of the Laminar-Flow Regime in Packed Beds

Longitudinal-dispersion studies by Jacques and Vermeulen[23] and by Carberry and Bretton,[7] as well as the experimental part of the present investigation, show the existence of a laminar and a turbulent region with a fairly sharp transition region between them.

When these results are compared with a typical packed-bed friction-factor plot (f vs N_{Re}), where $N_{Re} = d_p U_0/\nu$, with d_p the equivalent-sphere-volume diameter of the packing material, U_0 the superficial velocity, and ν the kinematic viscosity, it is seen that the transition for axial-dispersion occurs in the same Reynolds-number range (see Fig. I-1).

A second item of evidence can be found in studies by Garner et al. of the flow pattern around single spheres.[17] In these studies, the following changes in flow pattern with increasing Reynolds number were observed: At first, the flow is entirely streamline and satisfies Stokes' solution. The velocity then begins to decrease on the downstream surface of the sphere, and increases on the upstream surface. The trend continues until separation of the forward flow occurs at $d_p U_\infty/\nu$ of 15 to 25, when a very small, weak, toroidal vortex is forward near the rear stagnation point. The vortex gains strength as the Reynolds number increases further; the separation ring advances toward the equator until at $d_p U_\infty/\nu$ around 450 (with the angle of separation equal to 104 deg), the wake becomes unstable, oscillating about the axis of motion, and spilling its content downstream. Ranz has shown that the interstitial velocity in packed beds is often eight to ten times the superficial

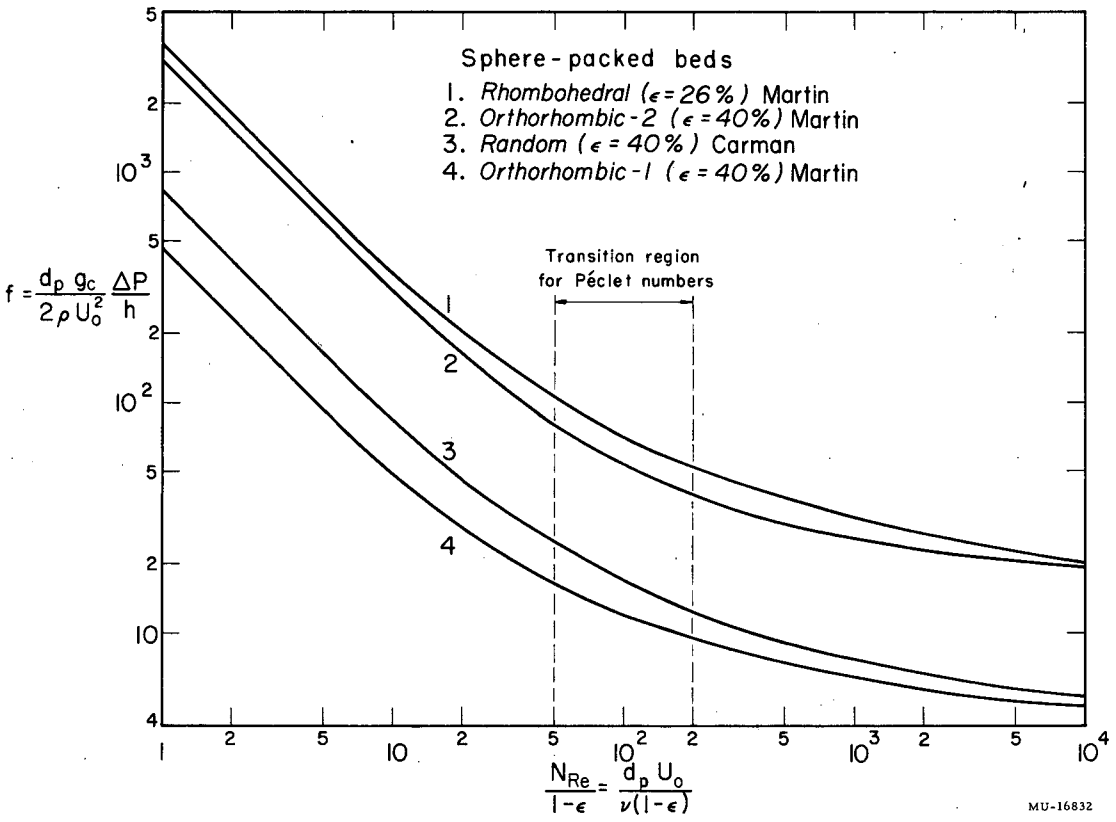

Fig. I-1. Friction factor for beds of solids.

velocity, upon which the packed-bed Reynolds number ($d_p U_0/\nu$) is based.[36] The wake instability can be identified with a flow condition in which the flow through a void space in the packing changes from predominantly streamline to near-perfect mixing. In terms of Garner's results, this change should occur at a $d_p U_0/\nu$ value of around 50 or $d_p U_0/\nu(1-\epsilon)$ of 80 to 90, where ϵ is the porosity.

Using a suspension of fine particles to indicate the fluid motion Hiby has cited photographic evidence of the transition from turbulent to laminar flow in packed beds; below $N_{Re}=10$, completely laminar flow was observed.[21]

A somewhat different investigation, dealing with liquid flow in a falling film over a single-file column of spheres in contact, also shows evidence for a laminar-turbulent flow transition.[11] The axial dispersion of liquid flowing over a system of 128 equal spheres in contact in a vertical line was studied by a tracer technique.[20] The experimental results indicate the presence of two different regions of behavior. One is representative of the very lowest flows ($d_p U_0/\nu<20$), whereas the other holds for higher flowrates ($d_p U_0/\nu>20$), with a quite sharp transition between the two. The reason for these two different regions was found to lie in the onset of rippling in the column at around $N_{Re}=20$, which causes a considerable increase in mixing at the junctions between the spheres.

Experimental evidence for the presence of a laminar-turbulent transition region has also been found in heat- and mass-transfer studies. Gamson and coworkers derived the following two relations for the Colburn j factor in mass-transfer:[16]

$$j_d = 1.46\, N_{Re}^{-0.41}(1-\epsilon)^{0.65} \text{ for } \frac{N_{Re}}{1-\epsilon} > 100,$$

and

$$j_d = 17\, N_{Re}^{-1}(1-\epsilon)^{1.2} \text{ for } \frac{N_{Re}}{1-\epsilon} < 100.$$

Due to experimental uncertainties, and perhaps also due to the gradual nature of the transition, the exact occurrence of the breakpoint is not well known.

From the various indications, it is concluded that ample justification exists for dividing the axial-dispersion phenomena into two different regions separated by a critical value (or range of values) of the Reynolds number.

2. Description of the Model

As just mentioned, the laminar regime of packed-bed flow (in columns having relatively uniform mean flow through all cellular elements of any one cross section--e.g., in circularly cylindrical columns) requires further study in order to obtain a physical model that will correspond accurately to the experimental outflow-concentration histories (breakthrough curves). A new model, which constitutes a step in this desired direction, is termed "segmented laminar flow."

In the actual laminar-flow behavior of a column, each fluid filament undergoes changes in velocity from point to point along its path. Such filaments can be considered to enter a new column "segment" each time their velocity crosses the mean velocity of the fluid. If the distribution of velocities is the same at each cross section as in randomly packed beds, one or more other filaments will be reduced in velocity at the cross section where a particular filament changes from a slow-moving to a fast-moving segment. The resulting interchange of fast-moving and slow-moving segments is equivalent to gradual but continual remixing of filaments. In the idealized model postulated here this gradual mixing is replaced by a sequence of cross sections at uniform intervals, where complete mixing occurs, with complete absence of mixing at intermediate points. The interval between the mixing cross sections becomes equivalent to a weighted average of the actual segment lengths. In each segment then, laminar flow occurs with well defined velocity profiles, and transverse molecular diffusion is treated as negligible.

In this study, two different velocity profiles are used. The first one is the usual quadratic (parabolic) profile, $u/u_{max}=1-r^2/R^2$, where u is the mean local velocity of a flow filament, and r/R is the mean ratio of its radius to the total radius of the passage. The second one, which we call "quartic," has the semi-empirical form $u/u_{max} = (1-r^2/R^2)^2$. While the quadratic velocity distribution might fit the flow through a bundle of parallel circular-bore tubes, the quartic distribution appears to provide a more accurate description of packed-bed flow, in the laminar regime.

At the end of each segment the liquid is assumed to be thoroughly mixed before it enters the next segment. Mathematically, a flow-average "cup-mixing" composition is computed after each segment, which represents the composition of the feed to the following segment.[2, 25] The boundary condition at the column inlet corresponds to a step input of a tracer material. The exact solution is not obtainable for the response curve after each segment, but a numerical solution has been derived by digital computation. The resulting theoretical breakthrough curves for different numbers of segments can be fitted to the individual experimental breakthrough curves. Each experimental run will thus exhibit a "number of dispersion units" which can be considered as a "column Péclet number", $N = h/\ell$ or hU_0/E, for purposes of defining an effective axial dispersion coefficient (here h is column height, ℓ is mixing length, U_0 is superficial velocity, and E is the superficial dispersion coefficient). From this, a "packing Péclet number", $P = d_p/\ell$ or d_pU_0/E, is calculated which presumably is constant over the entire length of the packed bed.

3. General Mathematical Approach

The equations were derived for a cylindrically symmetrical element of flow path having the cross-section S. The flow is assumed unidirectional. The concentration is a function of time t, of distance in the direction of flow z, and of a radius vector $\vec{r}$ which characterizes an element dS of the cross-sectional area. The local velocity is also a function of $\vec{r}$ as mentioned above. The flow-average concentration leaving one segment is taken as the feed concentration for the next segment. This flow-average concentration is defined as

$$c_b(z,t) = \frac{\int_S c(\vec{r},z,t)\, u(\vec{r},t)\, dS}{\int_S u(\vec{r},t)\, dS} . \qquad (1)$$

At each of the cross sections where mixing occurs, the $\vec{r}$-dependent concentration is replaced by its bulk average; i.e., $c(\vec{r},z,t)$

is replaced by $c_b(z,t)$. In a cylindrical element of flow path (one with uniform cross section) the velocity profile is only a function of $\vec{r}$. For steady-state laminar flow the concentration $c(\vec{r}, z_k, t)$ at a point z_k gives directly the concentration at a downstream point, $z > z_k$, in the corresponding radial location. Thus, we have

$$c(\vec{r}, z, t) = c(\vec{r}, z_k, t - t_1) , \tag{2}$$

where t_1 is the time necessary for the fluid to travel the distance $(z-z_k)$, and

$$t_1 = \int_{z_k}^{z} \frac{dz}{u(\vec{r}, t)} = \frac{z-z_k}{u(\vec{r})} . \tag{3}$$

In physical terms, the element of fluid observed earlier at z is the same as one which was observed earlier at z_k.

From these relations the general equation for a segment extending from z_k to z_{k+1} becomes

$$c_b(z_{k+1}, t) = \frac{\int_S c_b\left[z_k, t - \frac{z_{k+1}-z_k}{u(\vec{r})}\right] u(\vec{r})\, dS}{\int_S u(\vec{r})\, dS} . \tag{4}$$

In our study, the problem is analyzed with reference to a fluid in a circularly cylindrical volume element of radius R. For this case, Eqs. (1) and (4) become

$$c_b(z,t) = \frac{\int_0^R u(r)\, c(r)\, r\, dr}{\int_0^R u(r)\, r\, dr} \tag{5}$$

and

$$c_b(z_{k+1}, t) = \frac{\int_0^R c_b(z_k, t - \frac{z_{k+1}-z_k}{u(r)}) u(r)\, r\, dr}{\int_0^R u(r)\, r\, dr} . \tag{6}$$

By use of these equations, it is possible in principle to compute the

concentration of tracer material after any number of segments, if one knows the velocity distribution and the concentration distribution at the inlet as a function of time and position. In practice, the multiple integration required for successive segments becomes progressively more complex, and soon ceases to give relations in closed analytical form. The separate application of these basic equations to the quadratic and quartic velocity profiles is given in the following sections.

4. Quadratic Velocity Distribution.

For the case of quadratic velocity distribution it is assumed that the volume elements for flow through the packing have a circular cross section, in which the fluid moves with the usual laminar parabolic velocity profile

$$\frac{u(r)}{u_{max}} = 1 - \frac{r^2}{R^2} , \tag{7}$$

where u_{max} is the maximum velocity of the fluid and r is a radial coordinate. For the parabolic velocity profile the maximum velocity is equal to twice the average velocity.

From Eq. (7), the flow-average concentration is given by

$$c_b = \frac{4}{R^2} \int_0^R c(r) \left[1 - \frac{r^2}{R^2} \right] r dr . \tag{8}$$

This relation can be simplified by the following change of variable:

$$\zeta = 1 - \frac{r^2}{R^2} \tag{9}$$

here also

$$\zeta = \frac{u}{u_{max}} ; \tag{10}$$

ζ is thus the fraction of area enclosed between r and R. Differentiation gives

$$d\zeta = - \frac{2r\, dr}{R^2} . \tag{11}$$

The integration limits are at $r = 0$, $\zeta = 1$, and at $r = R$, $\zeta = 0$. Applying these relations to the segment (z_k, z_{k+1}) leads to the more specific relation

$$c_b(z_{k+1}, t) = 2\int_0^1 \left[c_b\left(z_k, t - \frac{z_{k+1}-z_k}{u_{max}\zeta}\right)\right]\zeta\, d\zeta . \qquad (12)$$

Equation (12) proves to be the key expression for evaluating the concentration breakthrough after any given number of segments. Applied to a column of total length h, divided into a number of segments N, each of length ℓ, it becomes

$$c_b(z_N, t) = 2\int_0^1 \left[c_b\left(z_{N-1}, t - \frac{z_N - z_{N-1}}{u_{max}\zeta}\right)\right]\zeta\, d\zeta . \qquad (13)$$

The initial condition can be described by the relation

$$c(0, r, t) = c_b(0, t) = c_0 H(t), \qquad (14)$$

where c_0 is the step-input concentration, and $H(t)$, the Heaviside unit function, is either zero or unity, depending on whether its argument is smaller or larger than zero. The Heaviside function expresses the fact that the tracer fluid takes a well defined time to emerge from the column.

After N divisions each of length ℓ, the remixed concentration is

$$c_b(N\ell, t) = c_0\, f_N(t)\, H\left(t - \frac{N\ell}{u_{max}}\right)$$

$$= c_N(t)\, H\left(t - \frac{N\ell}{2U}\right), \qquad (15)$$

where $f_N(t)$ is a dimensionless function of t that remains to be derived, $c_N(t)$ is the corresponding concentration $[= c_0\, f_N(t)]$, and U is the average linear velocity which for this case is equal to half the maximum velocity u_{max}. The Heaviside function in the above expression states that $c_b(N\ell, t)$ is nonzero only if $t \geq N\ell/2U$. Suppose c_{N-1} is known after $N-1$ segments; then, at the end of N segments,

$$c_N(T) = 2\int_0^1 \left[c_{N-1}\left(T - \frac{1}{2\zeta}\right)\right] H\left[T - \left(\frac{N-1}{2}\right) - \frac{1}{2\zeta}\right]\zeta d\zeta \,, \tag{16}$$

where $T = Ut/\ell$.

In the use of this relation, the argument of the Heaviside function serves to define a new lower limit of integration. Physically, the use of this function means replacing the lower limit by a quantity that avoids computing any negative concentration values. Thus, if we have $T - \frac{N-1}{2} - \frac{1}{2\zeta} > 0$, or hence, if we have $\zeta \geq (2T-N+1)^{-1}$, then

$$H\left[T - \left(\frac{N-1}{2}\right) - \frac{1}{2\zeta}\right] = 1 \,. \tag{17}$$

The general relation now becomes

$$X_N(T) = 2\int_{(2T-N+1)^{-1}}^1 \left[X_{N-1}\left(T - \frac{1}{2\zeta}\right)\right]\zeta d\zeta \,, \tag{18}$$

where $X_N(T) = c_b(N\ell, T)/c_0$ and similarly for X_{N-1} at its respective position and dimensionless time; with $X_N(T) = 0$ for $T \leq N/2$. These equations show that for each added segment, T is replaced by $T - (1/2\zeta)$, and the integration is then performed as indicated.

In dimensionless units, X can be given as a function of N, T, and ζ; or as a function of N, Θ, and ζ, where $\Theta_N = T/N$. For the latter case, the integrand function X_{N-1} is known in terms of Θ_{N-1}, but here one wishes to evaluate it in terms of Θ_N. This is equivalent to reducing the length of a column of $(N-1)$ segments from the constant value h to a new value $h' = (N-1)h/N$; then an extra segment is added to restore the column to length h. By use of the general definition $\Theta = T/N$ we have

$$\Theta_{N-1} = \frac{T}{N-1} - \frac{1}{2\zeta(N-1)}, \quad \text{and } \Theta_N = \frac{T}{N} \,. \tag{19}$$

Hence, we have

$$X_{N-1}(\Theta_{N-1}) = X_{N-1}\left(\frac{\Theta_N N}{N-1} - \frac{1}{2\zeta(N-1)}\right), \tag{20}$$

and Eq. (18) takes the form

$$X_N(\Theta_N) = 2 \int_{[N(2\Theta_N - 1)+1]^{-1}}^{1} \left\{ X_{N-1}\left(\frac{\Theta_N N}{N-1} - \frac{1}{2\zeta(N-1)} \right) \right\} \zeta d\zeta \,. \qquad (21)$$

The relations rapidly become very complex, and an exact solution seems to be impossible for $N > 2$. The solution must therefore be found by numerical methods on a high-speed digital computer.

a. Analytic relations. The expressions for beds consisting of only one or two segments can be derived analytically, and will now be given. Their mathematical form is of interest to show the complexity that is reached for beds with a larger number of segments, and also to indicate possible forms of empirical equations for representing the latter.

For $N = 1$, Eq. (18) becomes

$$X_1(T) = 2 \int_{\frac{1}{2T}}^{1} \left[X_0\left(T - \frac{1}{2\zeta}\right) \right] \zeta d\zeta \,. \qquad (22)$$

Here X_0, the value of inlet concentration, is constant at unity. From this,

$$X_1(T) = \left(1 - \frac{1}{4T^2}\right) \cdot H(T - 0.5) \,. \qquad (23)$$

This relation shows that $X_1(T)$ is zero as long as $T \leq 0.5$. We recall that $T = Ut/\ell$, where ℓ is the length of one segment, t is the elapsed time, and U is the mean linear velocity. Another dimensionless time can be defined as

$$\Theta = \frac{tU}{h} = \frac{tU}{N\ell} = \frac{T}{N} \,.$$

For $N = 1$ the form of Eq. (23) remains unchanged if Θ replaces T. If $N = 2$, the column consists of two segments of equal length. The mixing effluent from the first segment has the concentration X_1, as just derived. Then, we have

$$X_2(T) = 2 \int_{\frac{1}{2T-1}}^{1} \left[1 - \frac{1}{\left(2T - \frac{1}{\zeta}\right)^2}\right] \zeta d\zeta . \qquad (24)$$

This relation is obtained by replacing T by $[T-(1/2\zeta)]$ in the expression for X_1, and by changing the lower limit to avoid computing negative concentration values. Integration* of Eq. (24) between the specified limits yields

$$X_2(T) = \left\{2(t-1)\left[\frac{(2T)^3+(2T)^2-6}{(2T)^3(2T-1)}\right] - \frac{12}{(2T)^4}\ln(2T-1)\right\} H(T-1). \qquad (25)$$

The argument of the Heaviside function indicates that X_2 is zero for $T \leq 1$. In terms of Θ, the equation for X_2 is of identical form but with T replaced by 2Θ throughout.

5. Quartic Velocity Distribution

A major result of the quadratic velocity profile is that it takes at least half of the stoichiometric time (i.e., at least $\Theta = 0.5$) before any breakthrough sets in. This is unrealistic physically; many experimental curves start earlier, or have shapes that would correspond to N values smaller than 1. The reason for this partial failure of the quadratic model is believed to lie in the assumption of a circular shape for the flow element, in which the maximum fluid velocity is twice the average velocity. In reality the packing voids have a curved triangular, rectangular, or still more complex shape, with corners in which the fluid is practically stagnant. This tends to lead to an average fluid velocity larger than half of the maximum, and in turn frequently to breakthrough-curve X:Θ slopes smaller than those given by the quadratic distribution. As no exact expression for the velocity profile in these complex voids is available, an empirical relation giving $u_{max}/U=3$ has been adopted as a convenient and reasonable starting point.

---

*Details of the integration are given in Appendix I-1.

The steps in the derivation for the quartic velocity profile are identical with those for the quadratic distribution. Hence repetition is avoided here by showing only the respective equations with corresponding numbers.

The expression for the quartic velocity profile is

$$\frac{u(r)}{u_{max}} = \left(1 - \frac{r^2}{R^2}\right)^2 . \tag{7a}$$

Subsequent equations follow:

$$c_b = \frac{6}{R^2} \int_0^R c(r) \left[1 - \frac{r^2}{R^2}\right]^2 r\, dr, \tag{8a}$$

$$\zeta = 1 - \frac{r^2}{R^2} , \tag{9a}$$

$$\zeta = (u/u_{max})^{1/2} , \tag{10a}$$

$$d\zeta = - \frac{2r\, dr}{R^2} , \tag{11a}$$

$$c_b(z_{k+1}, t) = 3 \int_0^1 \left[c_b\left(z_k, t - \frac{z_{k+1} - z_k}{u_{max}\, \zeta^2}\right)\right] \zeta^2\, d\zeta , \tag{12a}$$

$$c_b(z_N, t) = 3 \int_0^1 \left[c_b\left(z_{N-1}, t - \frac{z_N - z_{N-1}}{u_{max}\, \zeta^2}\right)\right] \zeta^2\, d\zeta , \tag{13a}$$

$$c(o, r, t) = c_b(o, t) = c_b\, H(t) , \tag{14a}$$

$$c_b(N\ell, t) = c_0\, f_N(t)\, H\left(t - \frac{N\ell}{u_{max}}\right), \tag{15a}$$

$$= c_N(t)\, H\left(t - \frac{N\ell}{3\overline{U}}\right) ,$$

$$c_N(T) = 3\int_0^1 \left[c_{N-1}\left(T - \frac{1}{3\zeta^2}\right)\right] \cdot H\left[T - \left(\frac{N-1}{3}\right) - \frac{1}{3\zeta^2}\right] \zeta^2 d\zeta, \quad (16a)$$

If

$$T - \left(\frac{N-1}{3}\right) - \frac{1}{3\zeta^2} > 0 \quad \text{or} \quad \zeta \geq (3T-N+1)^{-1/2}, \; H\left[T-\left(\frac{N-1}{3}\right) - \frac{1}{3\zeta^2}\right] = 1, \quad (17a)$$

$$X_N(T) = 3\int_{(3T-N+1)^{-1/2}}^1 \left[X_{N-1}\left(T - \frac{1}{3\zeta^2}\right)\right] \zeta^2 d\zeta, \quad (18a)$$

$$\Theta_{N-1} = \frac{T}{N-1} - \frac{1}{3\zeta^2(N-1)}, \quad \text{with } \Theta_N = \frac{T}{N}, \quad (19a)$$

$$X_{N-1}(\Theta_{N-1}) = X_{N-1}\left[\frac{\Theta_N N}{N-1} - \frac{1}{3\zeta^2(N-1)}\right], \quad (20a)$$

and

$$X_N(\Theta_N) = 3\int_{[N(3\Theta_N-1)+1]^{-1/2}}^1 \left\{X_{N-1}\left[\frac{\Theta_N N}{N-1} - \frac{1}{3\zeta^2(N-1)}\right]\right\}\zeta^2 d\zeta. \quad (21a)$$

a. Analytic relations. The expressions for beds consisting of only one or two segments can again be derived analytically. For N = 1, they are

$$X_1(T) = 3\int_{(3T)^{-1/2}}^1 \left[X_0\left(T - \frac{1}{3\zeta^2}\right)\right]\zeta^2 d\zeta, \quad (22a)$$

and

$$X_1(T) = \left[1 - (3T)^{-3/2}\right] \cdot H\left(T - \frac{1}{3}\right). \quad (23a)$$

For N = 2, also, the expressions are

$$X_2(T) = 3\int_{(3T-1)^{-1/2}}^1 \left[1 - \left(3T - \frac{1}{\zeta^2}\right)^{-3/2}\right]\zeta^2 d\zeta, \quad (24a)$$

and

$$X_2(T) = \left[1 - \frac{2(3T)^3 + 6(3T)^2 - 24(3T) + 16}{(3T)^3(3T-1)^{3/2}}\right] \cdot H\left(T - \frac{2}{3}\right). \qquad (25a)$$

6. Numerical Methods of Solution

For both velocity profiles, the integrations required for successive segments (beyond N = 2) were computed by two different numerical methods. In Method 1 we evaluate the integral by a summation scheme using the exact concentration values calculated for the previous segment. This method is quite accurate, but very time consuming because of its use of a time scale with a constant increment which corresponds to a progressively smaller $\Delta\Theta$ as N increases. In Method 2 we evaluate the integral by Simpson's integration formula, getting the necessary concentration values by interpolation among the values calculated for the previous segment. This method is based on the Θ scale, and computes the minimum number of concentration values necessary to go up to a specified maximum N; it is very fast but becomes unstable for large values of N. It seems possible that an optimum method would be obtained by combining the favorable features of the two methods, but this has not been done.

In this section, these two methods are explained, using the quartic velocity profile for illustration. Results obtained for both velocity distributions are then given.

a. Method 1. This method numerically solves the analytical expression

$$X_N(T) = 3 \int_{(3T-N+1)^{-1/2}}^{1} \left[X_{N-1}\left(T - \frac{1}{3\zeta^2}\right)\right] \zeta^2 d\zeta , \qquad (26)$$

with

$$T = \frac{Ut}{\ell} = \frac{Ut}{h} N .$$

For ease of computation, a new time variable τ is introduced, for which all the curves begin at $\tau = 0$. The appropriate transformation is

$$\tau = 3T - N = N(3\Theta - 1) . \tag{27}$$

Physically, $\tau = 0$ corresponds to the time of arrival (at the outflow) of the maximum-velocity flow filament, for which $\zeta = 1$. When the X-vs-time behavior of a bed length corresponding to N segments is evaluated from that of a length corresponding to N - 1 segments, the values of τ (and T) used are based upon length N rather than upon length (N-1). Hence, when $\tau = 0$ for the evaluation of X_N, the function of τ at which X_{N-1} is evaluated (which can be termed τ_{N-1}) must also be zero when $\zeta = 1$. To state the problem another way, Eq. (27) can be extended to give

$$\tau_{N-1} = \tau_N + 3(T_{N-1} - T_N) - [(N-1)-N] . \tag{28}$$

From Eq. (26), T_{N-1} is seen to be $T_N - [1/(3\zeta^2)]$. Hence, we obtain

$$\tau_{N-1} = \tau_N - \frac{1}{\zeta^2} + 1. \tag{29}$$

A test of this relation shows that it does satisfy the condition stated above ($\tau_{N=1}=0$ when $\zeta = 1$).

To eliminate subscripts, the function τ_{N-1} will be redefined as a time variable W. Equation (26), the general formula, thus becomes

$$X_N(\tau) = 3 \int_{1/\sqrt{\tau+1}}^{1} \left[X_{N-1}\left(\tau+1 - \frac{1}{\zeta^2}\right)\right] \zeta^2 d\zeta$$

$$= \int_{1/\sqrt{\tau+1}}^{1} X_{N-1}(W)\, \zeta^2 d\zeta . \tag{30}$$

Method 1 involves approximating this integral by a summation, using directly the X values computed from the previous segment, with the corresponding ζ values as shown below. A time increment δ is selected such that

$$\tau = m\delta \tag{31}$$

and

$$W = m'\delta , \tag{32}$$

where m and m' are integers. From the definition of W, we have

$$\zeta = (1 + \tau - W)^{-1/2} = [1 + (m - m')\delta]^{-1/2} . \qquad (33)$$

with $m \geq m'$, ζ can take on an infinite sequence of values starting at unity and tending toward zero. The general equation, in summation form, becomes

$$X_N(\tau) = 3 \sum_{m'=0}^{m'=m-1} [X_N(W)]_{av} (\zeta^2)_{av} \Delta\zeta$$

$$= 1.5 \sum_{m'=0}^{m'=m-1} [X_N(W)]_{av} (\zeta^2_{m'} + \zeta^2_{m'+1}) (\zeta_{m'} - \zeta_{m'+1}) . \qquad (34)$$

Illustration of the use of these equations is given in Appendix I-2.

b. Method 2. Here the dimensionless time scale $\Theta = T/N$ is used directly, time being thus referred to the total length of the column rather than to the length of the individual segments. The general formula used in Method 2 is Eq. (21a):

$$X_N(\Theta) = 3 \int_{[N(3\Theta-1)+1]^{-1/2}}^{1} \left\{ X_{N-1} \left[\frac{N}{N-1} \Theta - \frac{1}{3(N-1)\zeta^2} \right] \right\} \zeta^2 d\zeta . \qquad (35)$$

For simplification, a new variable V is defined as

$$V = \frac{N}{N-1} \Theta - \frac{1}{3(N-1)\zeta^2} \qquad (36)$$

From this, we have

$$\zeta = [3N\Theta - 3(N-1)V]^{-1/2} , \qquad (37)$$

and

$$X_N(\Theta) = 4.5 \int_{1/3}^{\frac{3N\Theta-1}{3(N-1)}} X_{N-1}(V) \frac{(N-1)}{[3N\Theta - 3(N-1)V]^{2.5}} dV . \qquad (38)$$

To compute the concentration values X_N to a dimensionless time value Θ_N, it is necessary to know X_{N-1} values to a time Θ_{N-1} larger than Θ_N. The relation between the different time values is

$$\Theta_{N-i} = \Theta_N + \frac{i}{N-i}\left(\Theta_N - \frac{1}{3}\right), \qquad (39)$$

where i is an integer. After the largest Θ that is needed for the largest N has been specified, Eq. (39) indicates the largest Θ that must be carried for each lesser number of segments.

Computation was made with the analytic results for N=2 as starting values. In the computation for each new N, Θ was varied by constant increments up to the limit. For each Θ, Eq. (38) was evaluated by Simpson's integration rule, with the X values for a specified value of the argument V being obtained by interpolation. The number of points used in Simpson's rule was determined by specifying the maximum interval between any two successive points on the time scale.

The Fortran listings for both methods are given in Appendix I-2. Both programs also compute the area between the concentration-versus-time curve and a horizontal line drawn at X = 1. The stoichiometric point should occur at Θ = 1; thus, for correct computation, the above-mentioned area should also be unity.

c. Results. Numerical results for the quadratic and the quartic distribution obtained by Method 1 with δ (quadratic) = 0.100 and δ (quartic) = 0.1667 are given respectively in Tables I-I and I-II. In Figs. I-2 and I-3, the same results are presented graphically as semi-logarithmic plots of X vs Θ, the time scale being normalized by the stoichiometric time. The numerical results were limited to $N \leq 45$, due to the relatively large amount of computer time involved in going further (about 0.5 hr on the IBM 7090 was required for the present range of values). An exact estimate of the error involved in the use of Method 1 is not possible; however, trial runs for the quartic distribution up to N = 10 showed that by reducing the increment δ from 0.1667 to 0.0833 the X_{10} values changed only by 1 digit in the third place. Concentration

Table I-1. Breakthrough concentration values (X) for the segmented laminar-flow model with quadratic velocity

N	Θ=0.6	0.7	0.8	0.9	1.0	1.1	1.2	1.3	1.4	1.5	1.6	1.7	1.8
1	0.305556	0.489796	0.609375	0.691358	0.750000	0.793388	0.826389	0.852071	0.872449	0.888889	0.902344	0.913495	0.890
2	0.159055	0.366943	0.525802	0.638919	0.719336	0.777410	0.820196	0.852360	0.877001	0.896209	0.911418	0.923632	0.983
3	0.088238	0.287963	0.469662	0.605349	0.702030	0.770727	0.820143	0.856313	0.883281	0.903756	0.919565	0.931966	0.985
4	0.051324	0.232503	0.427527	0.580729	0.690576	0.767693	0.822088	0.861022	0.889400	0.910474	0.926414	0.938678	0.986
5	0.030608	0.190808	0.393416	0.560988	0.682131	0.766352	0.824747	0.865728	0.895004	0.916332	0.932177	0.944168	0.986
6	0.018543	0.158282	0.364627	0.544349	0.675502	0.765931	0.827667	0.870222	0.900078	0.921456	0.937087	0.948746	0.986
7	0.011357	0.132314	0.339684	0.529868	0.670079	0.766059	0.830657	0.874454	0.904672	0.925972	0.941323	0.952627	0.986
8	0.007013	0.111253	0.317680	0.516985	0.665512	0.766535	0.833630	0.878419	0.908847	0.929985	0.945020	0.955962	0.986
9	0.004357	0.093974	0.298014	0.505338	0.661580	0.767241	0.836541	0.882132	0.912657	0.933578	0.948278	0.958863	0.986
10	0.002721	0.079673	0.280262	0.494679	0.658138	0.768101	0.839372	0.885613	0.916149	0.936815	0.951173	0.961411	0.986
11	0.001706	0.067757	0.264113	0.484829	0.655083	0.769069	0.842114	0.888881	0.919365	0.939750	0.953765	0.963668	0.985
12	0.001073	0.057773	0.249331	0.475656	0.652342	0.770110	0.844763	0.891956	0.922337	0.942425	0.956100	0.965681	0.985
13	0.000677	0.049369	0.235729	0.467061	0.649859	0.771202	0.847320	0.894854	0.925093	0.944874	0.958215	0.967489	0.985
14	0.000428	0.042269	0.223161	0.458963	0.647594	0.772329	0.849788	0.897593	0.927658	0.947125	0.960140	0.969121	0.984
15	0.000272	0.036251	0.211506	0.451300	0.645513	0.773478	0.852170	0.900185	0.930052	0.949203	0.961901	0.970603	0.984
16	0.000173	0.031136	0.200664	0.444021	0.643589	0.774641	0.854470	0.902643	0.932293	0.951127	0.963518	0.971954	0.983
17	0.000110	0.026778	0.190551	0.437084	0.641803	0.775811	0.856692	0.904977	0.934394	0.952915	0.965007	0.973191	0.983
18	0.000070	0.023058	0.181097	0.430453	0.640137	0.776984	0.858839	0.907199	0.936371	0.954580	0.966385	0.974327	0.982
19	0.000045	0.019876	0.172239	0.424098	0.638577	0.778155	0.860915	0.909315	0.938233	0.956135	0.967661	0.975375	0.982
20	0.000029	0.017150	0.163925	0.417995	0.637110	0.779322	0.862925	0.911335	0.939991	0.957590	0.968849	0.976344	0.981
21	0.000018	0.014811	0.156109	0.412122	0.635728	0.780482	0.864871	0.913265	0.941655	0.958956	0.969956	0.977242	0.981
22	0.000012	0.012801	0.148750	0.406460	0.634420	0.781634	0.866756	0.915112	0.943230	0.960240	0.970990	0.978078	0.980
23	0.000007	0.011072	0.141813	0.400992	0.633181	0.782777	0.868585	0.916881	0.944725	0.961449	0.971958	0.978857	0.979
24	0.000005	0.009584	0.135265	0.395704	0.632003	0.783909	0.870359	0.918577	0.946146	0.962590	0.972867	0.979585	0.979
25	0.000003	0.008300	0.129077	0.390583	0.630881	0.785031	0.872081	0.920205	0.947498	0.963669	0.973722	0.	0.978
26	0.000002	0.007193	0.123224	0.385618	0.629810	0.786141	0.873755	0.921770	0.948787	0.964690	0.974527	0.	0.977
27	0.000001	0.006237	0.117683	0.380798	0.628787	0.787239	0.875381	0.923275	0.950016	0.965658	0.975286	0.	0.976
28	0.000001	0.005411	0.112433	0.376115	0.627806	0.788324	0.876963	0.924723	0.951190	0.966577	0.	0.	0.975
29	0.000001	0.004697	0.107453	0.371561	0.626866	0.789398	0.878502	0.926119	0.952312	0.967450	0.	0.	0.974
30	0.000000	0.004079	0.102728	0.367127	0.625963	0.790459	0.880000	0.927465	0.953386	0.	0.	0.	0.973
31	0.000000	0.003543	0.098240	0.362807	0.625094	0.791508	0.881459	0.928764	0.954416	0.	0.	0.	0.972
32	0.000000	0.003079	0.093976	0.358595	0.624257	0.792545	0.882881	0.930018	0.955403	0.	0.	0.	0.971
33	0.000000	0.002677	0.089922	0.354486	0.623449	0.793569	0.884268	0.931229	0.956350	0.	0.	0.	0.969
34	0.000000	0.002328	0.086065	0.350473	0.622670	0.794582	0.885620	0.932401	0.	0.	0.	0.	0.968
35	0.000000	0.002026	0.082393	0.346553	0.621917	0.795582	0.886940	0.933535	0.	0.	0.	0.	0.967
36	0.000000	0.001763	0.078897	0.342722	0.621188	0.796570	0.888228	0.934633	0.	0.	0.	0.	0.965
37	0.000000	0.001535	0.075566	0.338974	0.620482	0.797547	0.889486	0.935696	0.	0.	0.	0.	0.963
38	0.000000	0.001337	0.072391	0.335306	0.619798	0.798512	0.890715	0.	0.	0.	0.	0.	0.962
39	0.000000	0.001164	0.069363	0.331715	0.619134	0.799466	0.891915	0.	0.	0.	0.	0.	0.960
40	0.000000	0.001014	0.066475	0.328198	0.618489	0.800408	0.893089	0.	0.	0.	0.	0.	0.958

Table I-II. Breakthrough concentration values (X) for the segmented laminar-flow model with quartic velocity profile

N	ϑ=0.5	0.67	0.83	1.0	1.17	1.33	1.50	1.67	1.83	2.0	2.33
1	0.455669	0.646447	0.747018	0.807550	0.847279	0.875000	0.895243	0.910557	0.922472	0.931959	0.939657
2	0.313635	0.565152	0.703622	0.784933	0.836319	0.870817	0.895117	0.912907	0.926348	0.936769	0.945027
3	0.231530	0.512640	0.677476	0.773386	0.832528	0.871183	0.897734	0.916734	0.930801	0.941514	0.949870
4	0.176117	0.472610	0.658340	0.766012	0.831148	0.872814	0.900858	0.920568	0.934930	0.945718	0.954032
5	0.136300	0.439849	0.643069	0.760800	0.830892	0.874913	0.904035	0.924193	0.938690	0.949457	0.957673
6	0.106700	0.411951	0.630266	0.756895	0.831251	0.877198	0.907137	0.927589	0.942131	0.952828	0.960925
7	0.084218	0.387589	0.619182	0.753860	0.831978	0.879549	0.910129	0.930773	0.945307	0.955910	0.963879
8	0.066889	0.365939	0.609372	0.751442	0.832940	0.881911	0.913004	0.933773	0.948265	0.958759	0.966599
9	0.053388	0.346452	0.600544	0.749481	0.834060	0.884257	0.915768	0.936612	0.951041	0.961420	0.969132
10	0.042781	0.328740	0.592499	0.747873	0.835289	0.886573	0.918428	0.939313	0.953664	0.963926	0.971512
11	0.034396	0.312518	0.585095	0.746543	0.836593	0.888852	0.920993	0.941892	0.956157	0.966300	0.973767
12	0.027730	0.297569	0.578226	0.745439	0.837951	0.891092	0.923473	0.944366	0.958537	0.968564	0.975915
13	0.022410	0.283723	0.571809	0.744519	0.839349	0.893293	0.925875	0.946746	0.960821	0.970734	0.977973
14	0.018148	0.270844	0.565783	0.743755	0.840774	0.895454	0.928207	0.949044	0.963020	0.972821	0.979954
15	0.014723	0.258821	0.560095	0.743123	0.842220	0.897578	0.930475	0.951269	0.965145	0.974837	0.981869
16	0.011963	0.247563	0.554706	0.742604	0.843680	0.899666	0.932684	0.953428	0.967204	0.976790	0.983724
17	0.009735	0.236992	0.549581	0.742182	0.845151	0.901719	0.934840	0.955528	0.969204	0.978687	0.985529
18	0.007932	0.227044	0.544692	0.741845	0.846627	0.903740	0.936948	0.957575	0.971152	0.980536	0.987288
19	0.006470	0.217661	0.540015	0.741584	0.848108	0.905730	0.939010	0.959573	0.973053	0.982340	0.989006
20	0.005283	0.208797	0.535531	0.741390	0.849591	0.907691	0.941032	0.961527	0.974911	0.984105	0.990689
21	0.004318	0.200407	0.531222	0.741255	0.851075	0.909624	0.943015	0.963442	0.976731	0.985834	0.992339
22	0.003532	0.192456	0.527072	0.741173	0.852558	0.911532	0.944963	0.965319	0.978516	0.987531	0.993960
23	0.002892	0.184910	0.523069	0.741140	0.854039	0.913415	0.946879	0.967163	0.980268	0.989198	0.995524
24	0.002369	0.177739	0.519202	0.741150	0.855519	0.915275	0.948764	0.968975	0.981991	0.990839	0.996932
25	0.001942	0.170918	0.515459	0.741200	0.856995	0.917113	0.950621	0.970759	0.983688	0.992451	0.998103
26	0.001593	0.164423	0.511833	0.741287	0.858469	0.918930	0.952452	0.972516	0.985359	0.994003	0.999007
27	0.001308	0.158232	0.508315	0.741406	0.859939	0.920728	0.954258	0.974249	0.987008	0.995435	0.999627
28	0.001074	0.152327	0.504898	0.741556	0.861406	0.922508	0.956041	0.975958	0.988633	0.996703	0.
29	0.000883	0.146688	0.501576	0.741735	0.862869	0.924270	0.957802	0.977646	0.990226	0.997783	0.
30	0.000726	0.141302	0.498342	0.741940	0.864328	0.926015	0.959543	0.979315	0.991760	0.	0.
31	0.000597	0.136151	0.495192	0.742169	0.865783	0.927744	0.961265	0.980964	0.993204	0.	0.
32	0.000491	0.131224	0.492121	0.742420	0.867234	0.929458	0.962970	0.982596	0.994539	0.	0.
33	0.000404	0.126508	0.489124	0.742693	0.868682	0.931158	0.964657	0.984206	0.995747	0.	0.
34	0.000333	0.121990	0.486197	0.742986	0.870125	0.932844	0.966328	0.985787	0.	0.	0.
35	0.000274	0.117661	0.483337	0.743297	0.871564	0.934517	0.967984	0.987326	0.	0.	0.
36	0.000226	0.113511	0.480540	0.743625	0.873000	0.936178	0.969626	0.988810	0.	0.	0.
37	0.000186	0.109529	0.477803	0.743970	0.874431	0.937827	0.971254	0.990228	0.	0.	0.
38	0.000154	0.105709	0.475123	0.744330	0.875859	0.939465	0.972869	0.	0.	0.	0.
39	0.000127	0.102041	0.472498	0.744705	0.877283	0.941092	0.974469	0.	0.	0.	0.
40	0.000104	0.098518	0.469926	0.745094	0.878703	0.942709	0.976052	0.	0.	0.	0.
41	0.000086	0.095133	0.467403	0.745496	0.880120	0.944315	0.977614	0.	0.	0.	0.
42	0.000071	0.091880	0.464927	0.745910	0.881533	0.945913	0.979149	0.	0.	0.	0.
43	0.000059	0.088752	0.462498	0.746336	0.882943	0.947501	0.	0.	0.	0.	0.
44	0.000049	0.085744	0.460112	0.746773	0.884350	0.949081	0.	0.	0.	0.	0.
45	0.000040	0.082851	0.457768	0.747221	0.885754	0.950652	0.	0.	0.	0.	0.

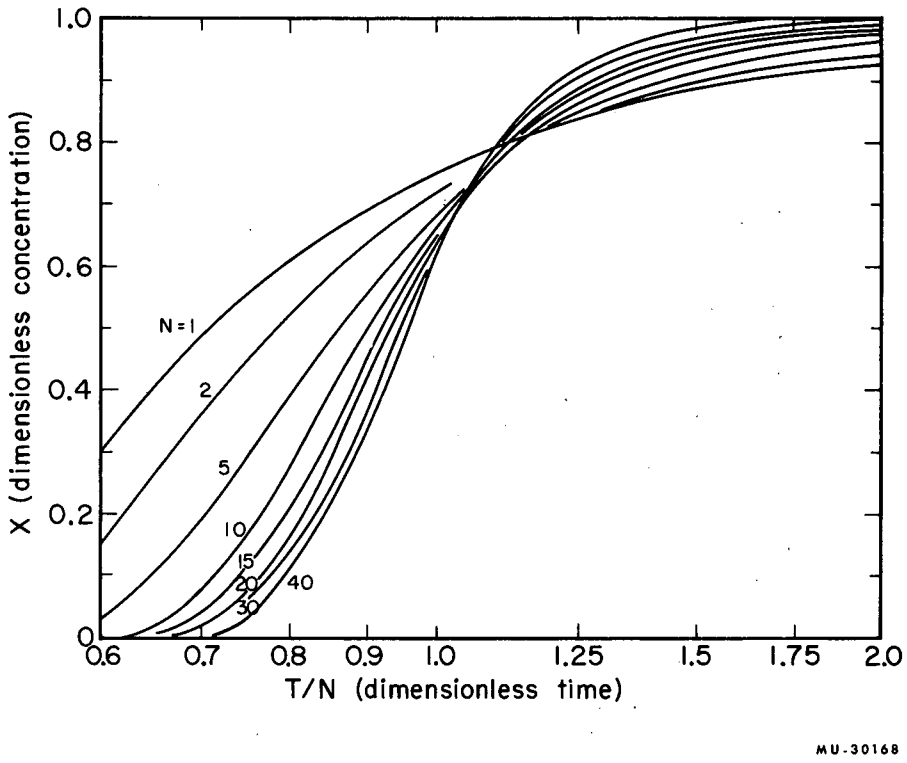

Fig. I-2. Breakthrough curves for the segmented laminar-flow model with quadratic velocity profile.

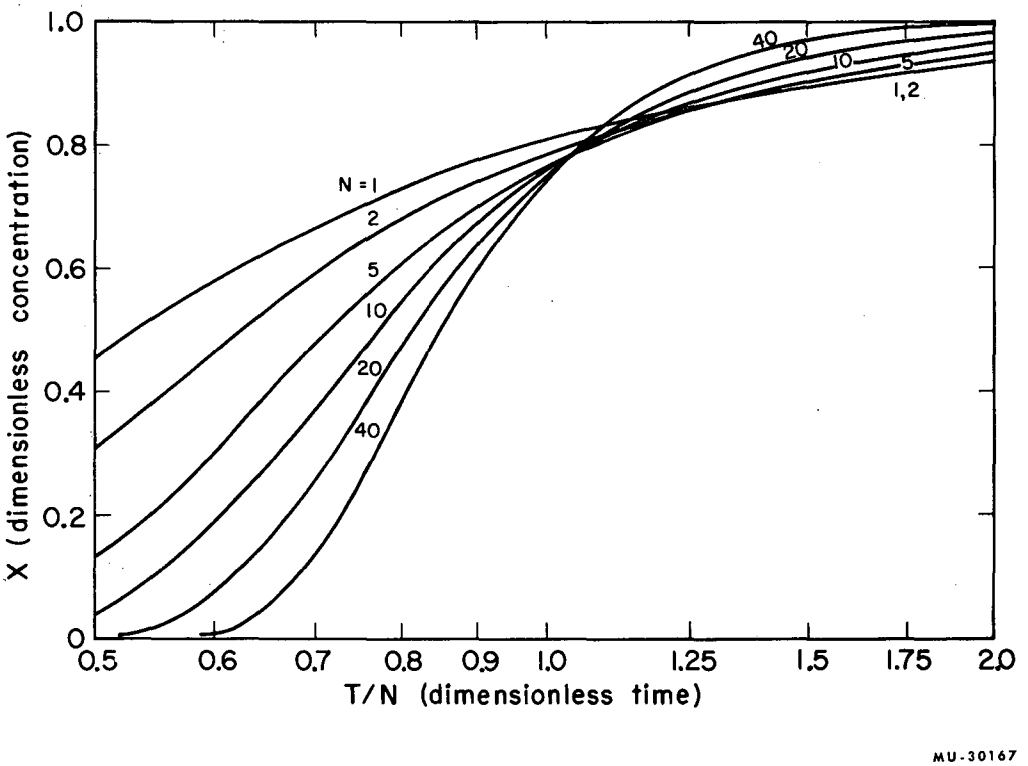

Fig. I-3. Breakthrough curves for the segmented laminar-flow model with quartic velocity profile.

values calculated by Method 2 with $\Delta\Theta = 0.042$ up to $N = 10$ did not differ more than 2 digits in the third place from those computed by Method 1. Beyond $N = 10$, cumulative errors led to erroneous results unless $\Delta\Theta$ was much further reduced, which in turn was very time consuming.

The coordinates of Figs. I-2 and I-3 are very convenient for comparing experimental breakthrough curves with the theoretical results, since a logarithmic scale of the experimental volume or time will only differ from the logarithm of dimensionless time by a constant additive term. Dimensionless slopes at the midpoint ($X = 0.50$), defined as $s' = \Theta_{50}(dX/d\Theta)$, are given in Tables I-III, and I-IV. In this definition Θ_{50} is the Θ value corresponding to $X = 0.50$, and $dX/d\Theta\,(=s)$ is the slope at Θ_{50}; the tabulated slopes were obtained graphically from plots of the data on rectangular coordinates. These slopes will be used later to compare the results from different models.

A frequency-response analysis for the quadratic velocity distribution, obtained from the step-input response, is given in Appendix I-3. A similar approach could be used for the quartic velocity distribution, if needed.

C. Diffusion Model

In the diffusion model for longitudinal dispersion, it is assumed that equations of exactly the same form apply as those describing the molecular-diffusion process. The governing equation is

$$\frac{E}{\epsilon}\frac{\partial^2 c}{\partial z^2} - \frac{U_0}{\epsilon}\frac{\partial c}{\partial z} = \frac{\partial c}{\partial t}, \tag{40}$$

where z is axial distance, t is time, c is the solute concentration of interest, E is the superficial axial-dispersion coefficient, ϵ is the void fraction, and U_0 is the superficial velocity of the fluid. The solution to this equation has been given for two different sets of boundary conditions corresponding to a finite-length column and to an infinite

Table I-III. Midpoint slopes for the segmented-laminar-flow model, with quadratic velocity profile

N	Θ_{50}	s	$\Theta_{50} \cdot s$
1	0.708	1.45	1.027
2	0.785	1.43	1.123
3	0.825	1.48	1.221
5	0.865	1.62	1.401
7	0.888	1.71	1.518
10	0.905	1.88	1.701
15	0.925	2.14	1.980
20	0.932	2.28	2.125
25	0.940	2.42	2.280
30	0.950	2.60	2.470
35	0.952	2.72	2.589
40	0.954	2.80	2.671

Table I-IV. Midpoint slopes for the segmented-laminar-flow model with quartic velocity profile

N	Θ_{50}	s	$\Theta_{50} \cdot s$
1	0.502	1.230	0.691
2	0.615	1.269	0.780
3	0.660	1.285	0.848
5	0.715	1.364	0.975
7	0.741	1.498	1.110
10	0.767	1.557	1.194
15	0.790	1.720	1.359
20	0.813	1.750	1.423
25	0.820	1.859	1.525
30	0.830	1.989	1.651
35	0.839	2.062	1.730
40	0.847	2.150	1.820

column; both of these are reviewed below; a semi-infinite column has also been treated by Aris and Amundson[1] and others.[23]

1. Finite-Length Column (Bounded Diffusion)

For a column of length h, the following conditions hold. The feed conditions representing a step-function input are

$$\text{for } z = 0, \text{ at } t \leq 0\ (-),\ c = 0,$$

and

$$\text{at } t \geq 0\ (+),\ c = c_0 .$$

The inlet boundary condition is determined as follows: At the inlet (i.e., $z = 0$) the rate of arrival of solute outside by convection is equal to the rate of removal of solute inside by diffusion and by convection, plus the rate of accumulation of solute at the interior boundary. To obtain a solution, the latter term is neglected; this is equivalent to assuming a steady state at the inlet. Then, from integration of Eq. (40), the boundary condition at $z = 0$ and at all $t > 0$ is obtained:

$$E \frac{dc(0+)}{dz} - U_0\, c(0+) = \text{const} = - U_0\, c(0-) . \tag{41}$$

At the bed outlet, a similar material balance (again assuming a negligible accumulation rate) gives

$$U_0\, c(h-) - E \frac{\partial c(h-)}{\partial z} = U_0\, c(h+) . \tag{42}$$

In a situation of rising concentration (an arriving breakthrough curve), regardless of the mechanism of material transport, we can never have a downstream concentration higher than an upstream value.[10,42] Since Eq. (42), with the negative dc/dz permissible in terms of this physical picture, would lead to $c(h+) > c(h-)$, the only physically acceptable condition is that, at $z = h$,

$$\frac{\partial c}{\partial z} = 0, \quad \text{for all } t > 0$$

and hence that $c(h-) = c(h+)$.

a. Exact expression. An exact solution for the diffusion equation, Eq. (40), applied to a column of finite length, has been given by Yagi and Miyauchi.[42] Brenner has shown that the general equation and the boundary conditions are similar to those governing heat loss to "sinks" at the ends of a slab,[3] for which Carslaw and Jaeger have given the general solution.[8]

The variables in Eq. (40) will be made dimensionless by introducing the relations $N = h/\ell = h\,U_0/E$, $X = c/c_0$, $T = U_0 t/\ell\epsilon$, and $Z = z/h$. Here N is a "column Péclet number," or total number of "dispersion units." Thus we have

$$\frac{\partial^2 X}{\partial Z^2} - N\,\frac{\partial X}{\partial Z} = N^2\,\frac{\partial X}{\partial Z} \tag{43}$$

The solution to this equation, at the exit of the column, has the form

$$\frac{c}{c_0} = \sum_{n=1}^{n=\infty} \exp\left\{\frac{N}{2}\left[1 - \frac{T}{2N}\left(1 + \frac{4\mu_n^2}{N^2}\right)\right]\right\} \tag{44}$$

$$\cdot\,\frac{N\mu_n(N\sin\mu_n + 2\mu_n\cos\mu_n)}{\left[(N/2)^2 + N + \mu_n^2\right]\left[(N/2)^2 + \mu_n^2\right]},$$

where μ_n is given by the transcendental equation

$$\mu_n = \cot^{-1}\left(\frac{\mu_n}{N} - \frac{N}{4\mu_n}\right). \tag{45}$$

b. Asymptotic solution. The formal solution given by Eq. (44) converges too slowly to be of much use when N is large or T is small. Therefore, Brenner developed the following asymptotic expansion by applying the Laplace transformation:[3]

$$X_e = 1/2 + 1/2\,\mathrm{erf}\left[(N/4\Theta)^{1/2}(1-\Theta)\right] - (N\Theta/\pi)^{1/2}\left[3 + (N/2)(1+\Theta)\right]$$
$$\cdot\exp\left[-N(1-\Theta)^2/4\Theta\right] + \left[1/2 + (N/2)(3+4\Theta) + (N^2/4)(1+\Theta)^2\right]$$
$$\cdot\exp(N)\cdot\mathrm{erfc}\left[(N/4\Theta)^{1/2}(1+\Theta)\right], \tag{46}$$
$$\text{with } \Theta = T/N.$$

This last expression can further be simplified by utilizing asymptotic expansions for all the error functions except those whose arguments are $(N/4\Theta)^{1/2}(1-\Theta)$. Brenner therefore presented the modified asymptotic expansion[3]

$$X_e = 1/2 + (1/2)\,\mathrm{erf}\left[(N/4\Theta)^{1/2}(1-\Theta)\right] + \frac{1}{\Theta+1}\left(\frac{\Theta}{\pi N}\right)^{1/2} \cdot \exp\left[-\frac{N(1-\Theta)^2}{4\Theta}\right]\psi(a)\,, \tag{47}$$

where

$$\psi(a) = (1 - 6a + 4a^2) - \frac{a(1-a)}{(N/2)}(1 - 18a + 24a^2) + \cdots + (-1)^K\left[\frac{a(1-a)}{(N/2)}\right]^K \phi_K(a) + \cdots, \tag{48}$$

and

$$\phi_K(a) = 1, 3, 5, \cdots (2K+1)\left[\frac{1}{2K+1} - 6a + 4(K+1)a^2\right], \tag{49}$$

and $a = \Theta/(\Theta+1)$. A different approach from that of Brenner, based on a semi-infinite column, has led to the following asymptotic expression as developed by Aris and Amundson[1] and extended by Jacques:[23]

$$X_e = 1/2\left[1 + \mathrm{erf}\left(\frac{T-N}{2\sqrt{T}}\right) - \exp N \cdot \mathrm{erf\,c}\left(\frac{T+N}{2\sqrt{T}}\right)\right] + \frac{1}{2\sqrt{\pi}}\int_0^T \frac{1}{\sqrt{T}}\exp\left[-\frac{(N-T)^2}{4T}\right]\left\{1 - \frac{2T}{N+T}\left[1 - \frac{2T}{(N+T)} + \frac{12T^2}{(N+T)^4} + \cdots\right]\right\}dT. \tag{50}$$

This relation is believed to give similar results to Eq. (47), and is only shown here for reference. It contains the same boundary condition at $z = 0$, but not at $z = h$.

c. Numerical evaluations. Calculations of outlet concentration were carried out in this investigation for a large number of N and Θ values, using the exact expression [Eq. (44)] with 18 roots. The roots of the transcendental relation Eq. (45), calculated on a digital computer, are given in Appendix I-4. The breakthrough values are given in Table I-V.

Table I-V. Breakthrough concentration values (X) for bounded-diffusion model

N	ϑ=0.4	0.5	0.6	0.7	0.8	0.9	1.0	1.1	1.2	1.3	1.4	1.5	1.6	1.7	2.0
1	0.2547	0.3359	0.4090	0.4742	0.5323	0.5840	0.6300	0.6710	0.7073	0.7397	0.7685	0.7941	0.8169	0.8371	0.8854
2	0.1862	0.2760	0.3613	0.4391	0.5086	0.5701	0.6241	0.6716	0.7130	0.7493	0.7810	0.8087	0.8330	0.8541	0.9028
3	0.1367	0.2269	0.3185	0.4053	0.4844	0.5547	0.6165	0.6703	0.7169	0.7570	0.7916	0.8213	0.8468	0.8687	0.9173
4	0.1015	0.1879	0.2823	0.3755	0.4623	0.5404	0.6091	0.6687	0.7200	0.7637	0.8008	0.8323	0.8588	0.8813	0.9294
5	0.0761	0.1568	0.2517	0.3493	0.4426	0.5275	0.6025	0.6675	0.7230	0.7699	0.8093	0.8422	0.8696	0.8923	0.9396
8	0.0184	0.0906	0.1821	0.2870	0.3945	0.4962	0.5875	0.6664	0.7327	0.7874	0.8319	0.8677	0.8963	0.9189	0.9617
10		0.0681	0.1502	0.2552	0.3690	0.4798	0.5803	0.6672	0.7396	0.7984	0.8453	0.8821	0.9106	0.9325	0.9715
16		0.0284[a]	0.0874	0.1858	0.3102	0.4422	0.5662	0.6733	0.7604	0.8281	0.8786	0.9155	0.9419	0.9605	0.9881
20		0.0150[a]	0.0614[a]	0.1525	0.2799	0.4226	0.5599	0.6786	0.7734	0.8448	0.8962	0.9319	0.9561	0.9720	0.9932
24		0.0085[a]	0.0441[a]	0.1267	0.2545	0.4059	0.5552	0.6843	0.7856	0.8597	0.9109	0.9448	0.9666	0.9801	0.9961
32		0.0028[a]	0.0232[a]	0.0890[a]	0.2135	0.3782	0.5483	0.6962	0.8077	0.8847	0.9339	0.9635	0.9804	0.9898	0.9988
40		0.0009[a]	0.0124[a]	0.0637[a]	0.1815[a]	0.3553	0.5435	0.7066	0.8267	0.9045	0.9504	0.9755	0.9884	0.9947	0.9995
80[a]			0.0006	0.0135	0.0886	0.2760	0.5311	0.7539	0.8932	0.9606	0.9873	0.9964	0.9905	0.9998	0.9999

[a]Values calculated by Brenner[3]

and presented graphically in Fig. I-3. Brenner's results, which became available subsequent to these calculations, have been used to expand the table in the low-T-high-N range. Outside this range there is close agreement between comparable values from the two calculations, but different N values from those shown were usually used by Brenner. Midpoint slopes are presented in Table I-VII; numerical results for different values of N and Θ are given in Table I-V and presented graphically in Fig. I-4.

2. Infinite-Length Column (Unbounded Diffusion)

The second type of boundary conditions applies to a column of infinite length (extending from $z = +\infty$ to $z = -\infty$). Initially, the section extending from $z = -\infty$ to $z = 0$ is filled with solute; at $t = 0$ it begins to flow into the test section. The initial condition can be written

$$\text{at } t = 0 \text{ and } z = 0(-),\ c = 0;\ z = 0(+),\ c = c_0 .$$

The boundary conditions, as stated by Danckwerts,[1] are

$$\text{at } z = \infty \text{ and } t > 0 \quad c = 0,$$

and

$$\text{at } z = -\infty \text{ and } t > 0 \quad c = c_0 .$$

With the use of these boundary conditions the following solution (in dimensionless form) to Eq. (40) is obtained for the outflow concentration:

$$X = 1/2\left[1 - \operatorname{erf}\frac{\sqrt{N}\,(1-\Theta)}{2\sqrt{\Theta}}\right]. \tag{51}$$

Numerical results for different values of N and Θ are given in Table I-VI and in Fig. I-5. The "unbounded" solution [Eq. (44)] and the "bounded" solution [Eq. (51)] approach each other at high N. Table I-VII gives the midpoint slopes, calculated from the relation

$$s = (N/4\pi)^{1/2}\ ; \tag{52}$$

these slopes are practically identical for $N > 20$.

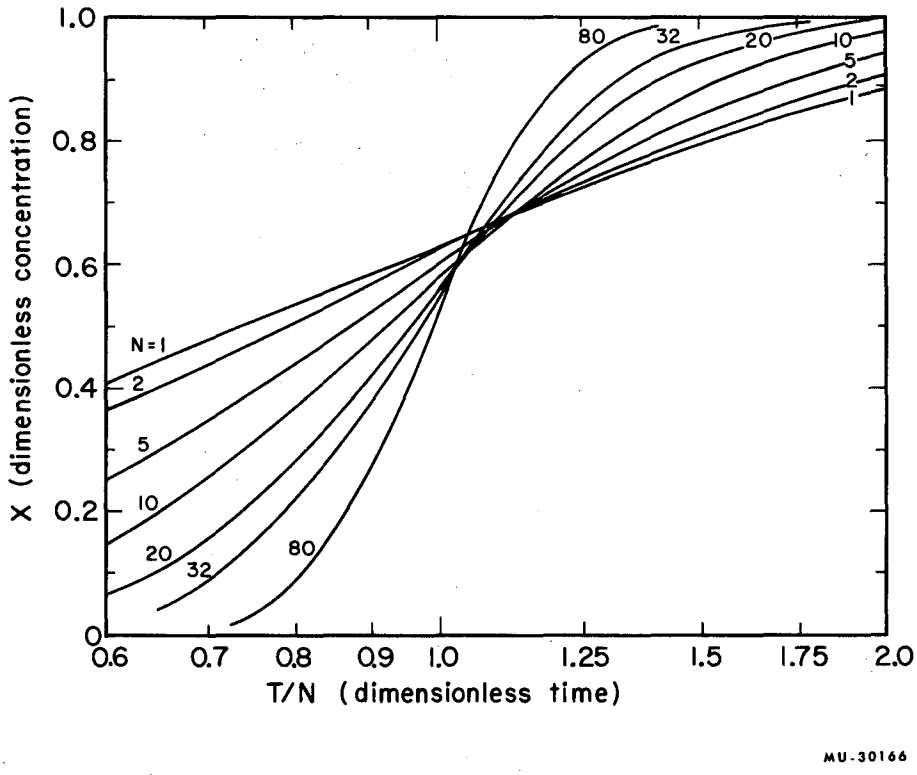

Fig. I-4. Breakthrough curves for bounded diffusion model.

Table I-VI. Breakthrough concentration values (X) for unbounded diffusion model

N	Θ=0.3	0.5	0.6	0.7	0.8	0.9	1.0	1.1	1.2	1.3	1.4	1.5	1.7	2.0
1	0.1831	0.3085	0.3575	0.3999	0.4372	0.4703	0.5000	0.5269	0.5514	0.5738	0.5945	0.6136	0.6479	0.6915
2	0.1006	0.2398	0.3028	0.3600	0.4115	0.4580	0.5000	0.5380	0.5724	0.6038	0.6323	0.6585	0.7043	0.7602
3	0.0588	0.1932	0.2635	0.3303	0.3921	0.4486	0.5000	0.5465	0.5885	0.6264	0.6606	0.6915	0.7446	0.8068
5	0.0217	0.1318	0.2071	0.2854	0.3618	0.4338	0.5000	0.5599	0.6136	0.6613	0.7035	0.7407	0.8020	0.8682
7	0.0084	0.0929	0.1670	0.2512	0.3379	0.4218	0.5000	0.5708	0.6337	0.6887	0.7365	0.7775	0.8424	0.9071
10	0.0021	0.0569	0.1241	0.2113	0.3085	0.4068	0.5000	0.5844	0.6585	0.7219	0.7752	0.8193	0.8850	0.9431
15	0.0002	0.0264	0.0786	0.1631	0.2701	0.3864	0.5000	0.6030	0.6915	0.7644	0.8227	0.8682	0.9293	0.9736
20	0.0000	0.0127	0.0512	0.1284	0.2398	0.3694	0.5000	0.6185	0.7181	0.7973	0.8575	0.9016	0.9552	0.9873
25		0.0062	0.0339	0.1024	0.2146	0.3547	0.5000	0.6320	0.7407	0.8239	0.8840	0.9255	0.9712	0.9938
30		0.0031	0.0228	0.0825	0.1932	0.3415	0.5000	0.6440	0.7602	0.8459	0.9048	0.9431	0.9812	0.9969
40		0.0008	0.0105	0.0544	0.1587	0.3187	0.5000	0.6651	0.7929	0.8803	0.9347	0.9661	0.9918	0.9992
50		0.0002	0.0049	0.0365	0.1318	0.2991	0.5000	0.6832	0.8193	0.9058	0.9545	0.9794	0.9964	0.9998
70		0.0000	0.0011	0.0169	0.0929	0.2664	0.5000	0.7136	0.8600	0.9402	0.9772	0.9921	0.9993	0.9999

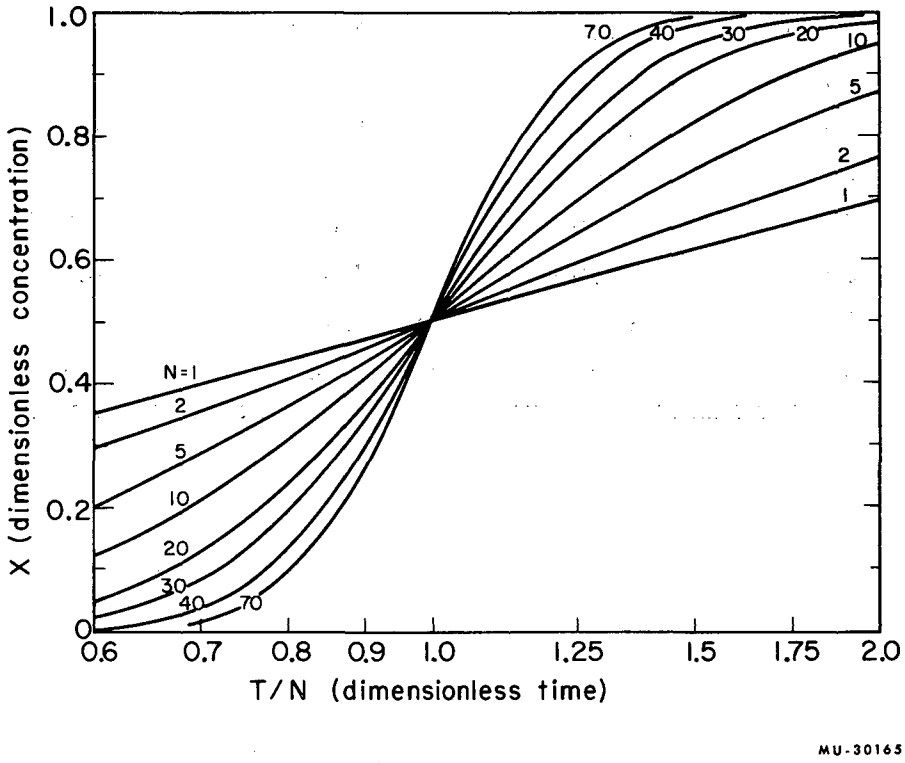

Fig. I-5. Breakthrough curves for unbounded diffusion model.

Table I-VII. Midpoint slopes for diffusion model

N	Bounded diffusion			Simple diffusion
	Θ_{50}	s	$\Theta_{50} \cdot s$	$\Theta_{50} \cdot s$
1	0.746	0.610	0.455	0.282
2	0.787	0.665	0.523	0.400
3	0.821	0.729	0.600	0.488
5	0.866	0.845	0.732	0.631
7	0.896	0.922	0.826	0.746
10	0.920	1.044	0.960	0.892
15	0.942	1.195	1.126	1.092
20	0.954	1.330	1.265	1.261
40	0.962	1.855	1.786	1.784
60	0.968	2.259	2.183	2.182
80	0.973	2.592	2.520	2.520
100	0.976	2.888	2.820	2.820

D. Random-Walk Model

The random-walk model applies to the motion of tracer molecules traveling through the column. Their path is made up of a succession of motion and rest phases, where the motion phases require negligible time compared to the rest phase. Physically, the motion phase may correspond to the narrow void channels in a packed bed, through which the liquid moves at high velocity; whereas the rest phases will then represent the wider void spaces. Diffusion, also, could be viewed as a random-walk process of individual molecules or of fluid packets, but one occurring with equal ease in the upstream and downstream directions. The distinguishing feature of the present model is that the random walk occurs in the downstream direction only.

In the derivation the fluid is considered to travel with a characteristic velocity $\bar{u}$, in a series of discrete jumps corresponding to a mean free path ℓ.[5, 23] For a column of length h, in which a particular portion of fluid has stayed for a time t, a number of mixing lengths $N = h/\ell$ and a dimensionless time scale $T' = \bar{u}t/\ell$ can be defined.

The analysis is based upon the probability of finding any one packet of fluid at N mixing lengths away from the inlet at time T', after it has taken $(n+1)$ jumps away from the inlet in its random walk; all possible paths for arriving at N at time T' are taken into account. This probability is

$$p(N, T') = \sum_{n=0}^{n=\infty} [\exp(-N-T)] \frac{N^n}{n!} \frac{T'^n}{n!} \tag{53}$$

This relation can be converted to a continuous function, which has the normalized form

$$p(N, T')dT' = [\exp(-N-T')] I_0 (2\sqrt{NT'})\, dT' . \tag{54}$$

Here I_0 is the zero-order Bessel function of the first kind with imaginary argument. If a step input of tracer is fed in continuously starting at time $\eta = 0$, the equation for the concentration at plane N is

$$X = \frac{c}{c_0} = \int_0^{T'} \exp(-N-\eta)\, I_0(2\sqrt{N\eta})\, d\eta \,, \tag{55}$$

with X increasing from zero toward unity as T' increases toward infinity. It may be noted that $X = 1-J(T', N)$, using a function J derived to describe heat and mass transfer in fixed beds.[18, 22] Two useful simplifications for Eq. (55), as developed by Klinkenberg,[27] are

$$X = 1/2\left[1 + \operatorname{erf}\left(\sqrt{T'} - \sqrt{N} - \frac{1}{8\sqrt{N'}} - \frac{1}{8\sqrt{T'}}\right)\right] \tag{56}$$

and

$$X = 1/2\left[1 + \operatorname{erf}\left(\sqrt{T' - 1/4} - \sqrt{N + 1/4}\right)\right]. \tag{57}$$

It is useful to define a time scale Θ such that, for any value of N, the stoichiometric point will occur for $\Theta = 1$. A material balance yields the result that when $t = h/U$, with U being the average linear velocity, $T' = N + 1$. The derivation of this important result is given in Appendix I-5. Through this relation, the characteristic velocity is related to the average linear velocity by the equation $\bar{u} = U(N + 1)/N$; the dimensionless time becomes $T' = (Ut/\ell) \cdot (N+1)/N$. These considerations lead to the following definition of Θ:

$$\Theta = \frac{T}{N} = \frac{T'}{N+1} \,. \tag{58}$$

Also, evidently, we have $T \equiv Ut/\ell = T'N/(N+1)$.

With these definitions, the Klinkenberg approximations become

$$X = 1/2\left[1 + \operatorname{erf}\left(\sqrt{(N+1)\Theta} - \sqrt{N} - \frac{1}{8\sqrt{N}} - \frac{1}{8\sqrt{(N+1)\Theta}}\right)\right] \tag{59}$$

and

$$X = 1/2\left\{1 + \operatorname{erf}\left[\sqrt{(N+1)\Theta - 1/4} - \sqrt{N+1/4}\right]\right\}. \tag{60}$$

Values of X for different values of Θ and N computed from Eq. (60) are given in Table I-VIII and Fig. I-6. Dimensionless slopes Θ_{50}'s are given in Table I-IX, Θ_{50} being the time when X=0.5, and s being $dX/d\Theta$ at this point.

Table I-VIII. Breakthrough concentration values (X) for the random-walk model

N	Θ=0.4	0.5	0.6	0.7	0.8	0.9	1.0	1.1	1.2	1.3	1.4	1.5	1.7	2.0
2	0.2305	0.2955	0.3596	0.4217	0.4808	0.5363	0.5880	0.6356	0.6791	0.7185	0.7540	0.7857	0.8390	0.8974
4	0.1487	0.2140	0.2845	0.3573	0.4298	0.4999	0.5661	0.6272	0.6826	0.7322	0.7758	0.8137	0.8740	0.9331
6	0.1011	0.1623	0.2345	0.3136	0.3958	0.4773	0.5551	0.6271	0.6920	0.7490	0.7980	0.8393	0.9016	0.9562
8	0.0705	0.1259	0.1970	0.2799	0.3693	0.4603	0.5482	0.6297	0.7024	0.7652	0.8180	0.8612	0.9228	0.9710
10	0.0499	0.0991	0.1676	0.2522	0.3474	0.4465	0.5434	0.6333	0.7127	0.7803	0.8356	0.8796	0.9390	0.9807
12	0.0357	0.0787	0.1437	0.2289	0.3285	0.4347	0.5398	0.6373	0.7227	0.7941	0.8512	0.8953	0.9516	0.9870
14	0.0258	0.0630	0.1240	0.2088	0.3118	0.4244	0.5370	0.6414	0.7322	0.8068	0.8651	0.9086	0.9614	0.9912
16	0.0187	0.0507	0.1075	0.1911	0.2968	0.4151	0.5347	0.6457	0.7413	0.8185	0.8774	0.9200	0.9692	0.9940
18	0.0137	0.0409	0.0936	0.1755	0.2832	0.4066	0.5328	0.6499	0.7499	0.8293	0.8884	0.9299	0.9753	0.9959
20	0.0100	0.0332	0.0817	0.1616	0.2707	0.3988	0.5311	0.6540	0.7580	0.8392	0.8982	0.9384	0.9801	0.9972
22	0.0073	0.0270	0.0715	0.1491	0.2592	0.3915	0.5297	0.6581	0.7658	0.8484	0.9071	0.9458	0.9840	0.9981
24	0.0054	0.0220	0.0627	0.1378	0.2485	0.3846	0.5285	0.6621	0.7732	0.8570	0.9150	0.9523	0.9871	0.9987
26	0.0040	0.0180	0.0551	0.1275	0.2385	0.3782	0.5274	0.6660	0.7802	0.8650	0.9222	0.9579	0.9895	0.9991
28	0.0030	0.0147	0.0485	0.1182	0.2291	0.3721	0.5264	0.6698	0.7870	0.8724	0.9288	0.9628	0.9915	0.9994
30	0.0022	0.0121	0.0427	0.1097	0.2203	0.3663	0.5255	0.6736	0.7934	0.8793	0.9347	0.9671	0.9931	0.9996
40	0.0015	0.0100	0.0231	0.0765	0.1831	0.3407	0.5222	0.6910	0.8218	0.9080	0.9572	0.9819	0.9975	0.9998
50		0.0700	0.0127	0.0543	0.1540	0.3192	0.5198	0.7067	0.8452	0.9290	0.9715	0.9899	0.9991	0.9999
60			0.0071	0.0389	0.1307	0.3006	0.5181	0.7209	0.8647	0.9448	0.9809	0.9943	0.9999	0.9999
80			0.0023	0.0205	0.0957	0.2693	0.5157	0.7459	0.8954	0.9661	0.9912	0.9982	0.9999	0.9999
100			0.0008	0.0110	0.0711	0.2435	0.5141	0.7672	0.9182	0.9788	0.9959	0.9994	0.9999	0.9999
120				0.0060	0.0535	0.2216	0.5128	0.7859	0.9355	0.9866	0.9980	0.9999	0.9999	0.9999
150				0.0025	0.0353	0.1939	0.5115	0.8099	0.9544	0.9932	0.9993	0.9999	0.9999	0.9999
200				0.0006	0.0182	0.1575	0.5100	0.8423	0.9738	0.9977	0.9999	0.9999	0.9999	0.9999

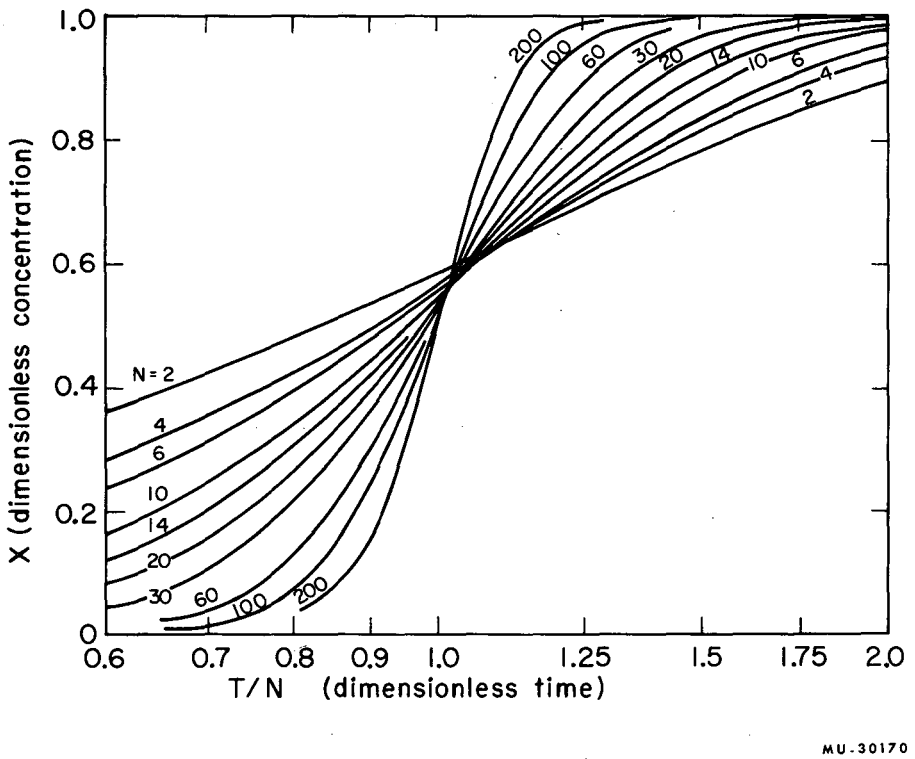

Fig. I-6. Breakthrough curves for the random-walk model.

Table I-IX. Midpoint slopes for the random-walk model

N	Θ_{50}	s	$\Theta_{50} \cdot s$
2	0.8333	0.568	0.473
3	0.8750	0.639	0.559
4	0.9000	0.695	0.626
5	0.9167	0.750	0.688
8	0.9444	0.894	0.844
10	0.9546	0.981	0.936
15	0.9688	1.164	1.128
20	0.9763	1.323	1.292
25	0.9808	1.466	1.438
30	0.9839	1.596	1.570
40	0.9878	1.832	1.810
50	0.9901	2.036	2.016

An eddy-dispersion coefficient E and a Péclet number P for the random-walk model are defined by comparison with the diffusion model:

$$E = U_0 \ell \ , \tag{61}$$

and

$$P \equiv \frac{d_p}{\ell} = \frac{d_p U_0}{E} \tag{62}$$

Consistent with this, we have $N \equiv h/\ell = Ph/d_p = hU_0/E$.

E. Mixing-Cell Model

Kramers and Alberta,[29] followed by other investigators,[1,6,7,33] proposed that the mixing effects occurring in process equipment could be described in terms of a cascade of mixing cells. In packed columns, the voids between the packing particles can be considered as unit cells for such mixing, the influent to a cell acting as a jet which sustains a mixing condition. At high Reynolds-number values, well within the turbulent-flow regime, the individual voids may each approach perfect mixing. Even if local mixing is not complete, a series of voids may be represented theoretically by a mixing cell.

In each "cell," perfect mixing is assumed to occur, such that the effluent from the cell has the same composition as the fluid at all points within the cell. For a step-function feed of a tracer solute (at concentration c_0) at the inlet to a sequence of mixing cells of equal size, the effluent from the Nth cell in the series has the dimensionless concentration

$$X_N = 1 - \left[1 + \frac{t}{\bar{t}} + \frac{1}{2!}\left(\frac{t}{\bar{t}}\right)^2 + \cdots \frac{1}{(N-1)!}\left(\frac{t}{\bar{t}}\right)^{N-1}\right] e^{-t/\bar{t}} \tag{63}$$

where $\bar{t}$ is the average residence time in the sequence.

The mixing-cell model is identical with a random-walk process in which the time for each step is variable, but the step length is fixed. The probability of encountering a tracer molecule in the outflow from the Nth cell, at a time t after it has entered the first cell, is

$$p(N, T) = \frac{e^{-T_T N}}{N!} \tag{64}$$

Integrating with respect to time, from T = 0 to T, leads to Eq. (63).

By comparing the diffusion model and the mixing-cell model, several investigators for one-phase[1, 29, 33] and two-phase studies[30, 35] have shown that the cell size in the mixing-cell model corresponds to twice the mixing length in the diffusion model. This comparison can be most easily seen by using the finite-difference form of the diffusion equation. The diffusion equation has the form

$$\frac{E}{\epsilon} \frac{\partial^2 X}{\partial z^2} - \frac{U_0}{E} \frac{\partial X}{\partial z} - \frac{\partial X}{\partial t} = 0 . \tag{65}$$

With division by U_0, and replacement of E by ℓU_0, and adoption of the finite-difference form, this becomes

$$\ell \frac{\Delta_2 X}{(\Delta z)^2} - \frac{\Delta X}{\Delta z} - \frac{\epsilon}{U_0} \frac{d X_N}{dt} = 0 , \tag{66}$$

where ΔX and $\Delta_2 X$ stand for the first and second differences, evaluated at plane N_D. We now adopt $\Delta z = 2\ell$ $(=2d_p/P)$, and obtain

$$\Delta_2 X - 2\Delta X - \frac{4\ell\epsilon}{U_0} \frac{d X_N}{dt} . \tag{67}$$

By evaluating the finite-differences over a distance of 2ℓ upstream and downstream from plane N_D, we obtain

$$(X_{N+1} + X_{N-1} - 2X_N) - (X_{N+1} - X_{N-1}) - \frac{4\ell}{U_0} \frac{d X_N}{dt} = 0, \tag{68}$$

or

$$X_{N-1} - X_N = \frac{2\ell\epsilon}{U_0} \frac{d X_N}{dt} . \tag{69}$$

The unsteady-state stirred-tank equation, without chemical reaction, can be written in the form

$$X_{N-1} - X_N = \bar{t} \frac{d X_N}{dt} , \tag{70}$$

$\bar{t}$ being the average residence time in the tank. If the unit length is 2ℓ, $\bar{t}$ becomes equal to $2\ell\epsilon/U_0$, and hence

$$X_{N-1} - X_N = \frac{2\ell}{U_0} \frac{dX_N}{dt}, \tag{71}$$

which is seen to be identical with Eq. (69). The key to this matching of the two models lies in the choice of $\Delta z = 2\ell$. Only for this particular interval will Eq. (67), the function of X_{N-1}, X_N, and X_{N+1}, reduce to a function solely of X_{N-1} and X_N. The stirred-tank equation likewise involves a function of X_{N-1} and X_N; and perhaps fortuitously, it is found to be the same function. The weak point in the match lies in the initial adoption of the finite-difference form; this is valid only if $\Delta z << h$, or hence if $N(= h/\ell)$ is large. A somewhat more explicit relation, as stated by Kramers and Alberta[29] is

$$N_c - 1 \approx \frac{U_0 h}{2E} = \frac{1}{2} \frac{h}{\ell} \tag{72}$$

where N_c is the number of mixing cells in series. Differentiation gives the relation $dN_c/dz = 1/2\ell$ [$= (1/2)\, dN_D/dz$], which is equivalent to the comparison just made. If every void in a packed bed were to be a perfect mixer, then $2\ell \approx 0.8 d_p$ and $P = 2.5$. Experimentally, $P \approx 2$ is often encountered.

Numerical results for different values of N, as given by Eq. (63), are presented in Table I-X and Fig. I-7. For comparison with other models, the dimensionless slopes for the cell model are given in Table I-XI, as computed analytically from the expression

$$\frac{dX_N}{d\Theta} = \frac{N^N}{(N-1)!} e^{-N\Theta} \Theta^{N-1}. \tag{73}$$

For large values of N, Stirling's approximation for the factorial $N! = e^{-N} N^N \sqrt{2\pi N}$ leads to

$$\frac{dX_N}{d\Theta} = \left(\frac{N}{2\pi}\right)^{1/2} e^{-N(\Theta-1)} \Theta^{(N-1)}. \tag{74}$$

Table I-X. Breakthrough concentration values (X) for the mixing cell model

N	ϑ=0.3	0.5	0.6	0.7	0.8	0.9	0.95	1.0	1.05	1.10	1.2	1.30	1.40	1.5	1.7	2.0
1	0.2592	0.3935	0.4512	0.5034	0.5507	0.5934	0.6133	0.6321	0.6501	0.6671	0.6988	0.7275	0.7534	0.7769	0.8173	0.8647
2	0.1219	0.2642	0.3374	0.4082	0.4751	0.5372	0.5663	0.5940	0.6204	0.6454	0.6916	0.7326	0.7689	0.8009	0.8532	0.9084
4	0.0338	0.1429	0.2213	0.3081	0.3975	0.4848	0.5265	0.5665	0.6046	0.6406	0.7058	0.7619	0.8094	0.8488	0.9072	0.9576
6	0.0104	0.0839	0.1559	0.2469	0.3490	0.4539	0.5050	0.5543	0.6012	0.6453	0.7241	0.7898	0.8427	0.8843	0.9401	0.9797
8	0.0033	0.0511	0.1133	0.2030	0.3127	0.4311	0.4900	0.5470	0.6014	0.6522	0.7416	0.8137	0.8693	0.9105	0.9607	0.9900
10	0.0011	0.0318	0.0839	0.1695	0.2834	0.4126	0.4782	0.5421	0.6029	0.6595	0.7576	0.8342	0.8906	0.9302	0.9739	0.9950
12	0.0004	0.0201	0.0629	0.1429	0.2588	0.3969	0.4684	0.5384	0.6050	0.6668	0.7722	0.8519	0.9080	0.9451	0.9825	0.9975
14	0.0001	0.0128	0.0475	0.1214	0.2376	0.3831	0.4599	0.5356	0.6075	0.6740	0.7857	0.8673	0.9222	0.9566	0.9882	0.9987
16	0.0000	0.0082	0.0362	0.1037	0.2190	0.3707	0.4524	0.5333	0.6102	0.6809	0.7979	0.8808	0.9341	0.9656	0.9920	0.9993
18	0.0000	0.0053	0.0277	0.0889	0.2025	0.3594	0.4456	0.5314	0.6130	0.6876	0.8093	0.8927	0.9439	0.9726	0.9945	0.9996
20	0.0000	0.0034	0.0213	0.0765	0.1878	0.3491	0.4394	0.5297	0.6157	0.6940	0.8197	0.9032	0.9522	0.9781	0.9962	0.9998
24	0.0000	0.0015	0.0127	0.0571	0.1624	0.3305	0.4283	0.5272	0.6213	0.7061	0.8385	0.9208	0.9650	0.9860	0.9982	0.9999
30	0.0000	0.0004	0.0059	0.0374	0.1321	0.3065	0.4140	0.5243	0.6293	0.7227	0.8621	0.9409	0.9779	0.9927	0.9994	0.9999
34	0.0000	0.0002	0.0036	0.0284	0.1158	0.2925	0.4055	0.5228	0.6345	0.7328	0.8755	0.9511	0.9836	0.9952	0.9997	0.9999
40	0.0000	0.0001	0.0017	0.0190	0.0956	0.2737	0.3941	0.5210	0.6419	0.7469	0.8927	0.9630	0.9894	0.9974	0.9999	0.9999
44	0.0000	0.0000	0.0011	0.0146	0.0844	0.2624	0.3871	0.5200	0.6467	0.7556	0.9026	0.9692	0.9921	0.9983	0.9999	0.9999
50	0.0000	0.0000	0.0005	0.0098	0.0703	0.2468	0.3774	0.5188	0.6535	0.7678	0.9156	0.9765	0.9949	0.9991	0.9999	0.9999
60	0.0000	0.0000	0.0002	0.0052	0.0523	0.2240	0.3629	0.5172	0.6642	0.7861	0.9331	0.9999	0.9999	0.9999	0.9999	0.9999
70	0.0000	0.0000	0.0000	0.0028	0.0392	0.2044	0.3499	0.5159	0.6741	0.8023	0.9999	0.9999	0.9999	0.9999	0.9999	0.9999

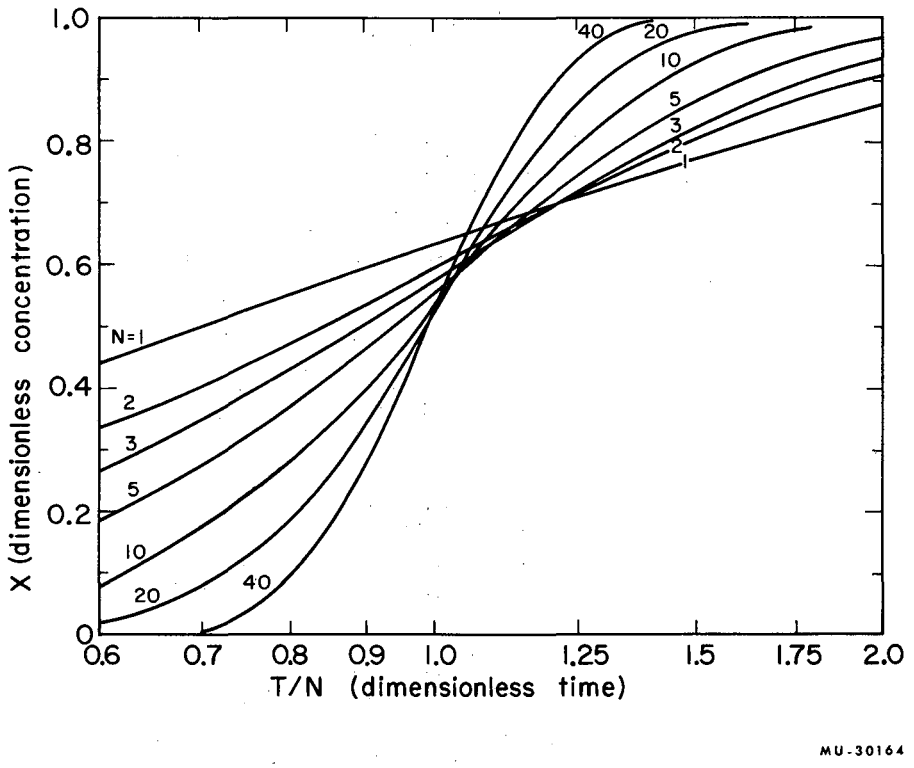

Fig. I-7. Breakthrough curves for the mixing-cell model.

Table I-XI. Midpoint slopes for the mixing-cell model

N	Θ_{50}	s	$\Theta_{50} \cdot s$
1	0.690	0.500	0.346
2	0.840	0.686	0.576
4	0.920	0.838	0.771
6	0.945	1.006	0.950
8	0.960	1.162	1.115
10	0.975	1.279	1.247
15	0.979	1.615	1.589
20	0.983	1.792	1.761
25	0.986	2.060	2.034
30	0.988	2.212	2.186
35	0.990	2.402	2.380
40	0.991	2.547	2.524

F. Relations Between the Different Models

Chemical-engineering interest in axial dispersion, up to the present, has centered upon fluid mixing in the turbulent (or nearly turbulent) flow regime. In this region, the diffusion, random-walk, and void-cell-mixing models are nearly equivalent, and all appear to give consistent descriptions of the experimental results. The analysis of liquid-liquid extraction in packed columns places new emphasis on the interpretation of longitudinal-dispersion behavior in laminar flow. From a theoretical viewpoint the void-cell mixing model cannot apply to this region, at least for liquids, owing to the fact that perfect mixing no longer is approached in each void cell. The diffusion model with finite boundary conditions and the random-walk model, as empirical treatments, may apply relatively well to all flow conditions. Clearly the segmented-laminar-flow model, with an appropriate velocity profile, is applicable only to the laminar-flow regime. For the most part, the step responses given by the different models do not coincide over their entire rise. Quantitative comparison hence has to be made at some reference condition; this is selected here as the (dimensionless) midpoint slope. A plot of dimensionless slopes for the different models, as functions of N, is given in Fig. I-8. This figure shows that, for small slopes, the use of one or the other model to analyze experimental data can easily lead to N values (or to packing Péclet numbers) differing by a factor of two.

The finite-boundary diffusion model and the random-walk have very similar midpoint-slope values. The entire breakthrough curves given by the two models have quite similar shapes, with the result that the t_{50} values for the diffusion model are only about 2% less than those for random walk. This small difference can be eliminated by use of a dimensionless midpoint slope as a comparison criterion; thus, for practical purposes, we can assume that the two models are identical.

The segmented-laminar-flow result with a quartic velocity distribution approaches the diffusion model at large values of N; in the

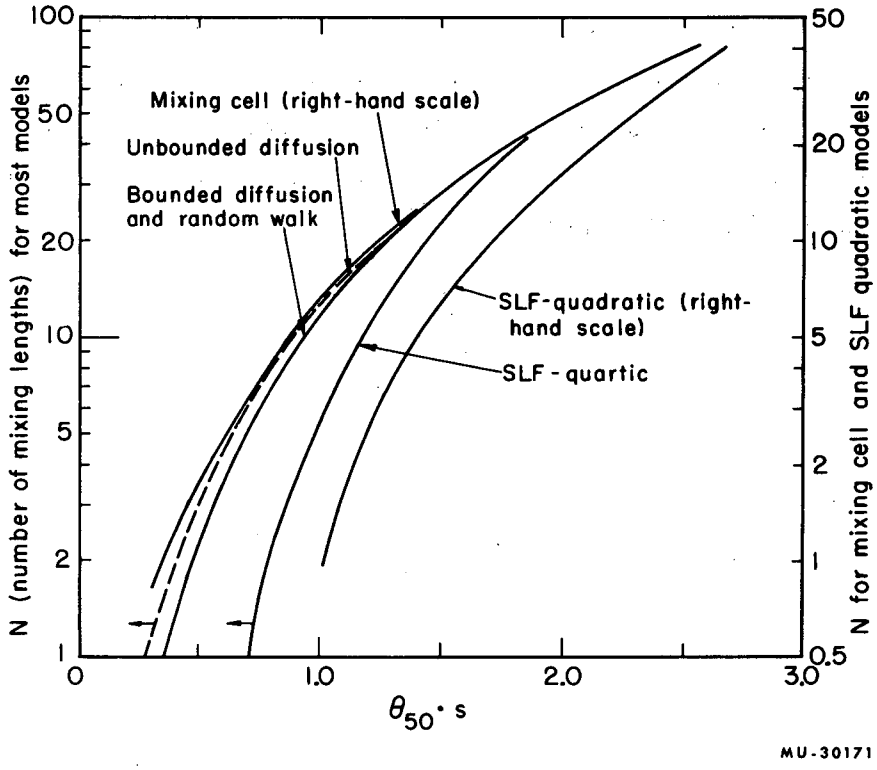

Fig. I-8. Midpoint slopes for different models.

low-N-value range, at any given N, it predicts less axial dispersion than the preceding models. The segmented-laminar-flow result with quadratic velocity profile (not recommended for use) seems to indicate that, for large N's, N_{SFP} approaches $N_D/2$.

For reference purposes only the unbounded-diffusion results are also shown, which for large N values become equivalent to the diffusion model with finite boundary conditions. The void-cell model at high N is approximately equivalent to the diffusion model (with $N_c \approx N_D/2$). At low N's it approximates the unbounded diffusion model.

In the low-N (shallow-bed) range the difference between the diffusion model and the segmented-laminar-flow model (quartic) is quite large. The proper choice between these models, for laminar flow in packed beds, must depend at present upon comparisons with experimental breakthrough curves.

G. Notation for Part I

A	Amplitude of inlet concentration wave.
B_1, B_2	Variables defined by Eqs. (38) and (39).
c	Concentration.
c_b	Flow average concentration.
c_0	Feed concentration.
c_m	Mean composition above which the concentration oscillates.
d_p	Particle diameter.
E	Longitudinal-dispersion coefficient, based on superficial velocity, $U_0 \ell$.
erf	Error function; $\frac{2}{\sqrt{\pi}} \int_0^X e^{-x^2} dx$.
erfc	Complementary error function; 1-erf X .
f	Friction factor.
$f(t)$	Dimensionless function of time.
F	Laplace transform of time-dependent functions.
h	Total height of bed.
h'	Modified height of bed = (N-1)h/N.
H	Heaviside unit function.
i	Integer.
I_0	Bessel function of zero order, with imaginary argument.
j_d	Colburn j factor, for mass transfer.
J	Function used in regenerative heat and mass transfer operations.
KG	System transfer function.
ℓ	Mixing length.
m, m'	Integers.
n	Number of random-walk jumps under consideration.
N	Number of dispersion units (mixing lengths), laminar-flow segments, or mixing cells.
N_{Re}	Reynolds number, $U_0 d_p / \nu$.
p	Probability.
P	Péclet number, d_p / ℓ.
r	Radial coordinate.

$\vec{r}$	Radius vector.
R	Total radius.
s	Slope of the breakthrough curve at X = 0.5 (based on Θ scale).
s'	Dimensionless midpoint slope (based on t/t_{50} scale).
S	Cross section.
t	Time.
t_1	Time defined by Eq. (3).
$\bar{t}$	Residence time.
T	Dimensionless time.
T'	Dimensionless time.
u	Characteristic, or local, velocity in segmented laminar-flow model.
$\bar{u}$	Characteristic velocity in random-walk.
u_{max}	Maximum velocity.
U	Interstitial velocity or mean linear velocity.
U_0	Superficial velocity; ϵU.
U_∞	Asymptotic uniform velocity of fluid past a single sphere.
V	Variable defined in Eq. (36).
W	Variable defined in Eq. (30).
X	Dimensionless concentration; c/c_0.
z	Axial distance.
Z	Dimensionless length; z/h.
α	Dimensionless time ; $\Theta/(\Theta+1)$.
δ	Time increment.
ϵ	Void-fraction.
ζ	Variable defined by Eq. (9), ($\zeta=1-r^2/R^2$); fraction of surface enclosed between r and R.
ξ	Dummy variable.
η	Dummy variable.
μ_n	Roots of transcendental equation [Eq. (45)] .
ν	Kinematic viscosity.
τ	Time, variable.
Θ	Dimensionless time T/N.

Θ_{50} Time corresponding to $X = 0.5$.

ψ Phase shift of outlet wave.

ω Angular frequency.

ω' Dimensionless frequency.

References for Part I

1. R. Aris, and N. R. Amundson, A. I. Ch. E. J. 3, 280 (1957).
2. R. B. Bird, W. E. Stewart, and E. N. Lightfoot, Transport Phenomena, 641 (John Wiley and Sons, Inc., New York, 1960), p. 297, 641.
3. Howard Brenner, Chem. Eng. Sci. 17, 229 (1962).
4. P. C. Carman, Trans. Inst. Chem. Engrs. (London) 15, 150 (1937).
5. E. J. Cairns and J. M. Prausnitz, Chem. Eng. Sci. 12, 20 (1960).
6. J. J. Carberry, A. I. Ch. E. J. 4, 13M (1958).
7. J. J. Carberry, and R. H. Bretton, A. I. Ch. E. J. 4, 367 (1958).
8. H. S. Carslaw, and J. C. Jaeger, Conduction of Heat in Solids, 1st ed. (Oxford University Press, England, 1947); 2nd ed. 114-119 (1959).
9. F. E. Crane, and G. H. F. Gardner, "Measurements of Transverse Dispersion in Granular Media," Technical Report from Gulf Research and Development Co., Pittsburgh, Pa. April 18, 1960.
10. P. V. Danckwerts, Chem. Eng. Sci. 2, 1 (1953).
11. J. F. Davidson, E. J. Cullen, D. Hanson, and D. Roberts, Trans. Inst. Chem. Engrs. (London) 37, 122 (1959).
12. H. A. Deans, A. I. Ch. E. 48th National Meeting, Preprint 7, Denver, Colorado, Aug. 26 to 29, 1962 (to be published).
13. P. F. Deisler, and R. H. Wilhelm, Ind. Eng. Chem. 45, 1219 (1953).
14. W. Eguchi, Proc. 25th Anniv. Congress, Soc. Chem. Eng. (Japan), Nov. 1961.
15. H. A. Einstein (Ph. D. Dissertation), Eidg. Techn. Hochschule, Zürich (1937).
16. B. W. Gamson, Chem. Eng. Progr. 47, 19 (1951).
17. F. H. Garner, V. G. Jenson, R. B. Keey, Trans. Inst. Chem. Engrs. 37, 191 (1959).
18. S. Goldstein, Proc. Roy. Soc. (London) A219, 151 (1953).
19. C. F. Gottschlich, A. I. Ch. E. J. 9, 88 (1963).
20. D. Harrison, M. Lane, and D. I. Walne, Trans. Inst. Chem. Engrs. 40, 214 (1962).

21. J. W. Hiby, Chem. Ing. Tech. 30, 180 (1958).
22. N. K. Hiester, and T. Vermeulen, Chem. Eng. Progr. 48, 505 (1952).
23. G. L. Jacques, and T. Vermeulen, University of California Radiation Laboratory Report UCRL-8029, 1958 (unpublished).
24. G. L. Jacques, J. E. Cotter, and T. Vermeulen, University of California Radiation Laboratory Report UCRL-8658, 1959 (unpublished).
25. M. Jakob, Heat Transfer, 1 (John Wiley and Sons, Inc., New York, 1949), p. 424.
26. G. de Josselin de Jong, Trans. Amer. Geophys. Union 39, 67 (1958).
27. A. Klinkenberg, Ind. Eng. Chem. 46, 2285 (1954).
28. V. Koump, (Ph. D. Thesis) Yale Univ., 1959 (unpublished).
29. H. Kramers and G. Alberta, Chem. Eng. Sci. 2, 173 (1953).
30. G. A. Latinen, (Ph. D. Thesis), Princeton Univ., 1954 (unpublished).
31. O. Levenspiel, and W. K. Smith, Chem. Eng. Sci. 6, 227 (1957).
32. I. I. Martin, W. W. McCabe, and C. C. Monrad, Chem. Eng. Progr. 47, 91 (1951).
33. K. W. McHenry and R. H. Wilhelm, A. I. Ch. E. J. 3, 83 (1957).
34. T. Miyauchi, University of California Radiation Laboratory Report UCRL-3911 (1957).
35. T. Miyauchi, Ind. Eng. Chem. Fundamentals 2, (1963).
36. W. E. Ranz, Chem. Eng. Progr. 48, 247 (1952).
37. P. G. Saffman, J. Fluid Mech. 6, 321 (1959); Chem. Eng. Sci. 11, 125 (1959); J. Fluid Mech. 7, 194 (1960).
38. C. A. Sleicher, A. I. Ch. E. J. 5, 145 (1959).
39. D. A. Strang, and C. J. Geankoplis, Ind. Eng. Chem. 50, 1305 (1958).
40. G. I. Taylor, Proc. Roy. Soc. (London) A219, 186 (1953); ibid A223, 446 (1954); ibid A225, 473 (1954).
41. J. F. Wehner and R. H. Wilhelm, Chem. Eng. Sci. 6, 89 (1956).
42. S. Yagi, and T. Miyauchi, Kagaku Kikai (Chem. Eng., Japan) 17, 382 (1953).

Appendixes for Part I

I-1. Analytic Integration for Columns Having One or Two Segments

For beds consisting of one or two segments, exact analytical expressions can be derived for the breakthrough curves.

A. Quadratic Velocity Profile

For N = 1, Eq. (18) can be written

$$X_1(T) = 2 \int_{\frac{1}{2T}}^{1} \left[X_0 \left(T - \frac{1}{2\zeta} \right) \right] \zeta \, d\zeta \; ; \tag{1}$$

because X_0, the inlet concentration, is unity, Eq. (1) simplifies to

$$X_1(T) = 2 \int_{\frac{1}{2T}}^{1} \zeta \, d\zeta = \left[1 - \left(\frac{1}{2T} \right)^2 \right] . \tag{2}$$

Finally, we have

$$X_1(T) = \left[1 - \left(\frac{1}{2T} \right)^2 \right] H(T-0.5) \; . \tag{3}$$

For N = 2, Eq. (18) can be written

$$X_2(T) = 2 \int_{\frac{1}{2T-1}}^{1} \left\{ 1 - \frac{1}{\left[2\left(T - \frac{1}{2\zeta} \right) \right]^2} \right\} \zeta \, d\zeta \tag{4}$$

$$= 2 \int_{\frac{1}{2T-1}}^{1} \left[\zeta - \frac{\zeta^3}{(2T\zeta - 1)^2} \right] d\zeta \; . \tag{5}$$

This integral can be solved in two parts; the first one is straightforward and leads to

$$\int_{\frac{1}{2T-1}}^{1} \zeta \, d\zeta = \frac{1}{2} - \frac{1}{2} \left(\frac{1}{2T-1} \right)^2 . \tag{6}$$

The solution to the second part is given in standard integral tables as follows:

$$\int_{\frac{1}{2T-1}}^{1} \frac{\zeta^3}{(2T\zeta-1)^2}\,d\zeta = \frac{1}{(2T)^4}\left[\frac{1}{2}(2T\zeta-1)^2 + 3(2T\zeta-1) + 3\ell n\,(2T\zeta-1) - \frac{1}{2T\zeta-1}\right]_{\frac{1}{2T-1}}^{1} \tag{7}$$

$$= \frac{1}{(2T)^4}\left[\frac{1}{2}(2T-1)^2 - \frac{1}{2}\left(\frac{1}{2T-1}\right)^2 + 4(2T-1) - \frac{4}{T-1} + 6\,\ell n(2T-1)\right], \tag{8}$$

and

$$X_2(T) = 1 - \frac{1}{(2T-1)^2} - \frac{(2T-1)^2}{(2T)^4} + \frac{1}{(2T)^4(2T-1)^2} - \frac{8(2T-1)}{(2T)^4} + \frac{8}{(2T)^4(2T-1)} - \frac{12}{(2T)^4}\,\ell n\,(2T-1)\,. \tag{9}$$

This expression can be further simplified by regrouping the following terms:

$$1 - \frac{1}{(2T-1)^2} = \frac{2T(2T-2)}{(2T-1)^2}\,,$$

$$-\frac{(2T-1)^2}{(2T)^4} + \frac{1}{(2T)^4(2T-1)^2} = -\frac{(2T-2)\left[(2T-1)^2+1\right]}{(2T)^3(2T-1)^2}\,, \tag{10}$$

and

$$-\frac{8(2T-1)}{(2T)^4} + \frac{8}{(2T)^4(2T-1)} = -\frac{8}{(2T)^3}\cdot\frac{2T-2}{(2T-1)}\,.$$

Adding these terms gives the following final form:

$$X_2(T) = \frac{2T-2}{(2T)^3(2T-1)}\left\{\left[(2T)^2+1\right](2T+1) - (2T-1) - 8\right\} - \frac{12}{(2T)^4}\,\ell n(2T-1) \tag{11}$$

or

$$X_2(T) = \left\{(2T-2)\left[\frac{(2T)^3+(2T)^2-6}{(2T)^3(2T-1)}\right] - \frac{12}{(2T)^4}\ \ell n(2T-1)\right\} H(T-1) . \qquad (12)$$

For columns of more than two segments, no exact analytical expression was found.

B. Quartic Velocity Profile

The steps in the derivation of the exact analytical expression for the quartic velocity profile are very similar to those for the quadratic distribution. For N = 1, Eq. (18a) becomes

$$X_1(T) = 3\int_{(3T)^{-1/2}}^{1}\left[X_0\left(T - \frac{1}{3\zeta^2}\right)\right]\zeta^2\, d\zeta\ ; \qquad (13)$$

with $X_0 = 1$, this equation simplifies to

$$X_1(T) = 3\int_{(3T)^{-1/2}}^{1}\zeta^2\, d\zeta = \left|\zeta^3\right|_{(3T)^{-1/2}}^{1} , \qquad (14)$$

or

$$X_1(T) = \left[1 - (3T)^{-3/2}\right]\cdot H(T-1/3) . \qquad (15)$$

For N = 2, Eq. (18a) becomes

$$X_2(T) = 3\int_{(3T-1)^{-1/2}}^{1}\left[1 - \left(3T - \frac{1}{\zeta^2}\right)^{-3/2}\right]\zeta^2\, d\zeta \qquad (16)$$

$$= 3\int_{(3T-1)^{-1/2}}^{1}\left[\zeta^2 - \frac{\zeta^5}{(3T\zeta^2-1)^{3/2}}\right] d\zeta . \qquad (17)$$

This integral will be solved in two parts; the first integral leads to

$$3\int_{(3T-1)^{-1/2}}^{1}\zeta^2 d\zeta = 1 - \left(\frac{1}{3T-1}\right)^{3/2} . \qquad (18)$$

The solution of the second integral is given in standard integral tables:

$$3\int_{(3T-1)^{-1/2}}^{1} \frac{\zeta^5}{(3T\zeta^2-1)^{3/2}}\,d\zeta = 3\int_{(3T-1)^{-1/2}}^{1} \frac{\zeta^5}{(3T)^{3/2}\left(\zeta^2-\frac{1}{3T}\right)^{3/2}}\,d\zeta \tag{19}$$

$$= \frac{1}{(3T)^3}\left[(3T\zeta^2-1)^{3/2} + 6(3T\zeta^2-1)^{1/2} - \frac{3}{(3T\zeta^2-1)^{1/2}}\right]_{(3T-1)^{-1/2}}^{1} \tag{20}$$

$$= \frac{1}{3T(3T-1)^{3/2}}\left[(3T-1)^3 + 6(3T-1)^2 - 3(3T-1)\right]$$

$$= \frac{1}{(3T)^3(3T-1)^{3/2}}\left[1 + 6(3T-1) - 3(3T-1)^2\right] \tag{21}$$

$$= \frac{(3T)^3 + 6(3T)^2 - 24(3T) + 16}{(3T)^3(3T-1)^{3/2}}\,. \tag{22}$$

Finally, we have

$$X_2(T) = \left[1 - \frac{2(3T)^3 + 6(3T)^2 - 24(3T) + 16}{(3T)^3(3T-1)^{3/2}}\right] H(T-2/3)\,. \tag{23}$$

For $N > 2$, no analytical expression for the breakthrough curve could be derived.

I-2. Numerical Solutions for Segmented Laminar Flow

A. Graphical Illustration of Method 1

Method 1 uses a complex summation scheme which can be most easily explained by a graphical illustration as follows:

The general equation of Method 1 [Eq. (34)] is

$$X_N(\tau) = 1.5 \sum_{m'=0}^{m'=m-1} [X_N(W)]_{av}(\zeta^2_{m'} + \zeta^2_{m'+1})(\zeta_{m'} - \zeta_{m+1}).$$

In the calculations based on Method 1, simple arithmetic averages were used starting with the exact analytical expression for $N = 1$ and $N = 2$.

The pattern of calculation is shown schematically in Fig. I-9. This figure is drawn for calculations from $N = 1$ to $N = 2$, with a time interval $\delta = 0.50$. The upper half of the graph shows X_{N-1} (in this case X_1) vs τ on linear coordinates. The lower half shows lines of constant $\tau_N = m\delta$, the ordinates being a logarithmic scale of $(\zeta^2)_{av}\Delta\zeta$. The calculation method involves obtaining the product of a value of X_{N-1} by a corresponding value of $(\zeta^2)_{av}\Delta\zeta$. Since a linear average of X is used, the lower part of the graph is displaced horizontally by the distance $+\delta/2$, to give an exact correspondence of abscissas (at the same m') between two points on the τ_{N-1} scale. Then for each value of m (or τ_N), the products are added together and the sum multiplied by 1.5.

A sample calculation for $\tau_2 = 2.0$ ($m = 4$, $\delta = 0.50$).

At m' = 0	$(\zeta^2)_{av}\Delta\zeta = 0.0404$	$X_{N-1} = 0.2279$	Product = 0.0092
1	= 0.0672	= 0.5511	= 0.0370
2	= 0.1274	= 0.6967	= 0.0888
3	= 0.3061	= 0.7773	= 0.2379
		Sum	= 0.3730

The resulting concentration $X_2 = 1.5 \times \text{Sum} = 0.5595$. The same procedure is repeated for all the values of m (or τ_N). The calculation is ended at an arbitrary high value, m_{max}, which is kept the same for all values of N.

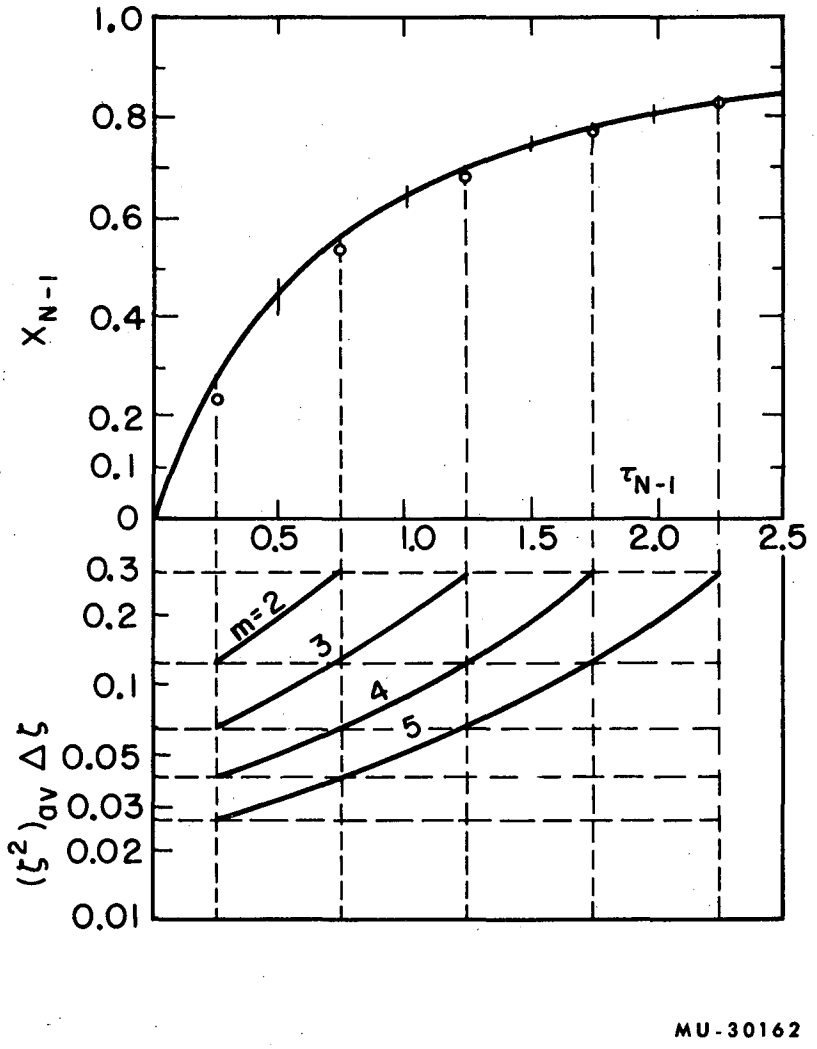

Fig. I-9. Illustration of Method 1 for numerical integration.

The true value of X_2 at $\tau_2 = 2.0$ (or $\Theta_2 = 0.667$) as given by Eq. (25a) is 0.5667. In the computer calculations, the error shown here was largely eliminated by taking $\delta = 0.25$, and by starting with the exact analytical expression for $N = 2$ which gives a less steep curve.

The X-value output from the computer was tabulated at specified values of Θ (=T/N) corresponding to particular values of τ included among those at which calculations were made.

1. Fortran Programs for Numerical Methods

The IBM-7090 Fortran programs for both velocity profiles and both methods are given in the following pages (see Table I-XII). A partial list of variable names follows; the mathematical symbols are those given in the nomenclature.

a. Variables having the same meaning in all programs

N	number of segments; N varies from 1 to NMAX
T	dimensionless time Θ
DT	time increments $\Delta\Theta$
C, C1	dimensionless concentration X
CP, CT	arrays used for printout
AR	area computed for checking purposes; AR should be close to 1.

b. Variables used in Method 1

A	corresponds to ζ^2
TAU	time variable τ
DT1	time increment δ
A1	ζ (used only in quartic distribution)

c. Variables used in Method 2

F1	time increment at which concentration values are printed out
T3	maximum time value for N = NMAX

DT11, DT12	distances separating the points used in Simpson's rule
TM1	quantity at which either DT11 or DT12 is used. If the variable is smaller than TM1, DT11 is used
TMAX 1	maximum time value for which concentration values are calculated for each N value
A	product under the integral sign of Eq. (38)
V	integration variable

Table I-XII. Fortran program for both velocity profiles and both methods.

```
      SEGMENTED LAMINAR FLOW MODEL  QUADRATIC  METHOD 1  A. HENNICO
      DIMENSION C(4000),C1(4000),A(4000),CP(1000),CT(100)
      READ IN DATA CHARACTERIZING NUMBER OF SEGMENTS,NUMBER OF TIME
      INTERVALS AND NUMBER OF PRINT OUT VALUES DESIRED
      READ INPUT TAPE 2,500,NMAX,MMAX,LMAX,DT,DT1
      DO 10 L=1,MMAX
      A(L)=1./(1.+FLOATF(L)*DT1-DT1)**2
   10 CONTINUE
      C(1)=0.
      SUM1=0.50
      EXACT EXPRESSION FOR FIRST SEGMENT
      N=1
      LMAX1=LMAX+1
      DO 20 M=2,LMAX1
      T=0.5+FLOATF(M)*DT-DT
      C(M)=1.-1./(2.*T)**2
      C1(M)=T
      SUM1=SUM1+(1.-C(M))
   20 CONTINUE
      AREA CALCULATION FOR CHECKING PURPOSES
      M1=MMAX
      SUM1=SUM1-(1.-C(M1))/2.
      AR=SUM1*DT + 0.5
      HEADINGS FOR PRINT OUT
      SET UP RESULTS FOR PRINT OUT
      DO 25 L1=1,LMAX
      M=1+L1
      CP(L1)=C(M)
      CT(L1)=C1(M)
   25 CONTINUE
      WRITE OUTPUT TAPE 3,300
      WRITE OUTPUT TAPE 3,400,(CT(L1),L1=1,LMAX)
      WRITE OUTPUT TAPE 3,600,N,(CP(L1),L1=1,LMAX),AR
      EXACT EXPRESSION FOR SECOND SEGMENT
      N=2
      C(1)=0.0
      SUM1=0.5
      DO 30 M=2,MMAX
      TAU=FLOATF(M)*DT1-DT1
      T1=(TAU+2.)/2.
      C(M)=(2.*T1-2.)*((2.*T1)**3+(2.*T1)**2-6.)/((2.*T1-1.)*(2.*T1
     1 )**3)-(12./(2.*T1)**4)*LOGF(2.*T1-1.)
      SUM1=SUM1+(1.-C(M))
   30 CONTINUE
      AREA CALCULATION FOR CHECKING PURPOSES
      M1=MMAX
      SUM1=SUM1-(1.-C(M1))/2.
      Z2=DT1/FLOATF(2*N)
      AR=SUM1*Z2 + 0.5
      SET UP RESULTS FOR PRINT OUT
      DO 55 L1=1,LMAX
      B=L1
      M=1.1+FLOATF(2*N)*B*(DT/DT1)
      CP(L1)=C(M)
   55 CONTINUE
      WRITE OUTPUT TAPE 3,600,N,(CP(L1),L1=1,LMAX),AR
      START OF NUMERICAL COMPUTATION FOR COLUMNS OF 3 OR MORE SEGMENTS
      DO 200 N=3,NMAX
      M=1
      C(M)=0.0
      SUM1=0.5
      DO 80 M=2,MMAX
```

```
      SUM=0.0
      DO 50 M1=2,M
      J=M-M1+1
      SUM=SUM+(A(J)-A(J+1))*(C(M1)+C(M1-1))/2.
   50 CONTINUE
      IF(SUM-1.)70,70,60
   60 SUM=1.0
   70 C1(M)=SUM
      SUM1=SUM1+(1.-C1(M))
   80 CONTINUE
      DO 86 M=1,MMAX
   86 C(M)=C1(M)
      AREA CALCULATION FOR CHECKING PURPOSES
      M1=MMAX
      SUM1=SUM1-(1.-C(M1))/2.
      Z2=DT1/FLOATF(2*N)
      AR=SUM1*Z2 + 0.5
      SET UP RESULTS FOR PRINT OUT
      DO 120 L1=1,LMAX
      B=L1
      M=1.1+FLOATF(2*N)*B*(DT/DT1)
      CP(L1)=C(M)
  120 CONTINUE
  200 WRITE OUTPUT TAPE 3,600,N,(CP(L1),L1=1,LMAX),AR
  300 FORMAT(1H1,40X,38HSEGMENTED LAMINAR FLOW MODEL METHOD 1 )
  400 FORMAT(2X,1HI,3X,2HT=F4.2,3X,2HT=F4.2,3X,2HT=F4.2,3X,2HT=F4.2
     1 3X,2HT=F4.2,3X,2HT=F4.2,3X,2HT=F4.2,3X,2HT=F4.2,3X,2HT=F4.2,
     2 3X,2HT=F4.2,3X,2HT=F4.2,3X,2HT=F4.2,3X,2HI=F4.2,5X,2HZ1)
  500 FORMAT(3I5,2F6.3)
  600 FORMAT(I3,1H ,12F9.6,F8.3)
      CALL EXIT
     END
```

```
      SEGMENTED LAMINAR FLOW MODEL  QUADRATIC  METHOD 2  A. HENNICO
      DIMENSION C(4000),C1(4000),A(4000),CP(1000),CT(100)
      READ IN DATA CHARACTERIZING NUMBER OF SEGMENTS,NUMBER OF TIME
      INTERVALS,NUMBER OF PRINT OUT VALUES DESIRED AND NUMBER OF POINTS
      USED IN SIMPSONS FORMULA.
      READ INPUT TAPE 2,500,NMAX,LMAX,DT,F1,T3,TM1,DT11,DT12
      EXACT EXPRESSION FOR FIRST SEGMENT
      N=1
      MAX. TIME AT WHICH CONC.VALUES ARE COMPUTED TO AVOID EXTRAPOL.
      A1=NMAX-N
      A2=N
      TMAX1=T3+(T3-0.5)*(A1/A2)
      M1=(TMAX1-0.5)/DT
      MMAX=M1+1
      C(1)=0.0
      SUM1=0.5
      DO 10 M=2,MMAX
      T=0.5+FLOATF(M)*DT-DT
      C(M)=1.-1./(2.*T)**2
      C1(M)=T
      AREA CALCULATION FOR CHECKING PURPOSES
      SUM1=SUM1+(1.-C(M))
10    CONTINUE
      M1=MMAX
      SUM1=SUM1-(1.-C(M1))/2.
      AR=SUM1*DT + 0.5
      HEADINGS FOR PRINT OUT
      SET UP RESULTS FOR PRINT OUT
      DO 30 L1=1,LMAX
      B=L1
      M=1.1+B*(F1/DT)
      CP(L1)=C(M)
      CT(L1)=C1(M)
30    CONTINUE
      WRITE OUTPUT TAPE 3,300
      WRITE OUTPUT TAPE 3,400,(CT(L1),L1=1,LMAX)
      WRITE OUTPUT TAPE 3,600,N,(CP(L1),L1=1,LMAX),AR
      EXACT EXPRESSION FOR SECOND SEGMENT
      N=2
      MAX. TIME AT WHICH CONC.VALUES ARE COMPUTED TO AVOID EXTRAPOL.
      A1=NMAX-N
      A2=N
      TMAX1=T3+(T3-0.5)*(A1/A2)
      M1=(TMAX1-0.5)/DT
      MMAX=M1+1
      C(1)=0.0
      SUM1=0.5
      DO 40 M=2,MMAX
      T=0.5+FLOATF(M)*DT-DT
      T1=2.*T
      C(M)=(2.*T1-2.)*((2.*T1)**3+(2.*T1)**2-6.)/((2.*T1-1.)*(2.*T1
     1 )**3)-(12./(2.*T1)**4)*LOGF(2.*T1-1.)
      AREA CALCULATION FOR CHECKING PURPOSES
      SUM1=SUM1+(1.-C(M))
40    CONTINUE
      M1=MMAX
      SUM1=SUM1-(1.-C(M1))/2.
      AR=SUM1*DT + 0.5
      SET UP RESULTS FOR PRINT OUT
      DO 60 L1=1,LMAX
      B=L1
      M=1.1+B*(F1/DT)
```

```
      CP(L1)=C(M)
   60 CONTINUE
      WRITE OUTPUT TAPE 3,600,N,(CP(L1),L1=1,LMAX),AR
      START OF NUMERICAL COMPUTATION FOR COLUMNS OF 3 OR MORE SEGMENTS
      DO 200 N=3,NMAX
      SUM1=0.5
      MAX. TIME AT WHICH CONC.VALUES ARE COMPUTED TO AVOID EXTRAPOL.
      A1=NMAX-N
      A2=N
      TMAX1=T3+(T3-0.5)*(A1/A2)
      M1=(TMAX1-0.5)/DT
      MMAX=M1+1
      Y=FLOATF(N)
      DO 130 M=2,MMAX
      T=0.50+FLOATF(M)*DT-DT
      IF(T-TM1) 90,90,92
   90 DT1=DT11
      GO TO 93
   92 DT1=DT12
      NUMBER OF POINTS USED IN SIMPSONS INTEGRATION FORMULA
   93 J4=((2.*T*Y-1.)/(2.*(Y-1.))-0.5)/DT1
      K1=2*J4+1
      B=((2.*T*Y-1.)/(2.*(Y-1.))-0.5)/(FLOATF(K1-1))
      VTBL=0.5
      DO 110 K=1,K1
      V=0.5+(FLOATF(K-1))*B
      CONCENTRATION VALUES COMPUTED BY INTERPOLATION ROUTINE TLUDX
      CALL TLUDX(V,VTBL,MMAX,C,F,DT)
      D=(Y-1.)/(Y*T-(Y-1.)*V)**3
      A(K)=D*F
  110 CONTINUE
      SIMPSONS FORMULA FOR INTEGRAL EVALUATION
      CALL ARSIMP(K1,B,A,R)
      SUMM=0.5*R
      IF (SUMM-1.) 125,125,120
  120 SUMM=1.0
  125 C1(M)=SUMM
      AREA CALCULATION FOR CHECKING PURPOSES
      SUM1=SUM1+(1.-C1(M))
  130 CONTINUE
      DO 135 M=1,MMAX
  135 C(M)=C1(M)
      M1=MMAX
      SUM1=SUM1-(1.-C(M1))/2.
      AR=SUM1*DT + 0.5
      SET UP RESULTS FOR PRINT OUT
      DO 140 L1=1,LMAX
      B=L1
      M=1.1+B*(F1/DT)
  140 CP(L1)=C(M)
  200 WRITE OUTPUT TAPE 3,600,N,(CP(L1),L1=1,LMAX),AR
  400 FORMAT(2X,1HI,3X,2HT=F4.2,3X,2HT=F4.2,3X,2HT=F4.2,3X,2HT=F4.2,
     1 3X,2HT=F4.2,3X,2HT=F4.2,3X,2HT=F4.2,3X,2HT=F4.2,3X,2HT=F4.2,
     2 3X,2HT=F4.2,3X,2HT=F4.2,3X,2HT=F4.2,3X,2HT=F4.2,5X,2HZ1)
  300 FORMAT(1H1,40X,38HSEGMENTED LAMINAR FLOW MODEL METHOD 2  )
  500 FORMAT(2I5,6F6.3)
  600 FORMAT(I3,1H ,12F9.6,F8.3)
      CALL EXIT
      END
      SUBROUTINE TLUDX(V,VTBL,MMAX,C,F,DT)
      SUBROUTINE TLUDX USES A LINEAR INTERPOLATION FORMULA
      DIMENSION C(4000)
```

```
      FN=MMAX
      VFIN IS THE LAST ARGUMENT FOR WHICH  INTERPOLATION IS POSSIBLE
      VFIN=VTBL+(FN-1.)*DT
      IF V IS LARGER THAN VFIN THE ROUTINE GIVES CONC.VALUE FOR VFIN
      IF V IS SMALLER THAN VTBL THE ROUTINE GIVES CONC.VALUE FOR VTBL
      IF (V-VFIN)110,125,125
  110 IF (V-VTBL)120,120,115
  115 ZEL=(V-VTBL)/DT
      L=ZEL
      ZEL1=FLOATF(L)
      PERCEN=ZEL-ZEL1
      LP=1+L
      LP1=LP+1
      THE INTERPOLATED CONC.VALUE DESIRED IS GIVEN AS F
      F=C(LP)+(PERCEN)*(C(LP1)-C(LP))
      GO TO 130
  120 F=C(1)
      GO TO 130
  125 M1=FN-1.
      L=MMAX
      F=C(L)
  130 RETURN
      END
      SIMPSONS INTEGRATION FORMULA
      SUBROUTINE ARSIMP(K1,B,A,R)
      THE NUMBER OF POINTS USED IN SIMPSONS RULE IS  COMPUTED BY
      THE MAIN PROGRAM
      THE RESULT OF THE INTEGRATION IS GIVEN AS R
      DIMENSION A(4000)
      SET=A(1)+A(K1)
      N1=K1-1
      N2=K1-2
      SUM=0.
      SUM1=0.
      DO 5 K=2,N1,2
      SUM=SUM+4.0*A(K)
    5 CONTINUE
      DO 15 K=3,N2,2
      SUM1=SUM1+2.0*A(K)
   15 CONTINUE
      R=(SET+SUM+SUM1)*B/3.0
      RETURN
      END
```

```
      SEGMENTED LAMINAR FLOW MODEL  QUARTIC  METHOD 1 ALPHONSE HENNICO
      DIMENSION C(4000),C1(4000),A(4000),A1(4000),CP(1000),CT(1000)
      READ IN DATA CHARACTERIZING NUMBER OF SEGMENTS,NUMBER OF TIME
      INTERVALS AND NUMBER OF PRINT OUT VALUES DESIRED
      READ INPUT TAPE 2,500,NMAX,MMAX,LMAX,DT,DT1
      DO 10 L=1,MMAX
      A(L)=1./(1.+FLOATF(L)*DT1-DT1)
      V=A(L)
      A1(L)=SQRTF(V)
   10 CONTINUE
      C(1)=0.
      SUM1=0.5
      EXACT EXPRESSION FOR FIRST SEGMENT
      N=1
      LMAX1=LMAX+1
      DO 20 M=2,LMAX1
      T=(1./3.)+FLOATF(M)*DT-DT
      T1=3.*T
      C(M)=1.-1./((T1)*SQRTF(T1))
      C1(M)=T
      SUM1=SUM1+(1.-C(M))
   20 CONTINUE
      AREA CALCULATION FOR CHECKING PURPOSES
      M1=LMAX1
      SUM1=SUM1-(1.-C(M1))/2.
      AR=SUM1*DT+(1./3.)
      HEADINGS FOR PRINT OUT
      SET UP RESULTS FOR PRINT OUT
      DO 25 L1=1,LMAX
      M=1+L1
      CP(L1)=C(M)
      CT(L1)=C1(M)
   25 CONTINUE
      WRITE OUTPUT TAPE 3,300
      WRITE OUTPUT TAPE 3,400,(CT(L1),L1=1,LMAX)
      WRITE OUTPUT TAPE 3,600,N,(CP(L1),L1=1,LMAX),AR
      EXACT EXPRESSION FOR SECOND SEGMENT
      N=2
      C(1)=0.
      SUM1=0.5
      DO 30 M=2,MMAX
      TAU=FLOATF(M)*DT1-DT1
      T1=TAU+2.
      C(M)=1.-(2.*(T1)**3+6.*(T1)**2-24.*T1+16.)/(((T1)**3)*(T1-1.)
     1 **1.5)
      SUM1=SUM1+(1.-C(M))
   30 CONTINUE
      AREA CALCULATION FOR CHECKING PURPOSES
      M1=MMAX
      SUM1=SUM1-(1.-C(M1))/2.
      Z2=DT1/FLOATF(3*N)
      AR=SUM1*Z2+(1./3.)
      SET UP RESULTS FOR PRINT OUT
      DO 55 L1=1,LMAX
      B=L1
      M=1.1+FLOATF(3*N)*B*(DT/DT1)
      CP(L1)=C(M)
   55 CONTINUE
      WRITE OUTPUT TAPE 3,600,N,(CP(L1),L1=1,LMAX),AR
      START OF NUMERICAL COMPUTATION FOR COLUMNS OF 3 OR MORE SEGMENTS
      DO 200 N=3,NMAX
      M=1
```

```
      C(M)=0.0
      SUM1=0.5
      DO 80 M=2,MMAX
      SUM=0.0
      DO 50 M1=2,M
      J=M-M1+1
      SUM=SUM+(A(J)+A(J+1))*(A1(J)-A1(J+1))*(C(M1)+C(M1-1))
   50 CONTINUE
      SUM=0.75*SUM
      IF(SUM-1.)70,70,60
   60 SUM=1.0
   70 C1(M)=SUM
      SUM1=SUM1+(1.-C1(M))
   80 CONTINUE
      DO 86 M=1,MMAX
   86 C(M)=C1(M)
      AREA CALCULATION FOR CHECKING PURPOSES
      M1=MMAX
      SUM1=SUM1-(1.-C(M1))/2.
      Z2=DT1/FLOATF(3*N)
      AR=SUM1*Z2 + (1./3.)
      SET UP RESULTS FOR PRINT OUT
      DO 120 L1=1,LMAX
      B=L1
      M=1.1+FLOATF(3*N)*B*(DT/DT1)
      CP(L1)=C(M)
  120 CONTINUE
  200 WRITE OUTPUT TAPE 3,600,N,(CP(L1),L1=1,LMAX),AR
  300 FORMAT(1H1,35X,46HSEGMENTED LAMINAR FLOW MODEL QUARTIC METHOD 2
     1       )
  400 FORMAT(2X,1HI,3X,2HT=F4.2,3X,2HT=F4.2,3X,2HT=F4.2,3X,2HT=F4.2,
     1 3X,2HT=F4.2,3X,2HT=F4.2,3X,2HT=F4.2,3X,2HT=F4.2,3X,2HT=F4.2,
     2 3X,2HT=F4.2,3X,2HT=F4.2,3X,2HT=F4.2,3X,2HT=F4.2,5X,2HAR)
  500 FORMAT(3I5,2F9.6)
  600 FORMAT(I3,1H ,12F9.6,F8.3)
      CALL EXIT
      END
```

```
      SEGMENTED LAMINAR FLOW MODEL  QUARTIC  METHOD 2 ALPHONSE HENNICO
      DIMENSION C(4000),C1(4000),A(4000),CP(4000),CT(100)
      INTERVALS,NUMBER OF PRINT OUT VALUES DESIRED AND NUMBER OF POINTS
      READ IN DATA CHARACTERIZING NUMBER OF SEGMENTS,NUMBER OF TIME
      USED IN SIMPSONS FORMULA.
      READ INPUT TAPE 2,500,NMAX,LMAX,DT,F1,T3,TM1,DT11,DT12
      T13=(1./3.)
      C(1)=0.
      SUM1=0.5
      EXACT EXPRESSION FOR FIRST SEGMENT
      N=1
      LMAX1=LMAX+1
      DO 20 M=2,LMAX1
      T=T13+FLOATF(M)*F1-F1
      T1=3.*T
      C(M)=1.-1./((T1)*SQRTF(T1))
      C1(M)=T
      AREA CALCULATION FOR CHECKING PURPOSES
      SUM1=SUM1+(1.-C(M))
   20 CONTINUE
      M1=LMAX1
      SUM1=SUM1-(1.-C(M1))/2.
      AR=SUM1*F1+T13
      HEADINGS FOR PRINT OUT
      SET UP RESULTS FOR PRINT OUT
      DO 25 L1=1,LMAX
      M=1+L1
      CP(L1)=C(M)
      CT(L1)=C1(M)
   25 CONTINUE
      WRITE OUTPUT TAPE 3,300
      WRITE OUTPUT TAPE 3,400,(CT(L1),L1=1,LMAX)
      WRITE OUTPUT TAPE 3,600,N,(CP(L1),L1=1,LMAX),AR
      EXACT EXPRESSION FOR SECOND SEGMENT
      N=2
      C(1)=0.
      SUM1=0.5
      MAX. TIME AT WHICH CONC.VALUES ARE COMPUTED TO AVOID EXTRAPOL.
      A1=NMAX-N
      A2=N
      TMAX1=T3+(T3-T13)*(A1/A2)
      M1=(TMAX1-T13)/DT
      MMAX=M1+1
      DO 30 M=2,MMAX
      T=T13+FLOATF(M)*DT-DT
      T1=6.*T
      C(M)=1.-(2.*(T1)**3+6.*(T1)**2-24.*T1+16.)/(((T1)**3)*(T1-1.)
     1 **1.5)
      SUM1=SUM1+(1.-C(M))
   30 CONTINUE
      M1=MMAX
      SUM1=SUM1-(1.-C(M1))/2.
      AR=SUM1*DT+T13
      SET UP RESULTS FOR PRINT OUT
      DO 60 L1=1,LMAX
      B=L1
      M=1.1+B*(F1/DT)
      CP(L1)=C(M)
   60 CONTINUE
      WRITE OUTPUT TAPE 3,600,N,(CP(L1),L1=1,LMAX),AR
      START OF NUMERICAL COMPUTATION FOR COLUMNS OF 3 OR MORE SEGMENTS
      DO 200 N=3,NMAX
```

```
      SUM1=0.5
      MAX. TIME AT WHICH CONC.VALUES ARE COMPUTED TO AVOID EXTRAPOL.
      A1=NMAX-N
      A2=N
      TMAX1=T3+(T3-T13)*(A1/A2)
      M1=(TMAX1-T13)/DT
      MMAX=M1+1
      Y=FLOATF(N)
      DO 130 M=2,MMAX
      T=T13+FLOATF(M)*DT-DT
      IF(T-TM1) 90,90,92
   90 DT1=DT11
      GO TO 93
   92 DT1=DT12
      NUMBER OF POINTS USED IN SIMPSONS INTEGRATION FORMULA
   93 J4=((3.*T*Y-1.)/(3.*(Y-1.))-T13)/DT1
      K1=2*J4+1
      B=((3.*T*Y-1.)/(3.*(Y-1.))-T13)/(FLOATF(K1-1))
      VTBL=T13
      DO 110 K=1,K1
      V=T13+(FLOATF(K-1))*B
      CONCENTRATION VALUES COMPUTED BY INTERPOLATION ROUTINE TLUDX
      CALL TLUDX(V,VTBL,MMAX,C,F,DT)
      D=(Y-1.)/(3.*Y*T-3.*(Y-1.)*V)**2.5
      A(K)=D*F
  110 CONTINUE
      SIMPSONS FORMULA FOR INTEGRAL EVALUATION
      CALL ARSIMP(K1,B,A,R)
      SUMM=4.5*R
      IF (SUMM-1.) 125,125,120
  120 SUMM=1.0
  125 C1(M)=SUMM
      AREA CALCULATION FOR CHECKING PURPOSES
      SUM1=SUM1+(1.-C1(M))
  130 CONTINUE
      DO 135 M=1,MMAX
  135 C(M)=C1(M)
      M1=MMAX
      SUM1=SUM1-(1.-C(M1))/2.
      AR=SUM1*DT + T13
      SET UP RESULTS FOR PRINT OUT
      DO 140 L1=1,LMAX
      B=L1
      M=1.1+B*(F1/DT)
  140 CP(L1)=C(M)
  200 WRITE OUTPUT TAPE 3,600,N,(CP(L1),L1=1,LMAX),AR
  300 FORMAT(1H1,35X,46HSEGMENTED LAMINAR FLOW MODEL QUARTIC METHOD 2
     1       )
  400 FORMAT(2X,1HI,3X,2HT=F4.2,3X,2HT=F4.2,3X,2HT=F4.2,3X,2HT=F4.2,
     1 3X,2HT=F4.2,3X,2HT=F4.2,3X,2HT=F4.2,3X,2HT=F4.2,3X,2HT=F4.2,
     2 3X,2HT=F4.2,3X,2HT=F4.2,3X,2HT=F4.2,5X,2HAR)
  500 FORMAT(2I5,6F9.6)
  600 FORMAT(I3,1H ,12F9.6,F8.3)
      CALL EXIT
      END
      SUBROUTINE TLUDX(V,VTBL,MMAX,C,F,DT)
      SUBROUTINE TLUDX USES A LINEAR INTERPOLATION FORMULA
      DIMENSION C(4000)
      FN=MMAX
      VFIN IS THE LAST ARGUMENT FOR WHICH  INTERPOLATION IS POSSIBLE
      VFIN=VTBL+(FN-1.)*DT
      IF V IS LARGER THAN VFIN THE ROUTINE GIVES CONC.VALUE FOR VFIN
```

```
      IF V IS SMALLER THAN VTBL THE ROUTINE GIVES CONC.VALUE FOR VTBL
      IF (V-VFIN)110,125,125
  110 IF (V-VTBL)120,120,115
  115 ZEL=(V-VTBL)/DT
      L=ZEL
      ZEL1=FLOATF(L)
      PERCEN=ZEL-ZEL1
      LP=1+L
      LP1=LP+1
      THE INTERPOLATED CONC.VALUE DESIRED IS GIVEN AS F
      F=C(LP)+(PERCEN)*(C(LP1)-C(LP))
      GO TO 130
  120 F=C(1)
      GO TO 130
  125 M1=FN-1.
      L=MMAX
      F=C(L)
  130 RETURN
      END
      SIMPSONS INTEGRATION FORMULA
      SUBROUTINE ARSIMP(K1,B,A,R)
      THE NUMBER OF POINTS USED IN SIMPSONS RULE IS COMPUTED BY
      THE MAIN PROGRAM
      THE RESULT OF THE INTEGRATION IS GIVEN AS R
      DIMENSION A(4000)
      SET=A(1)+A(K1)
      N1=K1-1
      N2=K1-2
      SUM=0.
      SUM1=0.
      DO 5 K=2,N1,2
      SUM=SUM+4.0*A(K)
    5 CONTINUE
      DO 15 K=3,N2,2
      SUM1=SUM1+2.0*A(K)
   15 CONTINUE
      R=(SET+SUM+SUM1)*B/3.0
      RETURN
      END
```

I-3. Frequency-Response Analysis for Segmented Laminar Flow (with Quadratic Velocity Distribution)

A. General

Experimental studies of packed-bed characteristics frequently involve using a sinusoidal concentration wave as the input. It is important to be able to interpret the response of a packed bed to this type of input in relation to the properties of the packed bed. We now assume that the input disturbance has the form

$$c(0,t) = c_m + A(0) \sin \omega t \ , \tag{1}$$

where c_m is the mean composition above which the concentration oscillates, $A(0)$ is the amplitude of the inlet concentration wave, and ω is the angular frequency of the oscillations. It can be shown* that the response to this sinusoidal disturbance has the form

$$c(z,t) = c_m + A(0) \left| KG(j\omega) \right| \sin (\omega t + \Psi), \tag{2}$$

where $\left| KG(j\omega) \right|$ is the absolute value of the complex transfer function $KG(j\omega)$, and Ψ is the phase shift of the outlet wave. We can calculate Ψ from the relation

$$\Psi = \tan^{-1} \left(\frac{\text{Imaginary part of } KG(j\omega)}{\text{Real part of } KG(j\omega)} \right) . \tag{3}$$

These relations show that the frequency response can be calculated from a known $KG(j\omega)$, which in turn can be obtained from the step-input response.

1. Derivation of System-Transfer Function from Step Response

From the definition of the system transfer function $KG(s)$, the following relation holds:

---

*S. B. Brown, and D. P. Campbell, Principles of Servomechanisms (John Wiley and Sons, Inc., New York 1948), p. 94.

$$F_0(s) = KG(s)\ F_i(s)\ , \tag{4}$$

where $F_i(s)$ is the Laplace transform of the input signal $f_i(t)$, and $F_0(s)$ is the Laplace transform of the output signal $f_0(t)$, the Laplace transform being by definition

$$F(s) = \int_0^\infty f(t)\ e^{-st}\ dt\ . \tag{5}$$

In this study the step input response is not known in exact analytical form; therefore, a numerical method is used. To use this method the following characteristics for the system are assumed:

(a) The system is linear.

(b) The system is at rest before the transient is applied.

(c) For a unit step function applied to the input at $t = 0$, the output approaches some constant value as t increases without limit.

When a unit step function is applied at $t = 0$, $F_i(s) = 1/s$ and $f_0(t) = h_0(t)$. The system relationship is stated as

$$F_0(s) = KG(s) \cdot F_i(s) = \frac{KG(s)}{s}\ . \tag{6}$$

The Laplace transform of the first derivative of the output with respect to time is

$$\frac{dF_0(s)}{dt} = s\ F_0(s) - h_0(t_{0+})\ . \tag{7}$$

From assumption (b), the last term is zero. Therefore, the transfer function is $KG(s) = dF_0(s)/dt$ and

$$KG(s) = \int_0^\infty \frac{dh_0(t)}{dt} \cdot e^{-st}\ dt\ . \tag{8}$$

From assumption (c), $dh_0(t)/dt$ approaches zero as t increases to ∞. The integral therefore converges if the real part of $s = s_r + j\omega$ is taken as zero (i.e., $s_r = 0$ and $s = j\omega$). Then,

$$KG(j\omega) = \int_0^\infty \frac{dh_0(t)}{dt}\ e^{-j\omega t}\ dt = \int_0^\infty e^{-j\omega t}\ d[h_0(t)]\ . \tag{9}$$

Previously, it has been shown that the system does not respond to any disturbance as long as $t \leq \tau/2$ where τ is the average residence time. Thus, one can replace the lower limit of integration by $\tau/2$ and Eq. (9) becomes

$$KG(j\omega) = \int_{\tau/2}^{\infty} \frac{dh_0(t)}{dt} \cdot e^{-j\omega t}\, dt . \qquad (10)$$

By introducing the dimensionless time $\Theta = t/\tau$ and defining a dimensionless frequency $\omega' = \tau\omega$, Eq. (10) can be written

$$KG(j\omega') = \int_{0.5}^{\infty} \frac{dh_0(\Theta)}{d\Theta} \cdot e^{-j\omega'\Theta}\, d\Theta = \int_{0.5}^{\infty} e^{-j\omega'\Theta} dh_0(\Theta) . \qquad (11)$$

This last equation is solved numerically in the following way:*† As indicated in Fig. I-10 the step response is approximated by the sum of a series of step functions of magnitude $(\Delta X_0)_1$, $(\Delta X_0)_2, \cdots (\Delta X_0)_i \cdots$ The first step function is delayed by time $\Delta\Theta/2$, the second step function is delayed by time $3\Delta\Theta/2$, the ith step function is delayed by time $(2i-1)\Delta\Theta/2$. Let $k_i = (2i-1)/2$, then for numerical calculations, Teasdale's formula can be written

$$KG(j\omega') = \sum_{i=1}^{\infty} (\Delta X_0)_i \, L - \omega' k_i \, \Delta\Theta. \qquad (12)$$

Equation (12) indicates that the phase of the output with respect to input for each component is $-\omega' k_i \Delta\Theta$ where ω' is a dimensionless frequency $(\tau\omega)$ and $k_i\Delta\Theta$ is the time delay of the nth step function component. For digital calculation the formula is rewritten as

$$KG(j\omega') = \sum_{i=1}^{\infty} (\Delta X_0)_i \cos(\omega' k_i \Delta\Theta) - j \sum_{i=1}^{\infty} (\Delta X_0)_i \sin(\omega' k_i \Delta\Theta) \qquad (13)$$

---

*W. I. Caldwell, G. A. Coon, and L. M. Zoss, Frequency Response for Process Control (McGraw-Hill Book Company, Inc., New York 1959), p. 364.

†A. R. Teasdale.Jr., Control Eng. 2, 56 (1955).

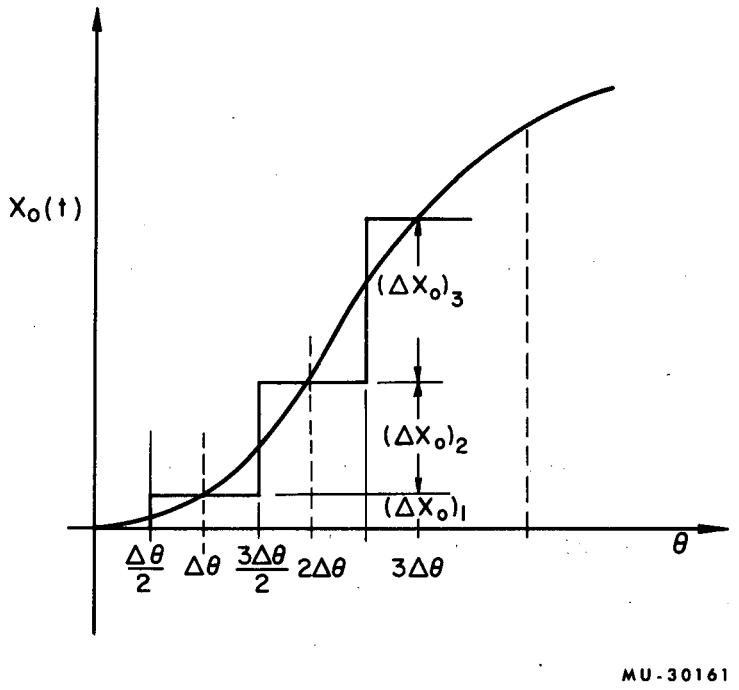

Fig. I-10. Approximation of response curve by a series of step functions.

Let

$$B_1 = \sum_{i=1}^{\infty} (\Delta X_0)_i \cos(\omega' k_i \Delta\Theta) \tag{14}$$

$$B_2 = \sum_{i=1}^{\infty} (\Delta X_0)_i \sin(\omega' k_i \Delta\Theta), \tag{15}$$

then we have

$$KG(j\omega') = B_1 - j\, B_2 \tag{16}$$

and

$$\left| KG(j\omega') \right| = (B_1^2 + B_2^2)^{1/2} . \tag{17}$$

The phase angle is

$$\psi = - \tan^{-1} (B^2/B_1) . \tag{18}$$

However, for this numerical calculation the origin has been changed from 0 to 0.5 because of the system's dead time. From process control theory it is well known* that dead time has the characteristic of a pure phase shift and that in combination with other dynamic elements the phase lag of dead time is added to obtain the total phase lag. For a dead time of $t = \tau/2$ the phase lag is $\omega\tau/2$ radians or $\omega'/2$ radians. Thus,

$$\psi = - \tan^{-1} B/A - \omega'/2 \tag{19}$$

For a column of only one segment, Eq. (11) can be solved analytically. For this special case we have

$$h_0(\Theta) = 1 - (1/2\Theta)^2, \tag{20}$$

$$\frac{dh_0(\Theta)}{d\Theta} = \frac{1}{2\Theta^3} , \tag{21}$$

and

$$KG(j\omega') = \int_{0.5}^{\infty} \frac{e^{-j\omega'\Theta}}{2\Theta^3}\, d\Theta \tag{22}$$

$$= \int_{0.5}^{\infty} \left[\frac{\cos(\omega'\Theta)}{\Theta^3} - j\, \frac{\sin(\omega'\Theta)}{\Theta^3} \right] d\Theta \tag{23}$$

---

*D. P. Eckman, Automatic Process Control (John Wiley and Sons, Inc.,) New York, 1958), p. 288.

The solution to these integrals is given in standard reference tables.

$$KG(j\omega') = \frac{e^{j\omega'/2}}{2} \left\{ \cos(\omega'/2) - (\omega'/2)\sin(\omega'/2) + (\omega'/2)^2 C_i(\omega'/2) \right.$$

$$\left. -j\left[\sin(\omega'/2) + (\omega'/2)\cos(\omega'/2) + (\omega'/2)^2 (Si(\omega'/2) - \pi/2) \right] \right\}, \quad (24)$$

where

$$Si(X) = \int_0^{\infty} \frac{\sin u}{u}\, du = \text{sine integral}$$

and

$$Ci(X) = \int_{\infty}^{X} \frac{\cos u}{u}\, du = \text{cosine integral.}$$

Numerical results, obtained by digital computer for N = 1, 2, 5, 10, and 20 are given in Table I-XIII, and plotted in Fig. I-11. For N = 1, the exact expression [Eq. (24)] for the frequency response was used; for N = 2, the computer used $(\Delta X_0)_i$ values computed by the analytical expression for the step response, whereas for other N's, the $(\Delta X_0)_i$ values were taken from graphs. For N = 2, the $\Delta\Theta$ selected was equal to 0.01; for N = 5, 10, and 20, $\Delta\Theta$ was set equal to 0.025. The results show that for columns of one and two segments the system gain is almost identical, and that for $\omega' > 3.0$ the numerical method was not accurate enough to differentiate between them.

Table I-XIII. Frequency response for segmented laminar-flow model with quadratic velocity distribution

N =	1		2		5		10		20	
ω'	$\lvert KG(j\omega)\rvert$	$-\psi_{rad}$	$\lvert KG(j\omega)\rvert$	$-\psi_{rad}$	$\lvert KG(j\omega)\rvert$	$-\psi_{rad}$	$\lvert KG(j\omega)\rvert$	$-\psi_{rad}$	$\lvert KG(j\omega)\rvert$	$-\psi_{rad}$
0.5	0.9496	0.4457	0.9601	0.4668	0.9669	0.4679	0.9796	0.4832	0.9853	0.4909
1.0	0.8779	0.8290	0.8967	0.8876	0.9353	0.9303	0.9544	0.9624	0.9671	0.9790
1.5	0.8164	1.1866	0.8346	1.2838	0.8873	1.3823	0.9157	1.4339	0.9390	1.4620
2.0	0.7571	1.5227	0.7725	1.6598	0.8289	1.8197	0.8680	1.8949	0.9038	1.9385
2.5	0.7075	1.8465	0.7171	2.0217	0.7665	2.2401	0.8157	2.3441	0.8643	2.4078
3.0	0.6606	2.1597	0.6645	2.3722	0.7057	2.6433	0.7627	2.7816	0.8227	2.8704
3.5	0.6210	2.4647	0.6178	2.7127	0.6504	3.0315	0.7117	3.2086	0.7804	3.3276
4.0	0.5836	2.7641	0.5742	3.0463	0.6019	3.4090	0.6641	3.6271	0.7382	3.7782
4.5	0.5515	3.057	0.5354	3.3719	0.5597	3.7803	0.6199	4.0393	0.6967	4.2246
5.0	0.5213	3.3470	0.4994	3.6932	0.5223	4.1490	0.5790	4.4467	0.6561	4.6666

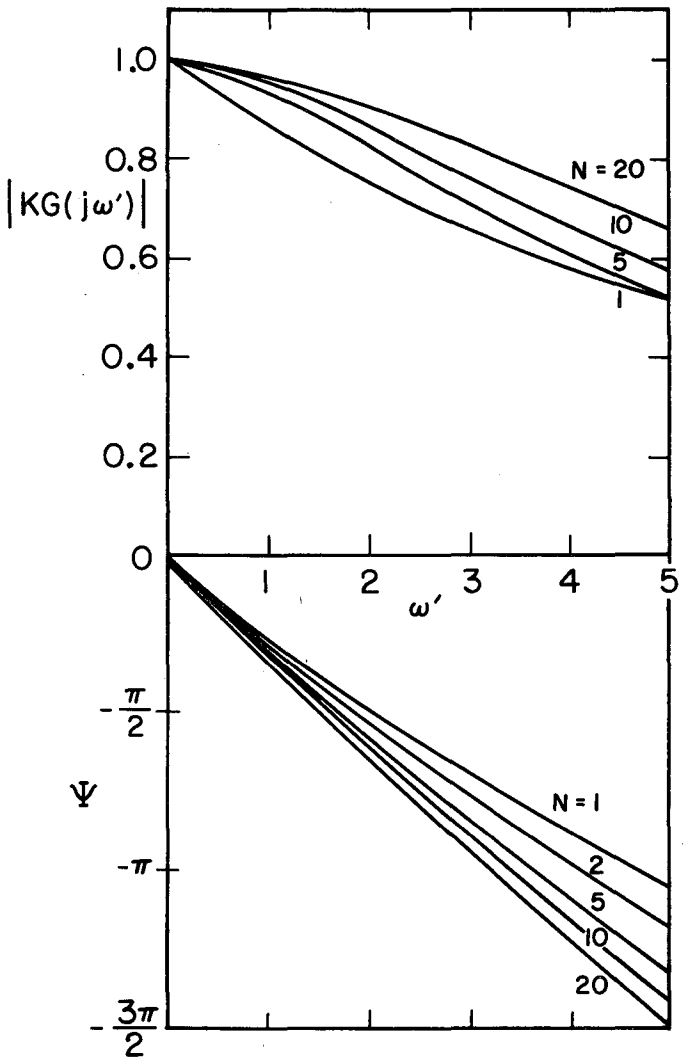

Fig. I-11. Frequency-response amplitudes and phase shifts for quadratic segmented laminar flow.

I-4. Numerical evaluation of bounded-diffusion solution

Roots of transcendental equation [Part I, Eq. (45)]

```
CARD
CARD     2*
CARD     3*      N=1
C        4*        0.960193   3.431015   6.438202   9.529614  12.645414  15.771352
CARD     5*       18.902444  22.036520  25.172465  28.309657  31.447724  34.586424
CARD     6*       37.725618  40.865170  44.005023  47.145103  50.285363  53.425790
CARD     7*      N=2
CARD     8*        1.306537   3.673192   6.584625   9.631683  12.723239  15.834101
CARD     9*       18.954971  22.081664  25.212025  28.344867  31.479434  34.615283
CARD    10*       37.752079  40.889606  44.027721  47.166291  50.305233  53.444497
CARD    11*      N=3
CARD    12*        1.542722   3.879476   6.722276   9.730673  12.799686  15.896132
CARD    13*       19.007066  22.126521  25.251405  28.379944  31.511060  34.644057
CARD    14*       37.778481  40.913994  44.050371  47.187443  50.325078  53.463169
CARD    15*      N=4
CARD    16*        1.720664   4.057513   6.851238   9.826367  12.874600  15.957335
CARD    17*       19.058670  22.171078  25.290569  28.414878  31.542567  34.672759
CARD    18*       37.804821  40.938334  44.072998  47.208571  50.344888  53.481828
CARD    19*      N=5
CARD    20*        1.861514   4.212757   6.971799   9.918597  12.947835  16.017615
CARD    21*       19.109723  22.215276  25.329506  28.449633  31.573953  34.701353
CARD    22*       37.831091  40.962614  44.095563  47.229651  50.364675  53.500463
CARD    23*      N=6
CARD    24*        1.976479   4.349257   7.084331  10.007293  13.019321  16.076926
CARD    25*       19.160188  22.259090  25.368167  28.484207  31.605196  34.729852
CARD    26*       37.857277  40.986834  44.118082  47.250696  50.384424  53.519063
CARD    27*      N=7
CARD    28*        2.072388   4.470142   7.189300  10.092416  13.088949  16.135181
CA      29*       19.209995  22.302473  25.406541  28.518566  31.636295  34.758230
CA      30*       37.883367  41.010983  44.140553  47.271704  50.404138  53.537639
CARD    31*      N=8
CARD    32*        2.153749   4.577856   7.287199  10.173969  13.156672  16.192322
CARD    33*       19.259118  22.345413  25.444602  28.552709  31.667226  34.786489
CARD    34*       37.909360  41.035047  44.162951  47.292653  50.423804  53.556178
CARD    35*      N=9
CARD    36*        2.223677   4.674377   7.378495  10.252010  13.222441  16.248324
CARD    37*       19.307522  22.387861  25.482329  28.586600  31.697966  34.814604
CARD    38*       37.935258  41.059027  44.185289  47.313541  50.443435  53.574670
CARD    39*      N=10
CARD    40*        2.284449   4.761266   7.463679  10.326612  13.286245  16.303128
CARD    41*       19.355159  22.429806  25.519696  28.620252  31.728525  34.842575
CARD    42*       37.961036  41.082923  44.207543  47.334369  50.463005  53.593126
CARD    43*      N=15
CARD    44*        2.498463   5.090553   7.813091  10.651732  13.575820  16.558547
CARD    45*       19.581122  22.631164  25.700621  28.784124  31.878065  34.979939
CARD    46*       38.087961  41.200836  44.317583  47.437494  50.560017  53.684685
CARD    47*      N=20
CARD    48*        2.627677   5.307323   8.067132  10.908709  13.819196  16.782688
CARD    49*       19.785501  22.817255  25.870438  28.939739  32.021323  35.112424
CARD    50*       38.211038  41.315645  44.425117  47.538557  50.655292  53.774795
CARD    51*      N=25
CARD    52*        2.713987   5.459595   8.257226  11.112920  14.022484  16.977268
CARD    53*       19.968188  22.987263  26.028186  29.086126  32.157404  35.239265
CARD    54*       38.329598  41.426799  44.529632  47.637115  50.748492  53.863142
CA      55*      N=30
CARD    56*        2.775646   5.571863   8.403457  11.277056  14.192480  17.145474
CARD    57*       20.130334  23.141356  26.173542  29.222794  32.285779  35.359922
CARD    58*       38.443149  41.533854  44.630754  47.732845  50.839297  53.949452
CARD    59*
CARD    60*      N=40
CARD    61*        2.857738   5.725548   8.611599  11.521114  14.456217  17.416629
CARD    62*       20.400531  23.405357  26.428375  29.466949  32.518728  35.581666
CARD    63*       38.654071  41.734481  44.821699  47.914741  51.012769  54.115098
CARD    64*      N=50
CARD    65*        2.909845   5.825329   8.751335  11.691482  14.647964  17.621595
C       66*       20.612160  23.618748  26.640040  29.674551  32.720782  35.777320
CARD    67*       38.842870  41.916282  44.996561  48.082832  51.174339  54.270437
CARD    68*      N=60
CARD    69*        2.945834   5.895125   8.850996  11.815962  14.791798  17.779559
CARD    70*       20.779591  23.791752  26.815525  29.850144  32.894733  35.948406
CARD    71*       39.010253  42.079423  45.155124  48.236673  51.323411  54.414787
CARD    72*      N=80
CARD    73*        2.992261   5.986085   8.982966  11.984185  14.990820  18.003700
CARD    74*       21.023338  24.050060  27.083960  30.124930  33.172791  36.227220
CARD    75*       39.287868  42.354341  45.426231  48.503118  51.584631  54.670387
CARD    76*      N=100
CARD    77*        3.020903   6.042651   9.066028  12.091815  15.120621  18.153035
CARD    78*       21.189463  24.230230  27.275551  30.325546  33.380214  36.439532
CARD    79*       39.503392  42.571651  45.644116  48.720607  51.800899  54.884796
```

I-5. Determination of Stoichiometric Time for the Random-Walk Model

The stoichiometric time is defined as the time necessary to fill one column volume with fluid. Usually a time scale Θ is adopted such that the stoichiometric time corresponds to $\Theta = 1$. From a material balance, this is equivalent to chosing a time scale such that the area between the breakthrough curve (X vs Θ) and the horizontal line corresponding to $X = 1$ is equal to unity.

The general equation for the random-walk model is

$$X(T', N) = \int_0^{T'} e^{-(N+\eta)} I_0 (2\sqrt{N\eta})\, d\eta \qquad (1)$$

with $X(\infty, N) = 1$. The area, mentioned above, which should be 1 is

$$S(N) = \int_0^{\infty} [1 - X(T', N)]\, dT'$$

$$= \int_0^{\infty} dT' \int_{T'}^{\infty} e^{-(N+\eta)} I_0(2\sqrt{N\eta})\, d\eta . \qquad (2)$$

Integrating by parts leads to

$$S(N) = \left[T' \int_{T'}^{\infty} e^{-(N+\eta)} I_0(2\sqrt{N\eta})\, d\eta \right]_0^{\infty} \qquad (3)$$

$$+ \int_0^{\infty} \eta\, e^{-(N+\eta)} I_0 (2\sqrt{N\eta})\, d\eta .$$

We first show that

$$\left[T' \int_{T'}^{\infty} e^{-(N+\eta)} I_0(2\sqrt{N\eta})\, d\eta \right]_0^{\infty} = 0 \qquad (4)$$

This expression can be simplified by the following change of variable:

$$\xi = 2\sqrt{N\eta}; \text{ then } \eta = \xi^2/4N, \text{ and } d\eta = (2\xi/4N)\, d\xi .$$

Equation (53) becomes

$$\left[T' \frac{e^{-N}}{2N} \int_{2\sqrt{NT'}}^{\infty} e^{-\xi^2/4N} I_0(\xi) \xi \, d\xi \right]_0^{\infty} = 0 . \qquad (5)$$

We first note that the expression under the integral is always positive and that the function $I_0(\xi)$ satisfies the inequality

$$I_0(\xi) < e^{\xi} \qquad (6)$$

for all positive values of ξ. From this, the expression between brackets clearly vanishes when $T' = 0$. To show that the same expression is zero at the upper limit, the expression will be replaced by a simpler and larger function which tends to zero when $T' \to \infty$. Using Eq. (6) we can write

$$e^{-\frac{\xi^2}{4N}} I_0(\xi) < e^{-\frac{\xi^2}{4N} + \xi} < e^{-\xi} \qquad (7)$$

for all $\xi > \xi_1$. Note that this relation holds for $\xi_1 > 8N$. Then, we have

$$\int_{2\sqrt{NT'}}^{\infty} e^{-\frac{\xi^2}{4N}} I_0(\xi) \, \xi \, d\xi < \int_{2\sqrt{NT'}}^{\infty} e^{-\xi} \, \xi \, d\xi . \qquad (8)$$

This last integral is equal to $(1 + 2\sqrt{NT'})\, e^{-2\sqrt{NT'}}$. Finally, Eq. (5) can be replaced by the dominating function

$$f = T' \frac{e^{-N}}{2N} (1 + 2\sqrt{NT'})\, e^{-2\sqrt{NT'}} , \qquad (9)$$

which tends to zero when T' tends toward ∞. As the expression between brackets in Eq. (5) is always positive and smaller than f, it also vanishes for $T' \to \infty$. Now, the area is given by

$$S(N) = \int_0^{\infty} \eta \, e^{-(N+\eta)} I_0 (2\sqrt{N\eta}) \, d\eta . \qquad (10)$$

Using the same change of variable as above, Eq. (10) becomes

$$S(N) = e^{-N} \frac{1}{2} \int_0^{\infty} \frac{\xi^2}{4N^2} e^{-\frac{\xi^2}{4N}} I_0(\xi) \xi \, d\xi \,, \tag{11}$$

or

$$S(N) = e^{-N} \frac{\partial}{\partial N} \left(\frac{1}{2} \int_0^{\infty} e^{-\frac{\xi^2}{4N}} I_0(\xi) \, \xi \, d\xi \right). \tag{12}$$

Also, Eq. (1) can be written

$$X(T', N) = \frac{e^{-N}}{2N} \int_0^{2\sqrt{NT'}} e^{-\frac{\xi^2}{4N}} I_0(\xi) \, \xi \, d\xi \,. \tag{13}$$

Since we have $X(\infty, N) = 1$ when $T' \to \infty$, we get

$$\frac{1}{2} \int_0^{\infty} e^{-\frac{\xi^2}{4N}} I_0(\xi) \, \xi \, d\xi = N \, e^N \,. \tag{14}$$

Using Eq. (14) in Eq. (12) it follows that

$$S(N) = e^{-N} \frac{\partial}{\partial N} (N \, e^N) = N+1 \,. \tag{15}$$

Thus, to normalize the breakthrough curves for the random walk model, the following time scale has to be used:

$$\Theta = T'/N+1 \tag{16}$$

With this time scale, the stoichiometric time occurs for $\Theta = 1$.

PART II. LONGITUDINAL DISPERSION IN LIQUID FLOW THROUGH ORDERED AND RANDOM PACKINGS

A. Introduction

Although the extent of axial mixing is of primary interest with respect to steady-state mass-transfer operations, it can most easily be evaluated quantitatively as a separate factor by unsteady-state tracer-injection techniques independently of mass transfer between phases. A tracer amount of a component is injected in a pattern approaching one of several kinds of idealized disturbance, and the concentration history (or "breakthrough curve") of tracer at a fixed distance downstream from the injection points is measured.

The characteristics of the experimental breakthrough or response curve may be compared with the forms predicted by a mathematical mixing model. The value of the mathematically calculated mixing parameter that gives the best fit to the experimental curve is designated as being characteristic of the experimental system.

Several different methods of analysis have been used to measure the breakthrough or response curve. These include ionization-current counting of radioactive tracers, electrical conductivity or electrode potential, and absorption of ultraviolet or visible light.

Three different forms of input disturbance are commonly used: a sinusoidal variation, a delta or pulse function, and a step function.

The frequency-response technique measures the result of a sinusoidally varying inlet concentration. When a sinusoidal concentration wave is passed through a packed bed, the wave suffers a reduction in amplitude and a phase lag which are characteristic of the longitudinal dispersion. A disadvantage of this method is that relatively complicated apparatus is required for production of the wave, and that it is very difficult to measure the phase lag.

In the pulse-wave method one determines the outlet concentration-history of an experiment in which tracer is injected over a short period of time; i.e., in the form of a unit pulse. The impulse response is also

called the residence-time distribution function (rtdf), in recognition of the fact that the normalized concentration function arising from an input pulse of identifiable (tracer) molecules gives the age distribution of all molecules passing through the system. Disadvantages of this method lie in the experimental difficulty of producing a unit pulse, and in the attendant need often encountered of having to measure extremely low concentration values on both sides of the peak.

A third method involves the response to an inlet step function. Experimentally this can be carried out by flowing a clear solution and a tracer solution successively through a fixed bed and determining exit concentration vs a function of time. Special care must be taken to obtain a sharp, uniform step function at the inlet. In the present investigation, the step input method is used. As tracer, a solution of $NaNO_3$ is injected into the system, and the breakthrough curve is measured by electrical conductivity.

1. Previous Studies

Until recently the transport of matter in the direction of flow by axial dispersion has been neglected in the study of rate processes in packed beds. Since 1953 several experimental investigations have been made to determine the nature and the magnitude of the axial dispersion mechanisms.

In one of the first studies of axial dispersion, Danckwerts presented a general discussion of residence-time distributions in pipes, packed beds, and stirred vessels.[8] He reported several measurements of axial dispersion in the flow of water through beds of 3/8-in. Raschig rings at a mean linear velocity of 0.4 cm/sec. These measurements involved the response of the system to a step change in the inlet concentration.

Using the response to a sinusoidally varying input, Kramers and Alberta investigated axial dispersion in water flowing through a column packed with 1-cm. Raschig rings at Reynolds numbers of 100 and 200.[15] Their phase-shift data yielded dispersion coefficients differing by 50 to 100% from the values based upon amplitude; the discrepancy was attributed to "trapping" in the interior of the rings.

McHenry and Wilhelm reported axial-dispersion data for gas flowing through a bed packed with 3-mm. spheres.[18] They used a sinusoidal-input signal and determined values of the axial-dispersion coefficient from the amplitude change. A value of the Péclet number (defined as $U_0 d_p/E$) equal to about 2 was found in a Reynolds-number range of from 26 to 1000.

Ebach and White reported the results of liquid-phase logitudinal-dispersion studies for beds of glass spheres, Raschig rings, Berl saddles, and Intalox saddles over a Reynolds-number range from 0.1 to 160.[9] They also investigated the influence of viscosity in a column packed with 1-mm. spheres for a flow rate corresponding to a Reynolds-number of 0.25 for water. In this flow region a change of viscosity from 0.95 to 27 cP did not influence the axial-dispersion-coefficient values; however, it does not necessarily follow that viscosity changes have no effect at higher Reynolds numbers. In comparisons between the different packings, the product of Péclet number and void-fraction was found to be nearly constant. In their experiments, both periodic and transient input signals were used, and the detection method was that of light absorption due to a dye tracer in the water stream.

Carberry and Bretton[5] employed pulse-injection techniques very similar to those of Ebach and White. They obtained dispersion coefficients at various flowrates in systems of 0.5, 1, 3, and 5-mm. spheres and 2 and 6-mm. Raschig rings, in a 1.5-in.-i.d. column. Their data consistently showed the presence of "long tails" in the output pulses; the authors suggested that the concept of "bed capacitance" would explain this phenomenon, but they did not include it in their analysis.

Jacques and Vermeulen investigated the axial dispersion during the flow of water through beds of ceramic spheres, Raschig rings, and Berl saddles.[14] The present work is a continuation of that study, and certain of those results will be included below.

Strang and Geankoplis studied axial dispersion through beds of glass beads, porous alumina spheres, and Raschig rings by the frequency-response technique, using 2-naphthol as a tracer.[24] Their

investigation, carried out over a relatively short Reynolds number range in the laminar region, gave results similar to those of Carberry and Bretton and Ebach and White.

Cairns and Prausnitz investigated longitudinal-mixing properties for a water stream flowing through a 2-in. column packed with 3.2-mm. glass spheres, over the Reynolds number range of 22 to 4500.[3] A step input was used in their experiments, with $NaNO_3$ solution as the tracer.

Besides the previously mentioned axial-dispersion studies, which are of primary importance for chemical engineers, many investigations reported in the literature have dealt with the mixing between miscible fluids in beds of sand or sandstone at very low flow rates.[1,6,21,22] For these conditions the effect of molecular diffusion becomes significant, and unstable flow behavior, resulting from density and viscosity differences, occurs. These studies, of primary interest to petroleum engineers and hydrologists, will not be discussed here.

Thus, previous investigations have resulted in many data concerning the axial mixing of liquids in packed beds. However, as pointed out by Hofmann, serious discrepancies exist between the results reported for low Reynolds numbers.[13] Further, no study of the influence of viscosity has been found in the literature for Reynolds numbers larger than 0.25.

B. Apparatus

1. General Specifications

Specifications for the experimental equipment were based upon the following objectives for single-phase breakthrough experiments:

(1) To develop the best possible experimental conditions for determining axial-dispersion coefficients. The variables to be considered were the concentration and proportion of tracer, the direction of injection (top or bottom of the column), and the sharpness of the step input. Electrolytic conductance was selected as the measure of tracer concentration.

(2) To study the influence of viscosity on the axial dispersion coefficient. Whereas the gas-phase axial dispersivity appears to remain nearly constant over a wide range of Reynolds numbers (for reasons to be discussed latter in this article), the liquid phase is believed to show a transition from a "laminar" to a "turbulent" flow regime[5, 14] coincident with changes in slope of the friction-factor and mass-transfer j-factor curves.

(3) To investigate the influence of different packing-particle types, size, and arrangements upon axial dispersion, over a range significant for predictions on industrial-scale packed-tower apparatus. Ordered arrangements of sphere packing were included so as to determine the possible occurrence of packing-orientation effects in axial dispersion, and to obtain a controlled variation of packing void-fraction.

Apparatus was designed for study over a wide range of flow rates with various sizes and types of packing, as just indicated. The experimental needs led to the following specifications:

(a) Owing to the labor involved in packing a column and in installing conductivity probes and an injection head in any chosen arrangement, a column once packed was kept intact for repeated experiments. Consequently, different column sections were designed and built, corresponding to the different packing arrangements chosen for investigation. For each column the packing was locked between retaining grids of suitable design. Table II-I lists the columns and their corresponding specifications.

(b) In order to avoid an expensive duplication of the accessories, everything except the packed column sections was a single installation, while the packed columns were interchangeable. The upper and lower column heads with their accessories (level control, pressure taps, and nozzles) were mounted permanently on the frame in a manner that permitted rapid exchange of the packed sections. A hand-wheel-operated sling supported the head for lifting or lowering, so that we could substitute any of the different column sections. Metallic flexible hoses were connected to the inlet and outlet manifolds for both the top and bottom

of the column. The packed sections (weighing approximately 100 lb.) were transported between the column frame and the storage bench by a hoist supported by an overhead rail.

(c) To meet the flow-rate requirements for one or two main phases plus a tracer stream, a complex assembly of valves, pumps, and rotameters had to be used.

(d) To provide the needed flexibility in breakthrough-curve measurements, conductivity cells in the individual columns were manifolded through switches into a plug connection; this plug was joined by a cable to a recording potentiometer through a second set of switches on the main operating panel.

2. Column Bodies

The adoption of regular as well as random packing arrangements placed many limitations upon the column design. First of all, the triangular and square arrangements chosen necessitated flat-sided columns; thus, hexagonal and octagonal columns of calculated cross section were built, in order to simulate as closely as possible a cylindrical symmetry. Considerations of corrosion resistance, minimum weight, cost, and deformation during the needed welding operation led to the choice of aluminum rather than stainless steel for the project. Specifically, 3/16-in. 61ST aluminum sheet (alloyed with 0.25% copper, 0.6% silicon, 1% magnesium, and 0.25% chromium) was used. Cylindrical columns of the same material were built for random packings. Fins were welded on the sides of each column for strengthening and to facilitate handling. Further, the design of each of the grids that locked the packing inside the column had to be selected according to the packing geometry.

The photograph in Fig. II-1 shows Column 1 (see Table II-1), before packing and before drilling for the introduction of conductivity leads and sampling tubes. The bottom grid is attached to the body; the top grid and the corresponding spacer plate are removed. There are two rings of bolts at each end; the inside rings are used for locking the grid to the body, and the outside rings to attach the column to the

Table II-I. Dimensions and packing of experimental columns

Column number	Packing	Effective diam (in.)	Equivalent diam (in.)	Arrangement	Distance between layer (in.)	Fraction of voids (%)	Column height (in.)	Useful height (in.)	Cross-sectional area(in.^{2})
1	Spheres	0.75	0.75	Tetragonal	0.53	32.0	26.9	23.6	30.3
2	Spheres	0.75	0.75	Ortho-rhombic-1	0.65	38.0	25.8	23.0	30.3
3[a]	Raschig Rings	0.25	0.22	Random	0.29	73.0	26.4	26.0	30.7
4[a]	Pellets (Tenite polyethylene)	0.25	0.23	Random	0.21	35.0	26.4	26.0	30.7
5	Spheres	0.75	0.75	Random	0.71	41.2	26.0	25.0	30.7
6	Spheres	0.75	0.75	Ortho-rhombic-2	0.75	39.5	26.3	24.0	30.6
7	Raschig rings	0.75	0.65	Random	0.88	64.8	26.3	23.6	30.7
8[a]	Intalox saddles	1.0	0.72	Random	0.96	74.0	26.4	26.0	30.7
9[b]	Berl saddles	1.0	0.76	Random	—	68.6	26.4	25.0	30.7
10[b]	Spheres	0.38	0.38	Random	0.35	42.0	26.4	25.0	30.7

[a] Packing used only by Jacques[14]

[b] Packing used only in the present investigation

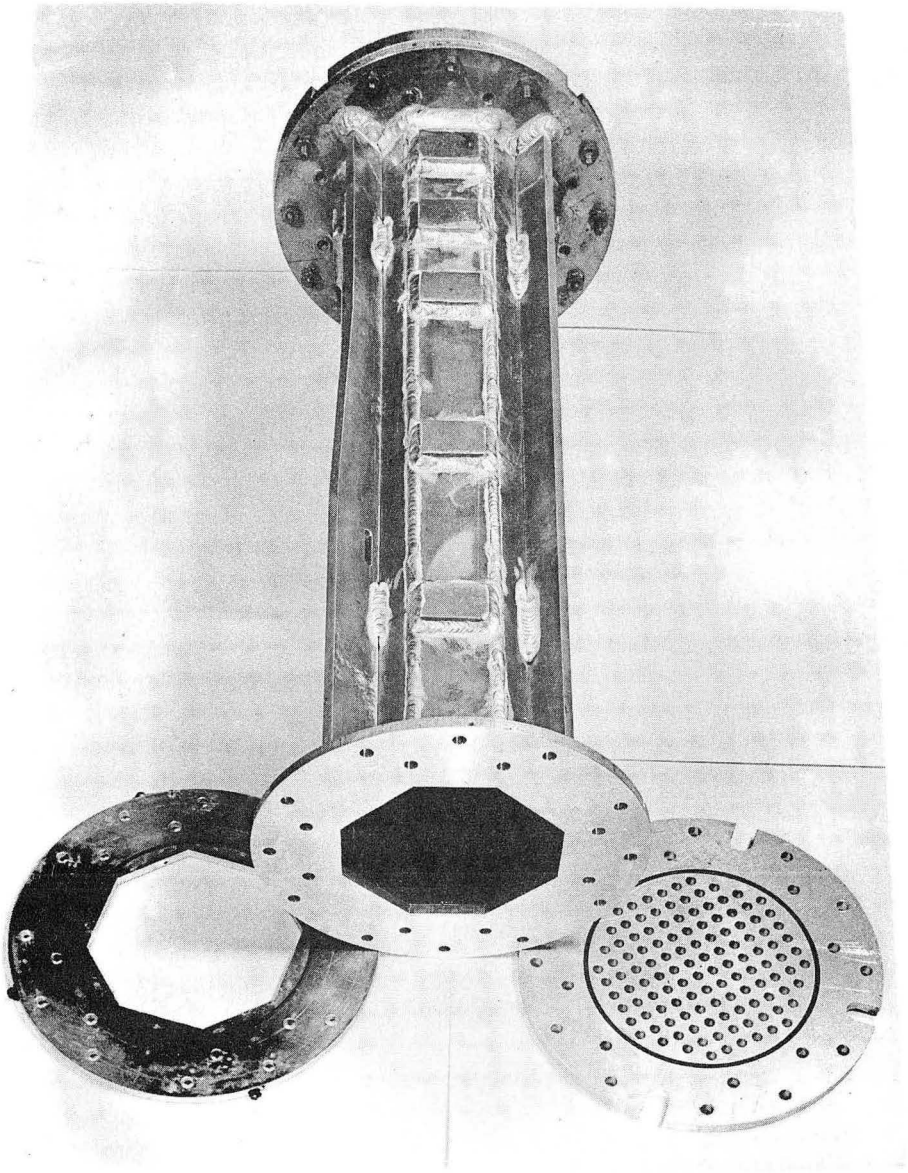

ZN-1818

Fig. II-1. Octagonal column before assembly.

permanent head and bottom; the four slots in the grid were cut out for the bolts attaching the bottom to the frame. We used O-rings to provide leakproof seals between the flanges. Finally, 3/16-in. reinforcing plates were welded on to provide needed thickness for installation of the sampling outlets. These outlets were placed at nominal distances of 0, 3, 6, 12, and 18 in. from the level of the injection manifold, the spacer plate corresponding to 24 in. The holes in the fins are for insertion of the lifting hoist.

3. Column Packing

The ordered arrangements of uniformly sized spheres correspond to known types of crystallographic lattice. For such arrangements in packed columns, one must select two parallel planes through the lattice that will represent the ends of the column, and several planes each perpendicular to these that will constitute the column walls. The different lattice structures for spheres, each available for columns in one or more orientations, have been reported by Graton and Frazer,[11] and Martin, McCabe, and Monrad.[17]

In the present investigation, three different regular packing arrangements of spheres were used: tetragonal sphenoidal (Column 1), orthorhombic-1 (Column 2) and orthorhombic-2 (Column 6). Spheres 0.75-in. in diam were obtained as over-sized ceramic balls with rough surfaces. They were wet-ground in a ball mill with granular alundum, and classified between 0.740 and 0.760 inch. Because of the geometry of the ordered packing, a boundary problem arose: as the design called for the spheres in one layer to be tangent to the wall, some of the spheres in the next layer would have to be either omitted or cut. This difficulty was avoided by insertion, in alternate layers, of spacers between the walls and the balls. Wall spacers for the second layer for Column 2 are shown in Fig. II-2. (The second layer is drawn in light lines; the first layer in heavy lines.)

Column 1, also equipped with wall spacers, was originally intended to have a rhombohedral arrangement (25.9% voids). It appears to have been packed somewhat loosely, as its measured void-fraction

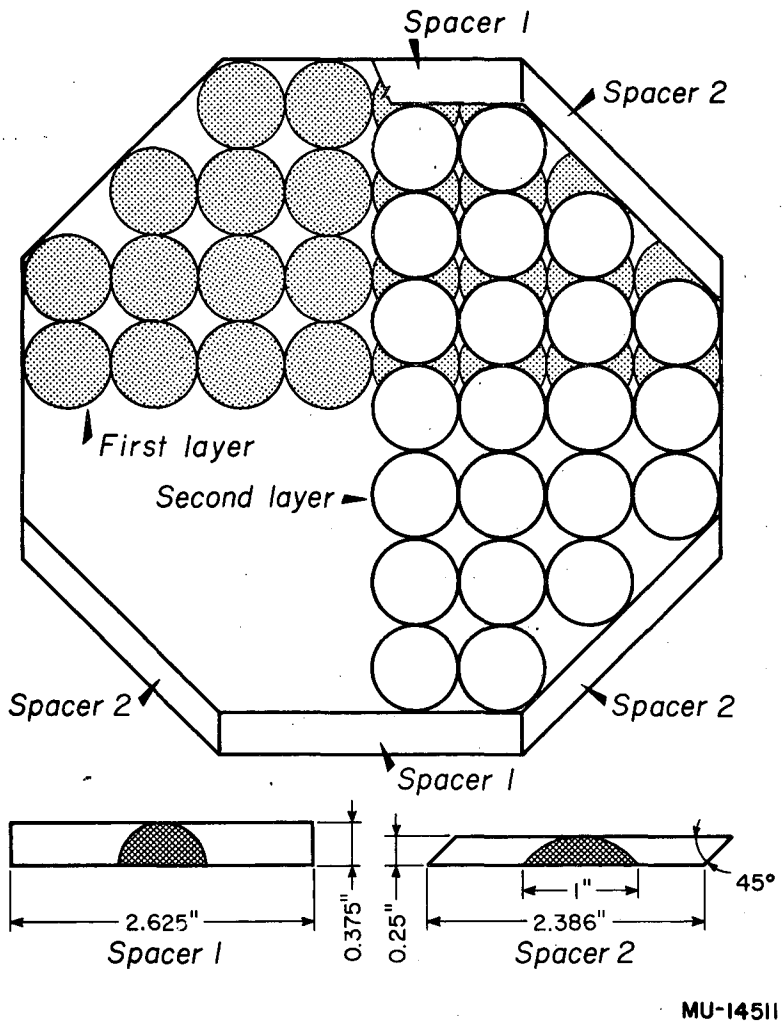

Fig. II-2. Arrangement of packing and spacers, column 2 (orthorhombic-1, octagonal).

was 32%. If this packing density is uniform, the packing corresponds to the tetragonal sphenoidal structure;[11,17] hence, this designation is used for Column 1. From Fig. II-2, we see that each sphere in the second layer is astride two in the first layer, and that these three spheres form an equilateral triangle that is perpendicular to the ends of the column. The tetragonal sphenoidal and rhombohedral structures are very similar, with each layer again in a square order, but with the equilateral triangle tilted so that the upper sphere lies more deeply in the hollow center of the square in the first layer. In the tetragonal structure, the angles of tilt (from the vertical) are 30 deg and 26 deg, 34 min; and in the rhombohedral structure, they are 30 and 30 deg.

The lattice structures of Columns 2 and 6 are identical, but the arrangement of Column 6 is perpendicular to that of Column 2. In Column 6 the triangles are parallel and the squares perpendicular to the ends of the column. Table II-I gives details on all the types and arrangements of packing used for the investigation.

The randomly packed columns were stacked by pouring the packing into the column with attendant shaking of the bed. They included not only spheres of 0.75-in. and 0.38-in. diam, but also 0.75-in. and 0.25-in. Raschig rings, 0.25-in. polyethylene pellets, and 1-in. Berl saddles and Intalox saddles.

The void fraction ϵ was measured for all packings by measuring the amount of water necessary to fill a column of known dimensions to a well specified height. The void-fraction of randomly packed spheres is generally close to that for the ordered rhombohedral arrangements. For packings other than spherical balls, several different "equivalent" diameters can be defined. The most common one is the "equivalent spherical diameter," $(d_p)_v$,[2,16] which corresponds to a sphere having the same volume as the packing unit. Pratt[20] introduced the "equivalent hydraulic diameter of the void space," $(d_p)_h$, as

$$(d_p)_h = \frac{4 \times \text{free space}}{\text{periphery}} = \frac{4\epsilon}{p} \quad . \qquad (1)$$

In the case of a stacked ring packing the periphery (ft/ft^2) is identical with the superficial area (excluding edges) expressed as ft^2/ft^3. The determination of the periphery of random packing is much more difficult; thus, it has been convenient to adopt empirically the same definition for the periphery as that just stated for regular packings. A third definition is the diameter of a sphere with the same surface-to-volume ratio as a packing particle.[19] From the properties of a sphere this diameter is defined as

$$(d_p)_a = \frac{6(1-\epsilon)}{a_p}, \qquad (2)$$

where a_p is the surface area per unit volume.

Another property of packed beds is the sphericity (ψ) of the particle. This is defined as the area of a sphere having the same volume as the particle, divided by the area of the particle. We note that $(d_p)_a = \psi(d_p)_v$.

The values used for the above mentioned parameters in this study are given in Table II-II.

4. Conductivity Probes

The tracer used was a sodium nitrate solution, with tap water was used as the main stream; the detection method was that of electrical conductivity. In the concentration range used, the electrical conductance of the aqueous salt solution was proportional to the concentration of the salt. Therefore a knowledge of the conductance of the mixed stream containing the salt tracer allows the direct determination of the concentration behavior in this stream.

The probes used to measure conductivity were constructed of two spherical sectors of 3/4-in. Bakelite balls connected by a pair of rhodium-plated pins, as shown in Fig. II-3. They were installed at different heights in the column (nominal 0, 3, 6, 12, 18 and 24 in.) with the plane of the probe being in each case perpendicular to the main direction of the fluid flow. Originally the equipment was also used for

Table II-II. Packing characteristics

Packing	ϵ	$(d_p)_v$ (in.)	$(d_p)_h$ (in.)	$(d_p)_a$ (in.)	a_p (ft^2/ft^3)	p (ft/ft^2)	ψ
3/4-in. Raschig rings	0.648	0.67	0.47	0.28	80	66	0.42
1-in. Berl saddles	0.686	0.76	0.42	0.25	78	77	0.33
1/4-in. Raschig rings	0.720	0.22	0.16	0.079	240	216	0.36
1-in. Intalox saddles	0.740	0.70	0.40	0.24	78	89	0.34

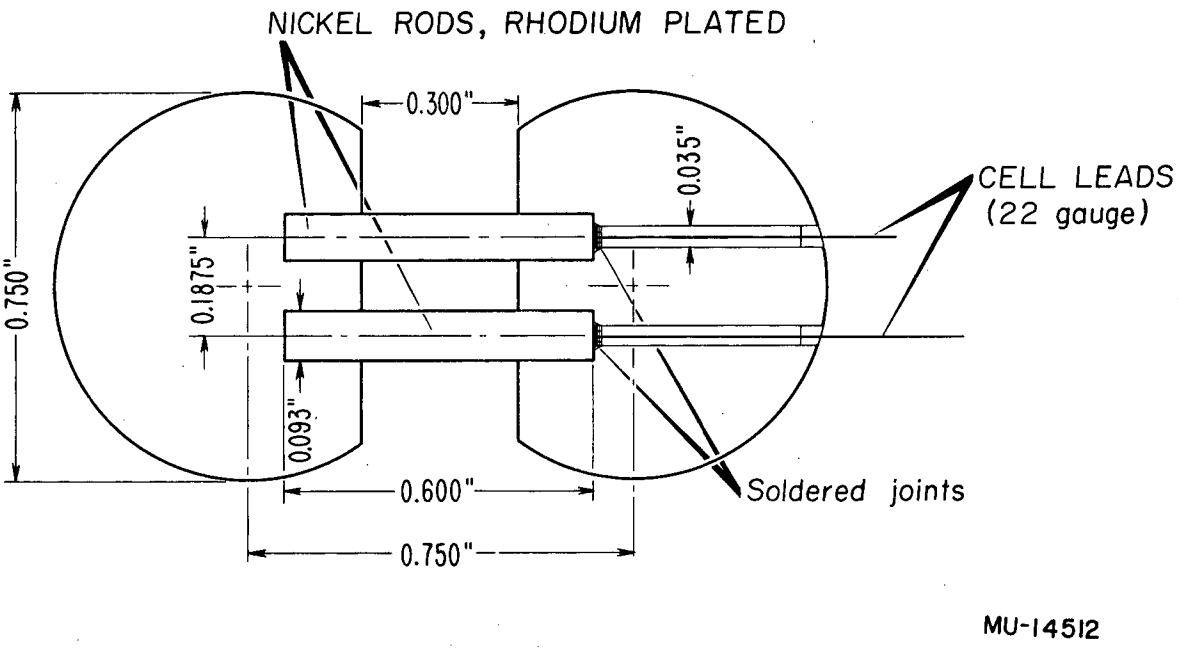

Fig. II-3. Construction of conductivity cell.

the study of radial dispersion, and thus several conductivity probes were installed at different radial positions.[14] In the present investigation, only longitudinal dispersion was studied, and only the conductivity probes at the center of the cross-section were selected for use.

5. Injector System

The injection device consisted of several tubes (0.0625-in. o. d., 0.031-in. i. d.) connected to a manifold. At the end of each injection tube an aluminum ball, 3/4-in. in diam, was fixed. For the central injector, the aluminum ball had 6 holes (0.059-in. diam) drilled, 60 deg apart, around a horizontal circle (perpendicular to the injection tube, here vertical). The arrangement and the number of injection tubes was dependent on the form of the cross-section; however, the number was normally around 8. The end of each off-center injector were anchored in the bed by being run through a 3/4-in. aluminum sphere. In Column 7, each such aluminum sphere was provided with six outlets.

A small pump continuously recirculated the tracer solution. A 3-way solenoid valve installed near the column allowed a very rapid action for either starting or stopping the flow of the injectant (tracer) into the test section. The pressure drops in the injection path and in the recirculation path were equalized by means of valves in each line adjacent to the solenoid valve.

6. Column Heads

Expanded end sections, identical in construction, were connected above and below the particular packed section in use (see Fig. II-4). As the columns were designed to operate in upward as well as in downward flow (see Figs. II-4 and 5), the same accessories were adopted for both upper and lower end sections: two windows for visual observation, a 6-in. -diam inlet nozzle with interchangeable orifice plates designed to give a velocity profile as flat as possible (see Fig. II-6), two symmetrically placed outlets, and a liquid-level control probe for subsequent two-phase experiments.

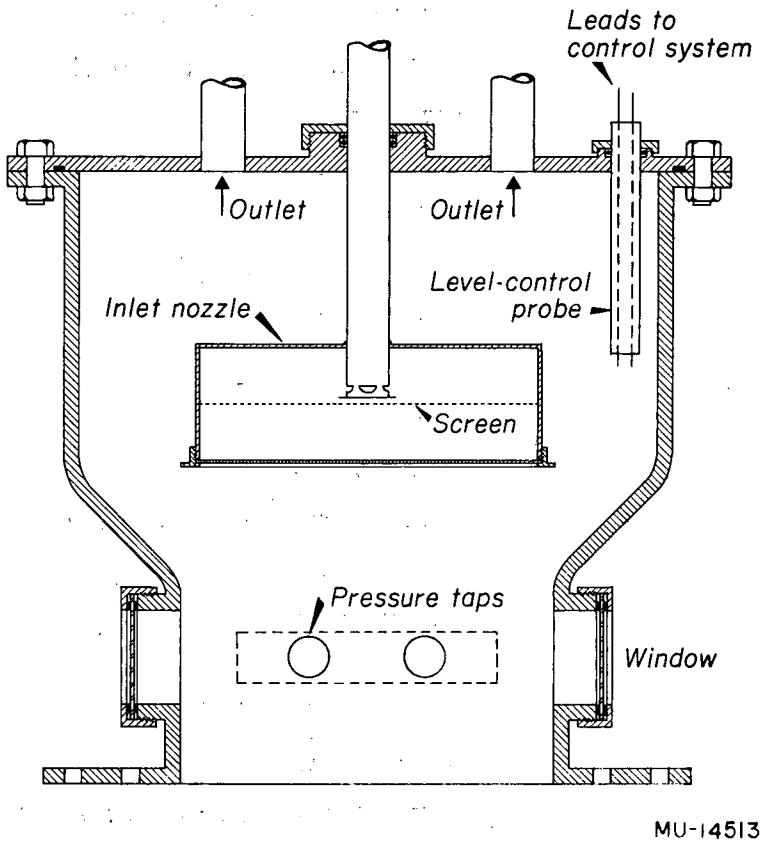

Fig. II-4. Diagram of column head.

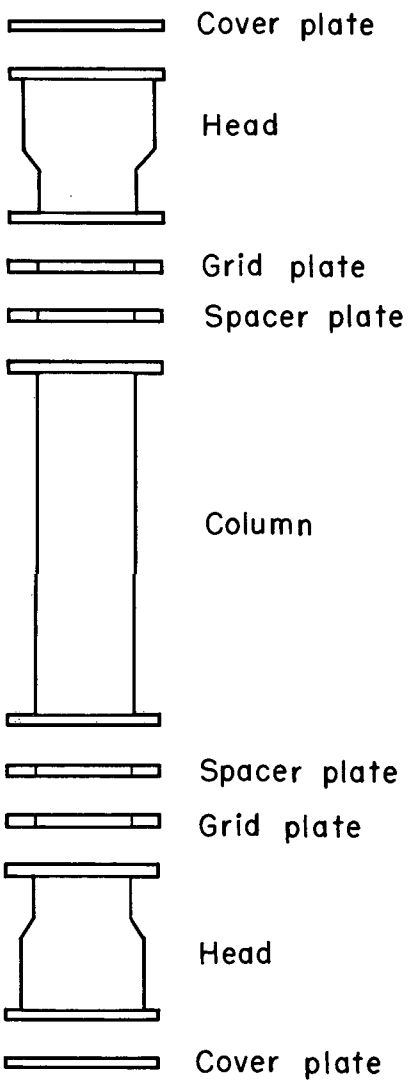

Fig. II-5. Exploded diagram of column assembly.

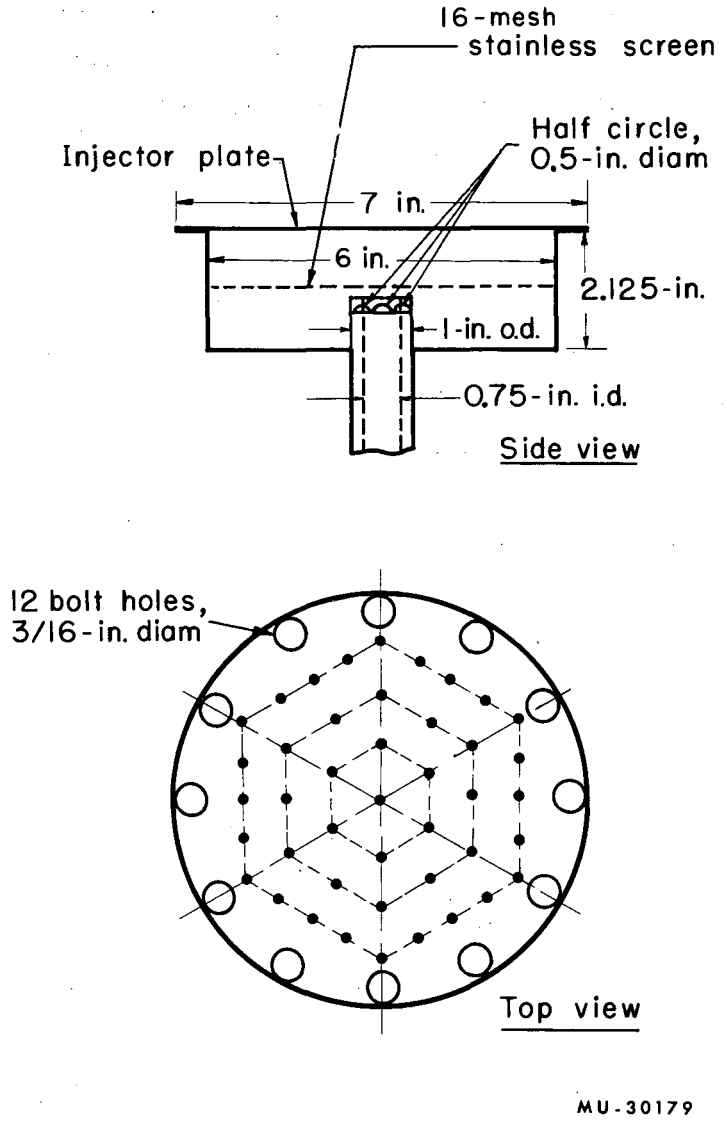

Fig. II-6. Detail of nozzle construction.

7. Circuitry

The basic electronic circuit used to measure the conductivity is shown in Figs. II-7, II-8, and II-9. It consists of four parts: an amplitude-stable oscillator, a low-impedance voltage source, an amplifier, and a self-balancing potentiometer which feeds the strip-chart recorder.

The 1000-cycle oscillator circuit employed (V_1, V_2) is of bridge "T" type, with thermal nonlinear-element stabilization. Negative feedback is supplied from the output of the grid of V_1 through the frequency determining network. The lamp and 600-Ω cathode resistor of V_1 form a variable positive-feedback path.

The output of the oscillator is fed into a power amplifier consisting of a cathode-coupled phase-inverter (V_3, V_5) driving a push-pull output stage (V_4, V_6). Power is delivered to the probes through an output transformer with a nominal output impedance of 4-Ω. A large amount of negative feedback is employed to reduce the output impedance further. In series with the probe is a resistor (R25) across which a voltage is developed that is proportional to the current drawn by the probe and thus also proportional to the conductance of the probe. This voltage is amplified (V_7, V_8) and transformer-coupled from a cathode-follower (V_9) to the detector (V_{10}). The detector output is fed to the recorder through a high impedance (R41). Through the use of manual potentiometric span control on the input to the recorder, and of gain controls in the cathode circuit of tube V7, a range of conductance from 10^{-5} to 10^{-1} mho can be monitored.

A panel board for wiring was attached to each column body, as shown in Fig. II-10. All the conductivity-cell leads of the column were connected to a rotary switch on the panel, corresponding to up to five combinations of six electrodes. The injection-tube manifold installed on the panel is also shown in Fig. II-10. Six double-pole double-throw switches on the column panel allowed the selection of any cell for measurement. Finally, an eight-wire-cable plug on the panel board provided a separate connection to the electronic measuring and recording system.

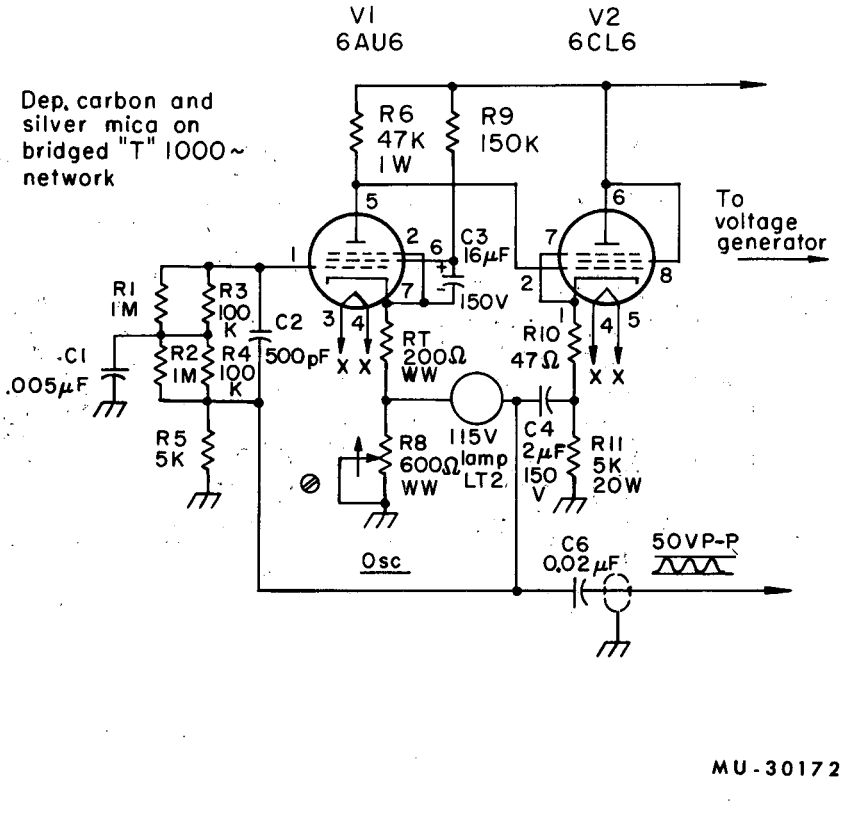

Fig. II-7. Oscillator circuit for conductance measurement.

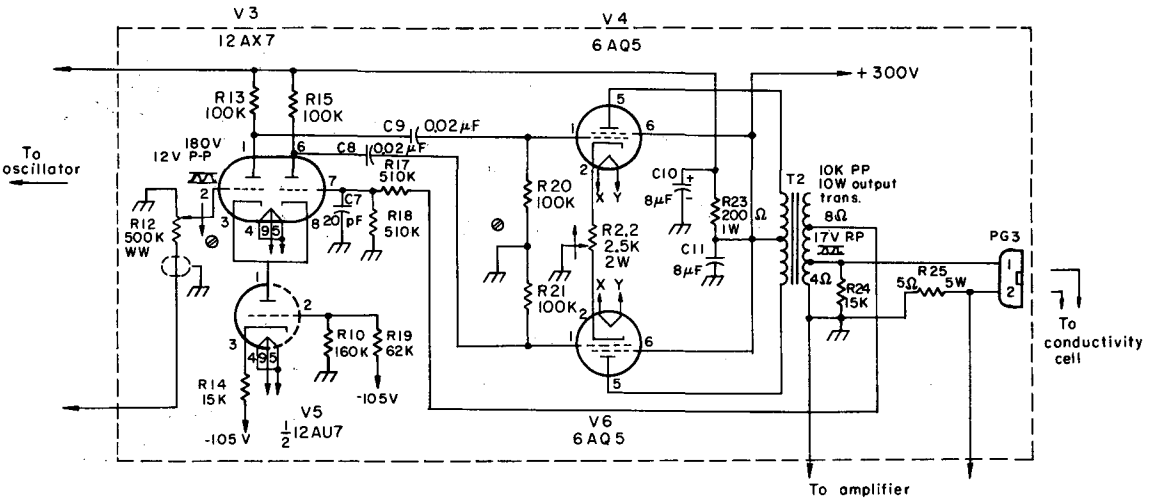

Fig. II-8. Voltage-generator circuit for conductance measurement.

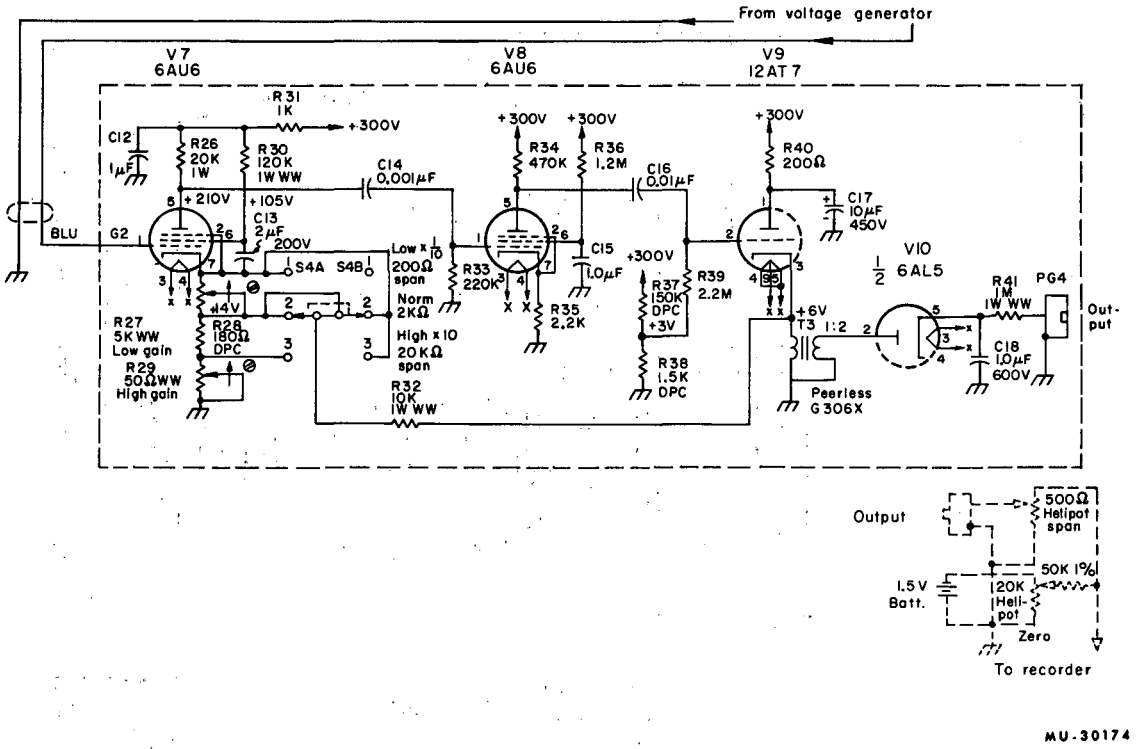

Fig. II-9. Amplifier circuit for conductance measurement.

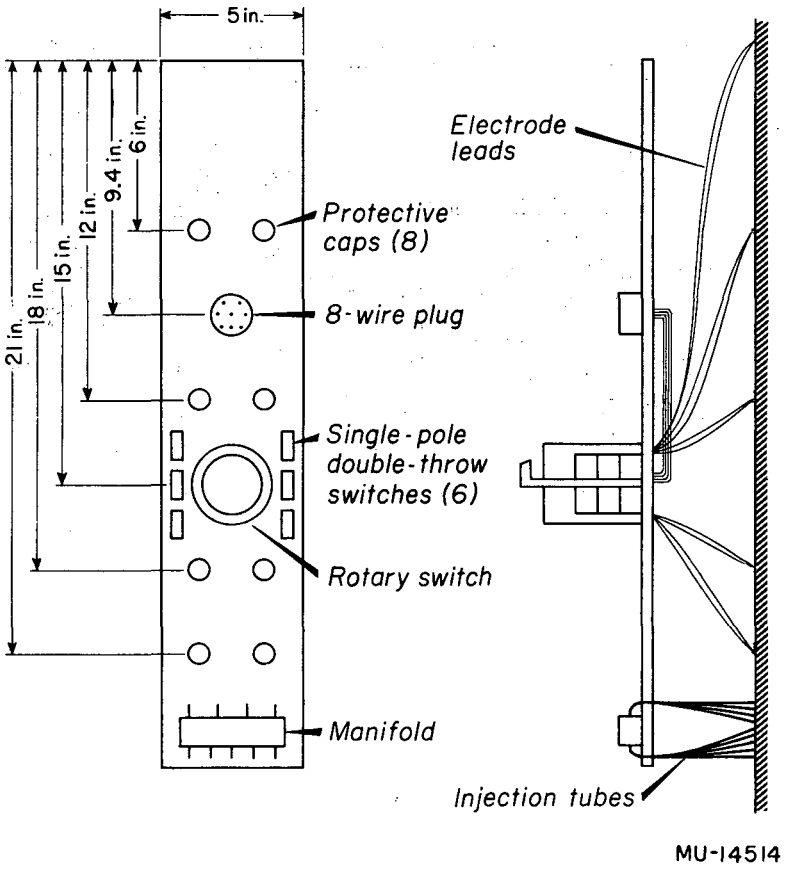

Fig. II-10. Design of metering panel for column section.

8. Layout and Accessories

As noted in the specifications, the design and construction of a complete pilot-plant unit with extensive manifolding was needed. The flow arrangement is shown in Fig. II-11, and the completed assembly in Figs. II-12 and II-13. A set of five pumps, five tanks, and six rotameters made it possible to feed and meter three different types of liquids at the same time for a range of 0.005 gpm to 40 gpm.

Water for the experiments was provided from a 150-gal constant-head tank mounted on the roof of the building, about 25 ft above the column.

The rotameters were each calibrated by weight-flow of water. Flow rates for kerosene were corrected by assuming that equal-weight flow rates gave equal readings, and by using standard correction charts supplied by the Fischer-Porter Company. The working ranges of water flow through the six rotameters were 0 to 40 gpm, 0 to 6 gpm, 0 to 6 gpm, 0 to 0.8 gpm, 0 to 0.3 gpm, and 0 to 0.005 gpm.

C. Experimental Measurements

1. Determination of Optimum Conditions

The equipment as designed allowed the injection of tracer solution at the top or at the bottom of the column. Theoretically, the same result should be obtained for either injection or shut-off of the tracer for either end of the column; however, it was found experimentally that for low flowrates large differences in behavior could occur. It thus became necessary to find experimentally the operating conditions that would minimize these differences. The smoothness of the breakthrough curve, and the proper correspondence between the calculated and measured stoichiometric times determined in two different ways (that is, by dividing the measured flowrate into the column void volume, and by integrating the experimental breakthrough curve) were also used as criteria for satisfactory operation.

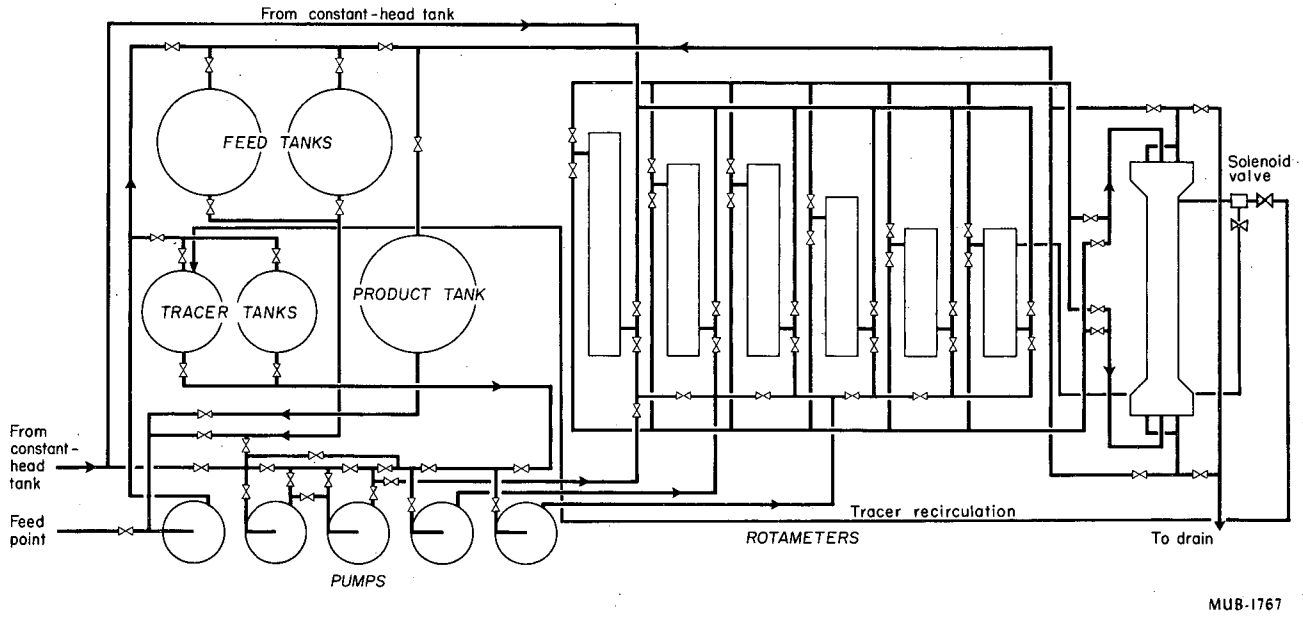

Fig. II-11. Layout of flow system.

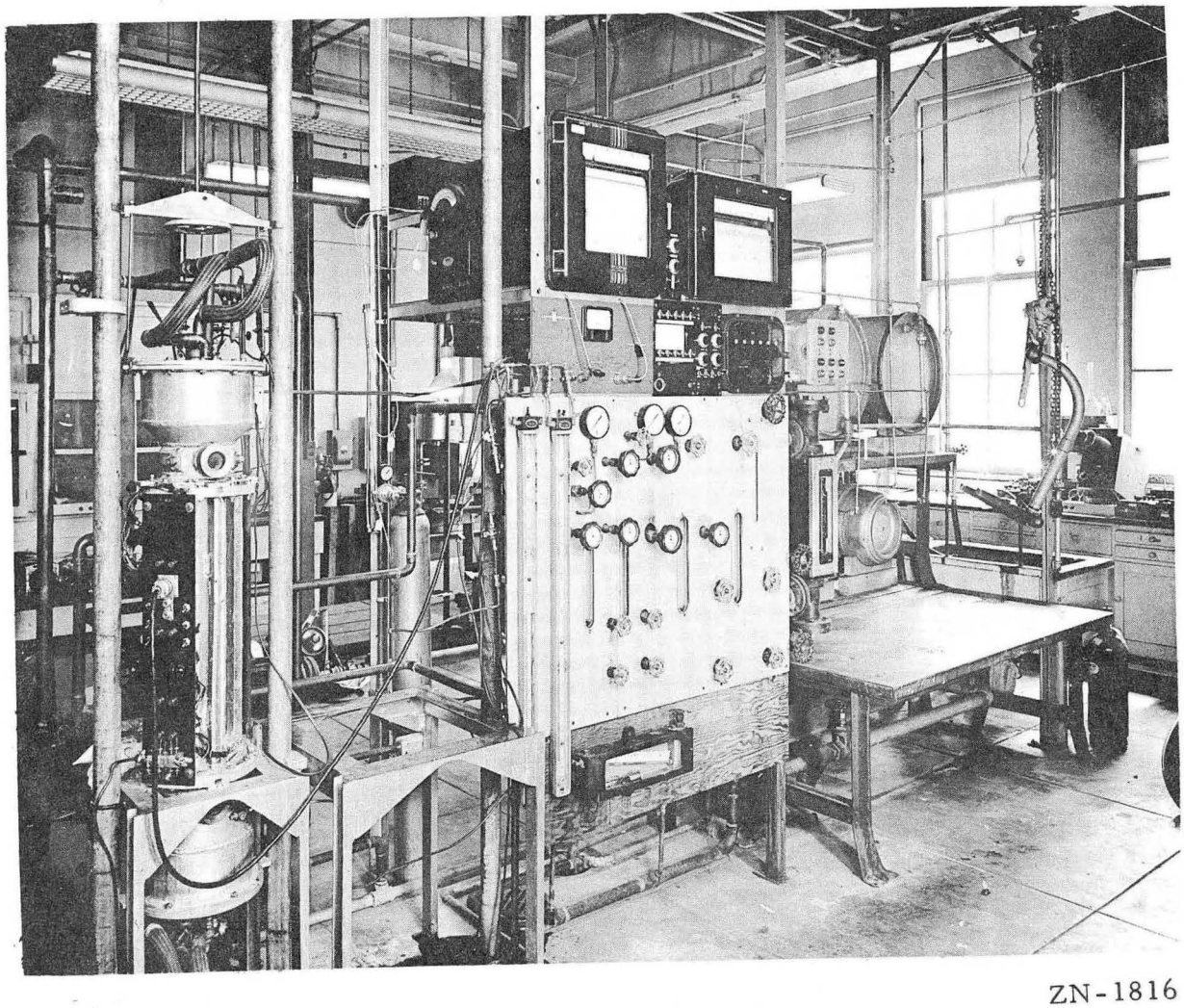

ZN-1816

Fig. II-12. Apparatus assembly, showing control valves and instruments.

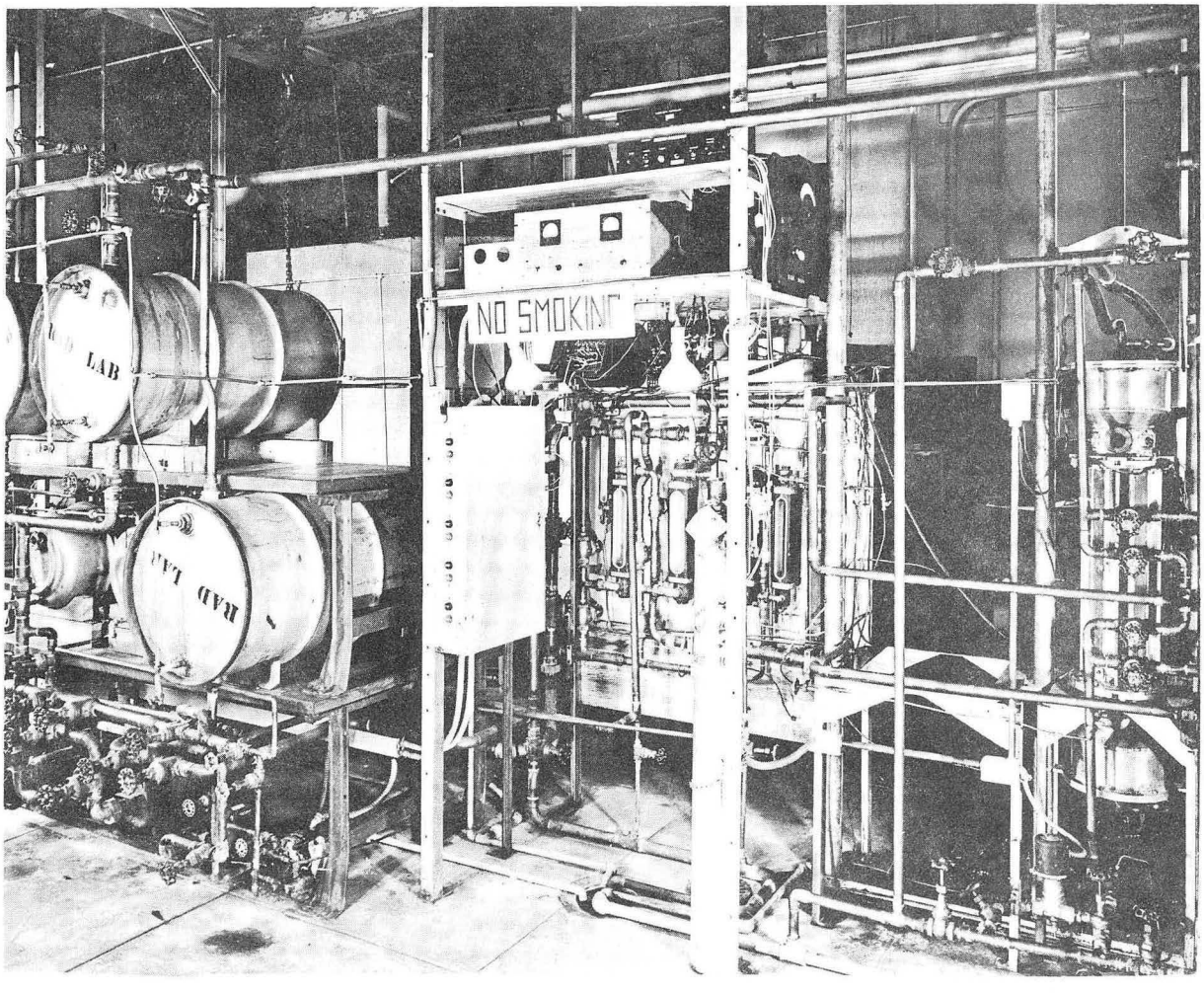

ZN-1814

Fig. II-13. Apparatus assembly, showing storage and piping.

Preliminary studies were therefore made of two columns with different packings: Column 1 (3/4-in. spheres, tetragonal arrangement) and Column 7 (3/4-in. Raschig rings). From this preliminary study, with water as the main stream, it was found for injection of salt ($NaNO_3$) at the top of the column that the purging curve resulting from shutting-off of tracer injection gave better breakthrough curves than the start-up of a step input of tracer. For the latter, the empirical stoichiometric point was much higher than the "exact" value. For injection at the bottom the start-up of tracer injection was better.

These experimental findings were believed to be caused by a hydrodynamic instability, resulting from the density difference between the main stream and the tracer solution, which may cause a preferential but irregular downward flow of the denser fluid (or upward flow of the lighter one). Such an effect is well known in displacement processes;[7, 12, 23, 26] the boundary between adjacent dissimilar bands of liquid can become peculiarly distorted by having "fingers" or "channels" of the displacing liquid intrude deeply into the liquid being displaced.

In principle, this gravity effect may be partially or even completely offset by a viscosity effect, although viscosity seems to have had very little influence in the present study. Displacement by the more viscous liquid favors stability of the boundary, whereas displacement by the less viscous one favors instability. The viscosity effect has been described by Helfferich in the following terms:[12] "Due to packing irregularities, the displacing liquid will slightly bulge out the boundary. If the displacing fluid is the less viscous, the flow resistance in the bulge is smaller and the flow larger than elsewhere; thus the fingers grow. On the other hand, if the displacing fluid is more viscous than the liquid being displaced, the flow resistance is larger in the bulge than next to it, and thus the channels vanish."

Thus the tendency toward "instability" could explain why "top-out" and "bottom-in" run conditions give the better breakthrough curves. The curves corresponding to the reverse conditions (indicating unstable behavior) show an unusual breakthrough shape, with a very fast response

at the start followed by a very long tail which eventually approaches saturation; such a shape can result from the presence of "fingers."

In our experiments it was also found that by reducing the salt concentration from 1 N to 0.05 N, the shape of the curves was improved, the two stoichiometric times showed better agreement, and a good match was obtained between equivalent tracer-in and tracer-out runs except at flowrates smaller than 0.3 gal/min.

2. Procedure

As a result of the preliminary runs, the following experimental conditions were adopted: For flowrates smaller than 0.5 gal/min 0.05 N $NaNO_3$ solution was injected at a rate corresponding in all cases to less than 5% in volume (in most cases around 1 to 2%). For higher flowrates, the amount of tracer injected was less than 1% in volume, but the salt concentration was increased to 0.1 N. The injection was made at the top of the column for nearly all experiments. Both injection- and purge-breakthrough curves were recorded; in the low-flowrate region, when the two curves did not agree, data were taken from the tracer-out or purging curves.

The experimental procedure for typical runs was as follows: Preliminary experiments determined the input "span" to the recorder and the amplifier-gain setting in the cathode circuit to tube V_7 (Fig. II-8) that were needed for the recorder to span nearly the full chart width for the breakthrough curve, for a specified salt injection. Before each set of runs, the electrical measuring unit was tested for linearity by replacing the conductivity probe by a potentiometer; for all the runs this error was within 1%. Then, the actual run was started, with tap water from a constant-head tank flowing through the column at a chosen flow rate. The tracer ($NaNO_3$) solution was started through the recirculation line at the appropriate flowrate (usually around 1 to 2 volume-percent of the main stream), and the pressure drops in the injection line and the recirculation line were equalized by means of two manual valves adjoining the solenoid valve.

After a final check of the flowrates, tracer injection into the column was started by opening the solenoid valve, with the starting time for injection marked electrically on the recorder chart. The voltages recorded during each run were proportional to the conductance of the main stream, and thus, as noted previously, proportional to the concentrations of the injected component. Tracer injection was stopped after a constant reading was reached on the chart; the conductivity was again followed as a function of time to give the purging breakthrough curve. The recorder results were then analyzed as explained below.

3. Calculation of Data

From a critical review of the different mixing models (see Part I) it was concluded that for low flowrates, the data would be analyzed both by the random-walk model (which is equivalent to the diffusion model with finite boundary conditions) and by the segmented-laminar-flow model with quartic velocity profile. For high flowrates the data would be analyzed solely by the random-walk model.

Output concentrations measured by the recorder were plotted as percentages of the total concentration-increment range, against the logarithm of relative time, t/t_{50}, where the reference time, t_{50}, corresponds to the 50% concentration point. The experimental breakthrough curve was then compared with theoretical breakthrough curves predicted by the mixing models. This graphical method has the advantage of comparing entire curves, and thus shows whether the theoretical model used is predicting the right overall shape. Once the theoretical models were shown to be applicable, it was found more convenient to compare experimental slopes for different values of column Péclet number N.

For the random-walk model, the dimensionless slope s can be converted to a column Péclet number by the relation

$$N = 4\pi s^2 - 0.80 \qquad (3)$$

as derived in Appendix II-1. For the segmented-laminar-flow model, the column Péclet number was obtained from a graph giving the

theoretical slopes for different values of N (Fig. II-14). Finally, the packing Péclet number (P) is obtained by multiplying column Péclet number (N) by the ratio of packing diameter to column height (d_p/h).

D. Results and Discussion

The variables affecting axial mixing which were investigated were viscosity, column length, packing characteristics, and liquid velocity. As indicated above, the experimental breakthrough curve can be analyzed either by curve matching on logarithmic time coordinates, or by taking the midpoint slope on linear t/t_{50} coordinates. Figure II-15 is a plot of data from both injection and purging breakthrough steps of a run in Column 2 at a Reynolds number of 31.4, matched to the random-walk model with N = 24 and to the segmented-laminar-flow (quartic) model with N = 18. The method of data analysis is discussed in detail in Appendix II-2.

Full results as obtained from 60 run conditions (approximately 400 separate breakthrough curves) are tabulated in Appendix II-3. A separate table is given for each column; within each table, for the different flow rates used, values are listed for Reynolds number, midpoint slope, and the number of mixing units N and the Péclet number for each theoretical model used.

1. Effects of Viscosity and Velocity

To study the effect of varying the viscosity, breakthrough curves were measured in three different columns; numbers 2, 5, and 7. Aqueous solutions of glycerol were used to obtain a kinematic viscosity of 5 to 6 centistokes. In Fig. II-16 the results are given and compared with those obtained from pure water (ν = 1.0 centistokes) under the same experimental conditions. All runs were made at ambient temperature, 68 ± 2° F. The figure shows that for the viscosity range considered, there is a definite variation in axial dispersion as the velocity changes. The Péclet number for pure water and for water-glycerol solution are found to be equal for the same Reynolds number.

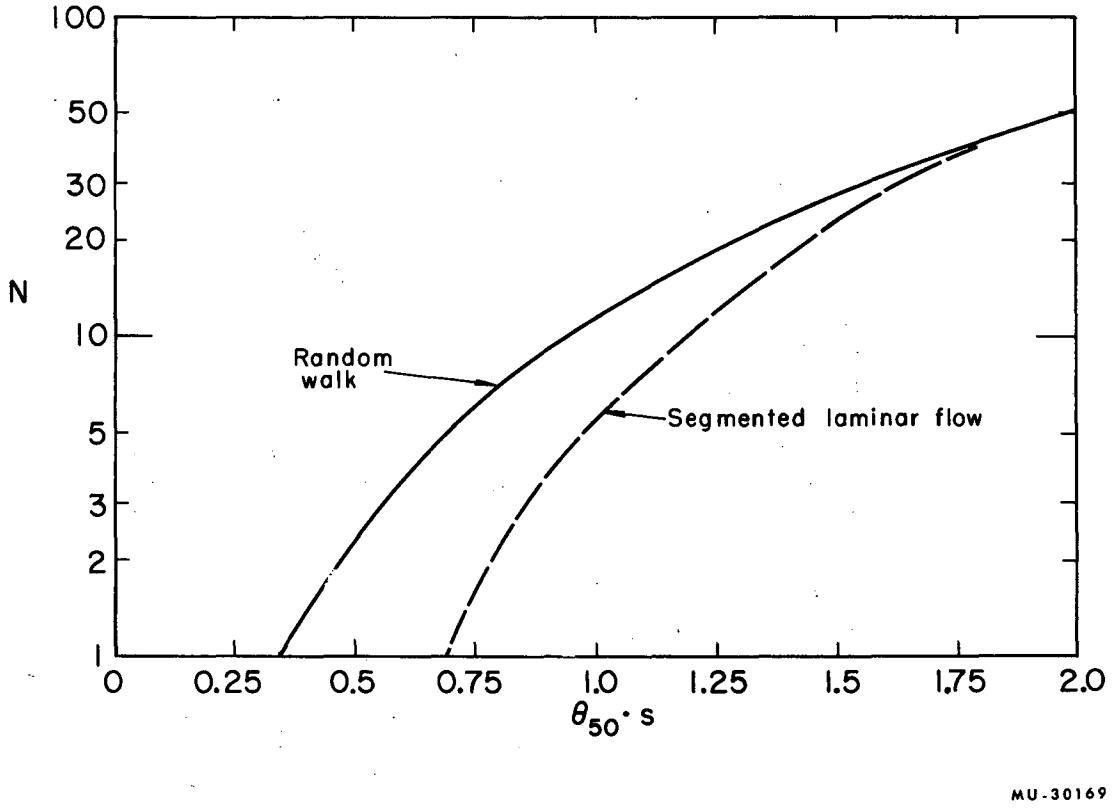

Fig. II-14. Dimensionless shops for random-walk and segmented laminar flow.

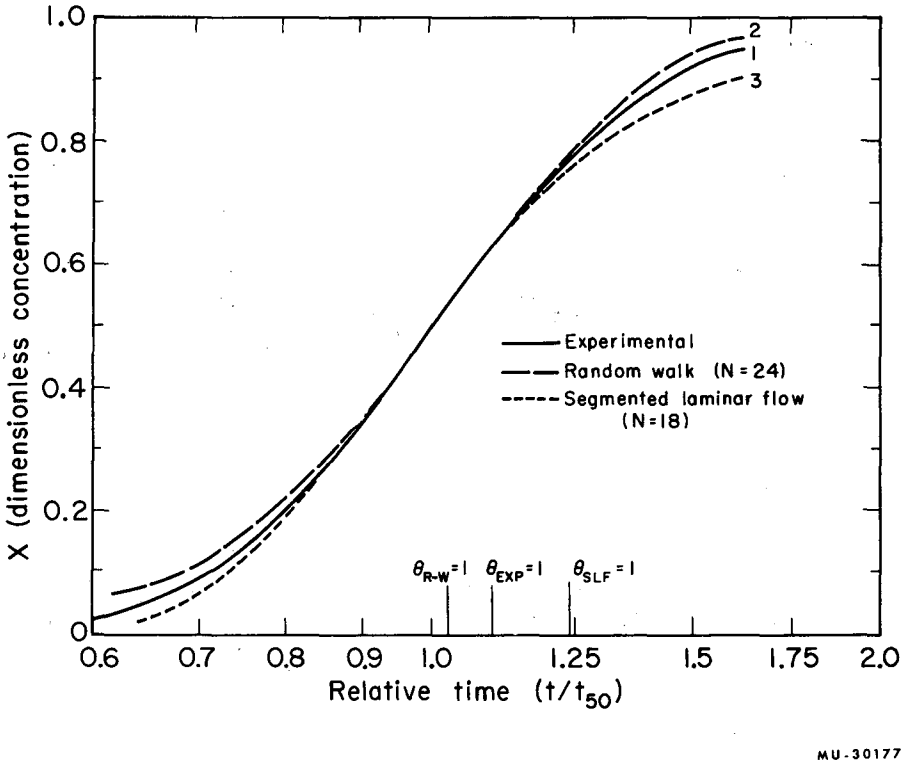

Fig. II-15. Comparison of experimental with theoretical results.

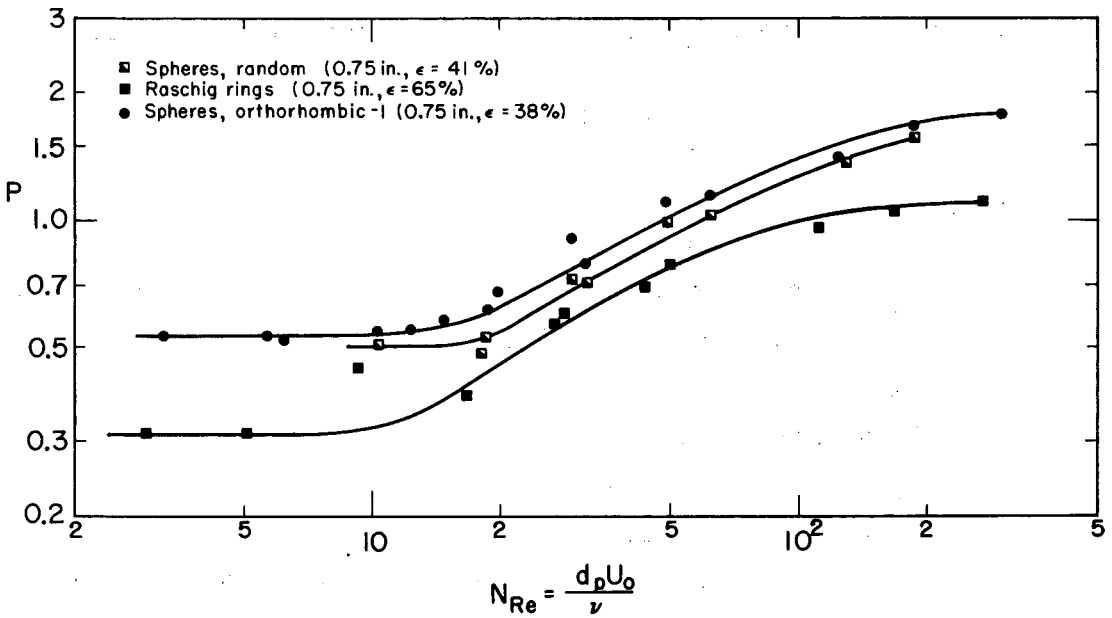

Fig. II-16. Influence of viscosity.

2. Effects of Packing-Particle Characteristics

Various types of packing were investigated to determine the effects of particle shape and packing arrangement, as listed in Tables II-I and II-II. Empirical shifting of the plots in Fig. II-15, and others, has shown that the points can be consolidated into a single curve, provided the ordinate (Péclet number) is multiplied by the void-fraction ϵ to give

$$\epsilon P \left(= \epsilon \, d_p / \ell \right)$$

and the abscissa (Reynolds number) is divided by $(1-\epsilon)$ to give

$$\frac{N_{Re}}{1-\epsilon} = \left(\frac{U_0 \, d_p}{(1-\epsilon)\nu} \right) \tag{4}$$

where

ϵ = void fraction,

d_p = particle diameter (equivalent spherical diameter for non-spherical particles),

ℓ = mixing length,

U_0 = superficial velocity,

and

ν = kinematic viscosity.

The dependence of axial mixing upon the factor $N_{Re}/(1-\epsilon)$ was adopted from Carman's and Ergun's work on pressure drops in packed beds.[4,10] The factor $(1-\epsilon)$ relates the area per unit volume of particles to the area per unit volume of packed bed. In Ergun's correlation the Reynolds number was not based upon the equivalent spherical diameter, as here, but upon the diameter $(d_p)_a$ of a sphere with the same surface-to-volume ratio as a packing particle. Quite possibly a more complex function of ϵ and of ψ (the sphericity) is involved, which we were not able to develop from data only on high-ψ low-ϵ packings and low-ψ high-ϵ packings. In any event, the form of Reynolds number selected by Ergun and Carman to bring together the pressure-drop data differs from the form that we have needed to use in order to match the Péclet-number shifts for different packings.

3. Effect of Bed Length; Choice of Theoretical Model

A crucial factor in determining a longitudinal dispersion coefficient is the selection of the proper theoretical model for interpreting the experimental data.

At least three experimental criteria are available for choosing from among several different theoretical models, in order to determine which model provides the most accurate measure of dispersions behavior. These are:

(1) The shape of the experimental breakthrough curve, in relation to the shapes predicted by the various models.

(2) Related to the shape criterion, the agreement between the observed and the empirical stoichiometric times. (The empirical time is obtained by matching the experimental breakthrough curve to one of a family of theoretical curves, with observation of the point on the actual time scale that matches the stoichiometric point given by the theory.)

(3) Constancy of the Péclet number, or mixing length, for different bed lengths. The different theoretical models all postulate a constant mixing length for the entire packing.

To measure the effect of the bed length, one column unit (Column 10, packed with 0.38-in. ceramic spheres in random arrangement) was equipped with conductivity probes at its center (12-in. level) as well as at the downstream end. Experiments in this column were conducted at four different flowrates; the results are summarized in Tables II-III and II-IV.

In Table II-IV the Péclet-number values in parentheses were determined by the random-walk model; in the high-N region, these approach the values for the segmented-laminar-flow model. The values calculated from the random walk or bounded-diffusion model indicate no effect of bed length, confirming the observations of other investigators;[3,9] whereas the values given by the segmented-laminar-flow model do vary with the bed length.

Table II-III. Effect of bed length; data analyzed by the random-walk model

Flowrate (gpm)	N_{Re}	$\frac{N}{L=23.6 \text{ in.}}$	$\frac{N}{L=12.0 \text{ in.}}$	$\frac{P}{L=23.6 \text{ in.}}$	$\frac{P}{L=12.0 \text{ in.}}$
0.3	9.6	36.2	15.5	0.595	0.526
0.5	16.3	36.3	17.3	0.605	0.586
1.0	32.0	46.3	23.4	0.774	0.794
2.0	64.0	61.0	31.4	1.020	1.040

Table II-IV. Effect of bed length; data analyzed by the segmented-laminar-flow model (quartic)

Flowrate (gpm)	N_{Re}	$\frac{N}{L=23.6 \text{ in.}}$	$\frac{N}{L=12.0 \text{ in.}}$	$\frac{P}{L=23.6 \text{ in.}}$	$\frac{P}{L=12.0 \text{ in.}}$
0.3	9.6	34.9	8.5	0.576	0.288
0.5	16.3	35.0	10.0	0.579	0.339
1.0	32.0	(46.3)	17.3	(0.774)	0.585
2.0	64.0	(61.0)	29.0	(1.020)	0.980

For the run plotted in Fig. II-15, both models represent the experimental data equally well for the range of X between 0.30 and 0.70; outside this range, the experimental curve lies between the two theoretical predictions. Similar comparisons on other runs have shown that there were curves where the segmented-laminar-flow model with quartic velocity profile gave a better prediction of the experimental curve shape than the random-walk model, for X between 0.1 and 0.9. In all cases, however, the segmented-laminar-flow model predicted stoichiometric times that were at least 10% higher than the "exact" values.

This discrepancy, accompanied by the fact that the Péclet number calculated by segmented-laminar-flow does depend upon column length, indicates that the random-walk model is somewhat more satisfactory even in the laminar-flow region. At the same time, the segmented-laminar-flow model, based as it is on the filamental nature of laminar flow in packed beds, should be viewed as a necessary step in the development of a better understanding of axial-dispersion phenomena. Its partial failure might be due to the velocity profile selected, and to the particular methods it involves of averaging the properties of the flow.

4. Graphical Correlation of Results

Using the modified dimensionless parameters just discussed, we have plotted all the experimental points of the present study (on logarithmic coordinates) in Fig. II-17. Our data clearly show the predicted laminar- and turbulent-flow regimes, with a well defined transition region occurring, for an $N_{Re}/(1-\epsilon)$ of from 25 to 1000. The data given at high flowrates, for $N_{Re}/(1-\epsilon)$ about 700 (and only these) are from a previous investigation in the same apparatus.[14] Figure 18 shows the data corresponding to the laminar-flow regime and part of the transition region, for a 2-ft column length, analyzed by the segmented-laminar-flow model with a quartic velocity profile. It is seen that the Péclet-number values thus obtained are appreciably smaller at low flowrates than those given by the random-walk model, whereas at higher flowrates they are more nearly equal. As already shown, however, the laminar-

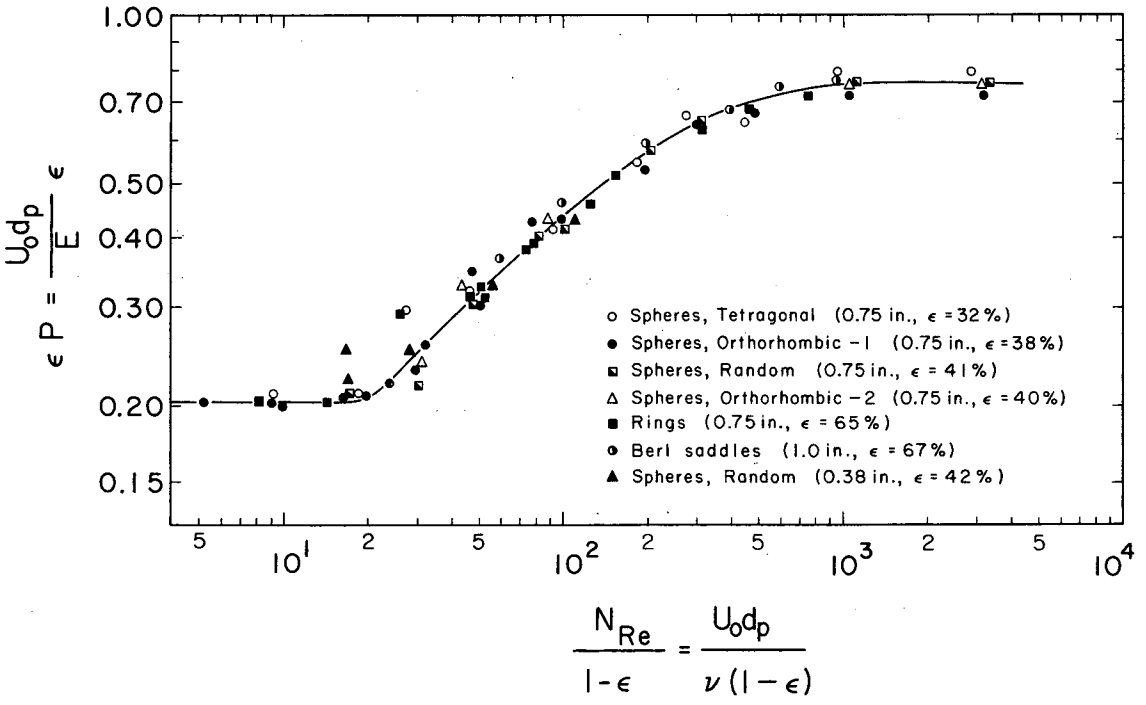

Fig. II-17. Experimental results analyzed by random-walk.

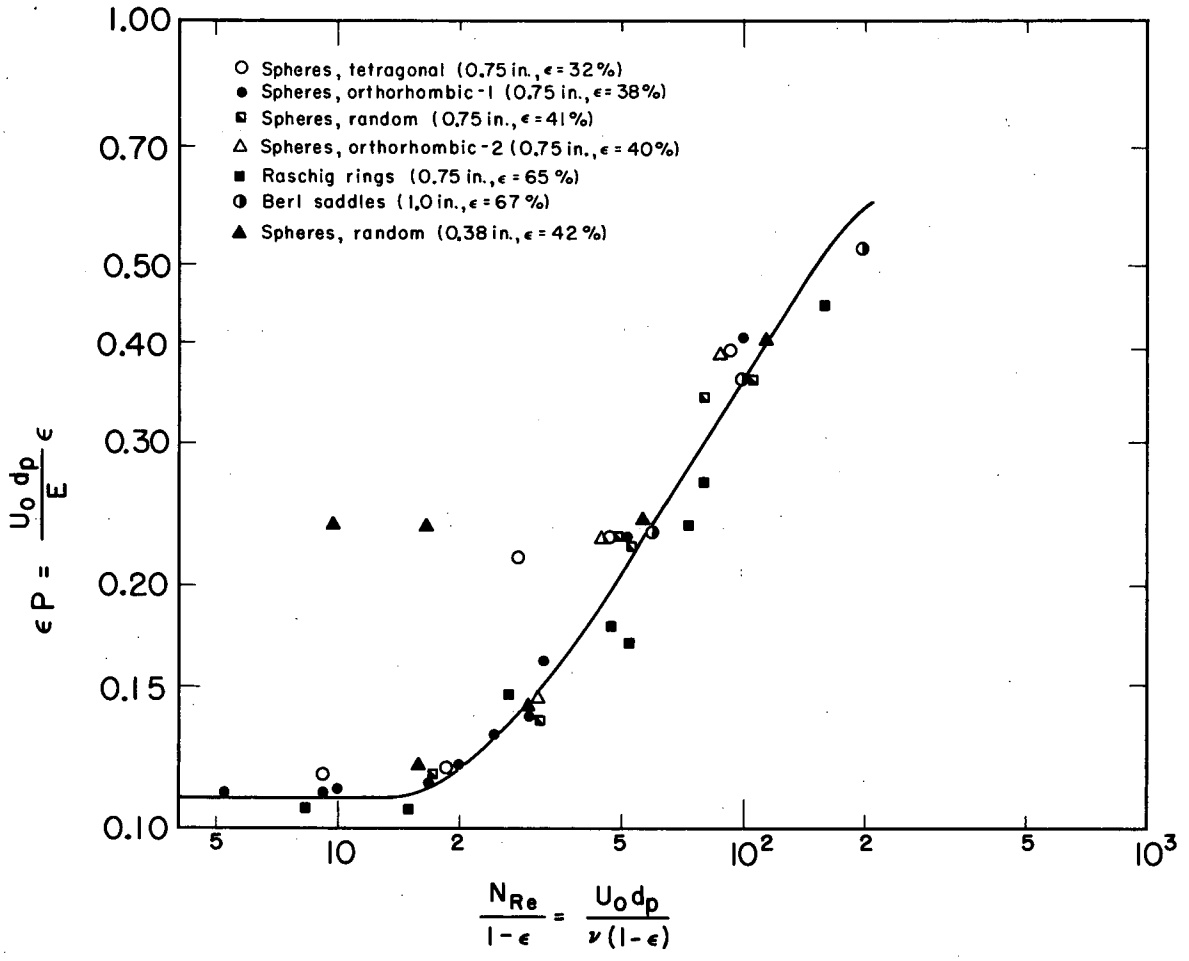

Fig. II-18. Experimental results analyzed by segmented laminar flow.

flow Péclet values obtained from the segmented-flow model appear to depend upon column length. If points had been shown at different lengths, it would not be possible to represent them by a single curve.

5. Comparison with Other Studies

a. Liquid phase. The experimental results of the present study are compared in Fig. II-19 with the data of several earlier investigations. Collectively these data confirm the presence of a transition effect between lower and higher values of Reynolds number. Beyond this general feature, the reproducibility of measurements within any one study seems much better than its agreement with any other one.

Strang and Geankopolis[24] used a sinusoidal imput of dye, for 0.23-in. glass spheres and 0.27-in. Raschig rings in a 1.65-in. diam column 22.5-in. in height.

Jacques's data[14] are from a preliminary study using the presently described apparatus. Subsequent to that study, improvements were made in both the recording and the injection systems, and the tracer-concentration level was greatly reduced.

Cairns and Prausnitz used 0.125-in. glass spheres in a column 2.0 in. in diam and 24 in. high.[3] A step-function input was selected with upward injection of $NaNO_3$ tracer solution, and purging-step curves were used for the analysis.

Ebach and White used sinusoidal injection and also pulse injection in a 2.0-in.-diam column 2.0 to 5.0 ft high, with glass spheres 0.0083, 0.04, 0.13, or 0.27 in. in diam and 0.25-in (nominal) Raschig rings, Berl saddles, and Intalox saddles.[9]

Carberry and Bretton used pulse injection of dye tracer in a 1.5-in.-diam column at various bed lengths, with spheres ranging from 0.02 to 0.20-in. in diam, 0.08-in. doughnut rings, and 0.25-in. Raschig rings.[5]

To compare these experiments, a number of possible sources of error must be kept in mind:

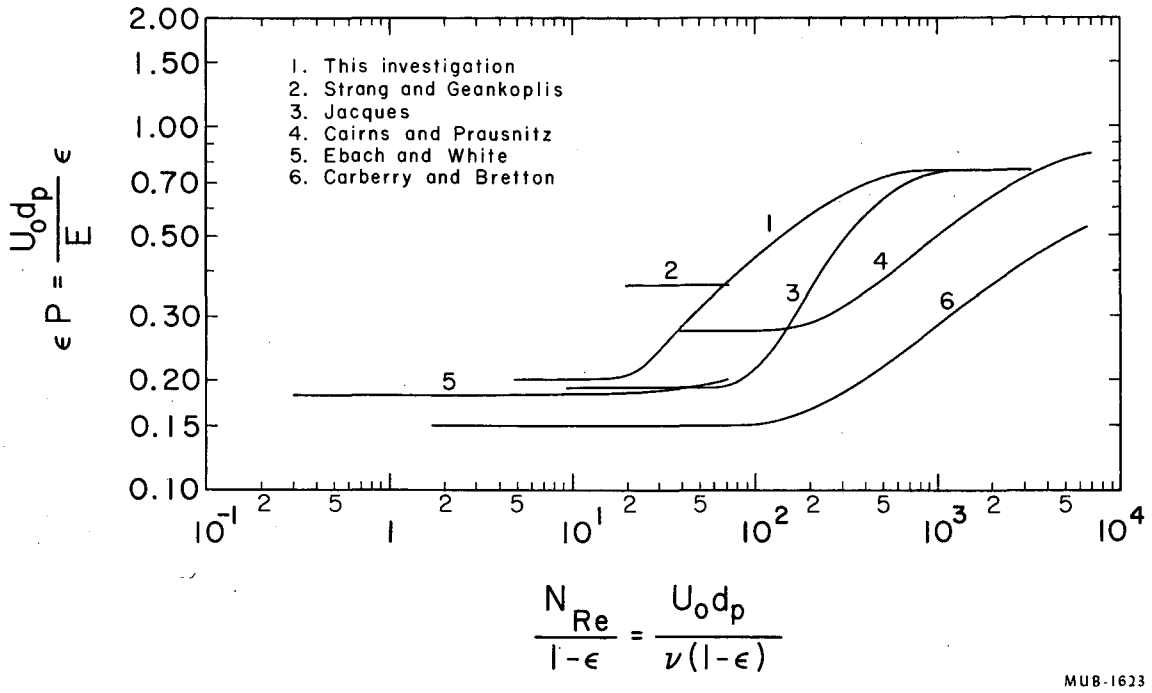

Fig. II-19. Comparison with other investigation.

(1) Hydrodynamic instability
(2) Adsorption of tracer on particle surfaces
(3) Instrument lags
(4) Injection end effects
(5) Flow irregularities in tracer-injection system
(6) Column wall effect and other channeling.

A possibility exists that the correct plotting functions have not yet been found, and that the different curves of Fig. II-19 are in better agreement than this plot indicates. However, it would be difficult to reconcile the different results for small glass spheres on any such basis.

The present results were obtained on the largest particles used in any study. Wall effects could have occurred in the randomly packed columns, but not in the ordered ones (Columns 1, 2, and 6). Injection end effects could occur; but both the close agreement of the stoichiometric times observed from the input and the output, and the good agreement between 1-ft and 2-ft column lengths, suggest that such end effects are minimal. The possibility of hydrodynamic instability, which clearly interfered with our reproducibility at higher tracer-concentration levels, has been almost entirely excluded by the agreement between injection and purging runs for both upflow and downflow operation.

b. Gas phase. McHenry and Wilhelm have reported the only thorough study of gas-phase longitudinal dispersion in packed beds, with sinusoidal input of hydrogen or ethylene into a nitrogen stream.[18] Their measurements were made with 0.127-in. glass spheres in a column 1.94 in. in diam, with several different bed heights. With some evidence for a dip at $N'_{Re} = 250$, their data led to a P value of 1.88 ± 0.15 or a ϵ P value of 0.73 ± 0.06 over the range of N'_{Re} from 20 to 1000. Carberry and Bretton reported a few values for helium tracer in air in the fine-particle low-flowrate region.[5] Taken together, these results indicate that the gas-phase Péclet-number values are essentially the same in the turbulent and the laminar regimes, but that at sufficiently low Reynolds numbers molecular diffusion predominates and causes the Péclet number to decline.

As already noted, the liquid-phase values from both this and other investigations tend to join McHenry's gas-phase data in the turbulent region, but then decrease to a level one-fourth to one-third of this value in the laminar region. It appears likely that, in gas-phase laminar flow, lateral molecular diffusion in the void spaces compensates for the segregation due to velocity distribution, and maintains the individual voids in an almost entirely mixed condition.

Figure II-20 has been drawn to examine and illustrate the logical consequences of this assumption. Except for axial molecular diffusion, the range of possible modified Péclet numbers appears to be bounded by a segregated-flow value of 0.202 and a void-cell-mixing value of 0.75. A justification for the upper limit to P_j will be given shortly. Thus, the actual gas-phase behavior is indicated by dashed lines, and liquid behavior is indicated by solid lines.

G. I. Taylor has shown for laminar flow inside pipes that the segregation of residence times (resulting from the velocity profile) can be represented by an effective axial-dispersion ("Taylor-diffusion") coefficient.[25] As radial dispersion becomes appreciable, it serves to reduce the apparent axial coefficient; for this region, in a tube of diameter d_t, in which the average fluid velocity is U, the longitudinal-dispersion coefficient is E and the molecular-diffusion coefficient is D, Taylor derived the relation

$$\frac{E}{Ud_t} = \frac{1}{192}\,\frac{Ud_t}{D} \quad . \tag{5}$$

For a column randomly packed with spheres we may assume a "tube" diameter equal to half the particle diameter. Then, with $\epsilon = 0.40$, we have

$$\frac{E}{U_0 d_p} = \frac{1}{123}\,\frac{d_p U_0}{D} \quad , \tag{6}$$

where U_0 is the superficial velocity ($= U\epsilon$). Introduction of the dimensionless groups,

$$P' = \epsilon P = \frac{U_0 d_p}{E} \quad , \tag{7}$$

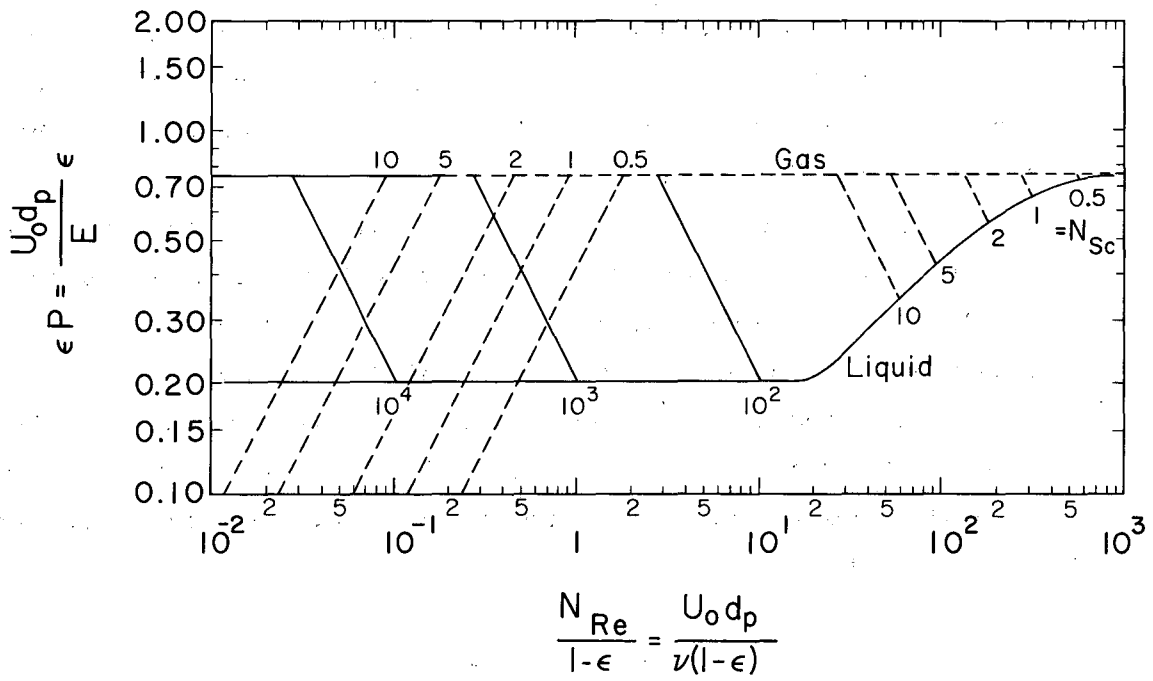

Fig. II-20. Relation between liquid- and gas-phase dispersion coefficients.

$$N'_{Re} = \frac{N_{Re}}{(1-\epsilon)} = \frac{U_0 d_p}{\nu(1-\epsilon)}, \tag{8}$$

and $N_{Sc} = \nu/D$, provides the relation

$$P' = \frac{205}{N_{Sc} N'_{Re}} . \tag{9}$$

Thus, for any given Schmidt number, reducing the Reynolds number should eventually increase the Péclet number from the lower curve to the upper curve. The lines of constant N_{Sc} rising from right to left correspond to the behavior indicated by Eq. (9). With gases, having $N_{Sc} \approx 1$, the rising curves are intersected almost before the fully turbulent region is departed from (McHenry's curve does show a relatively narrow dip at $N'_{Re} = 250$, of perhaps 15%).

With liquids, the rising curves apparently are not reached within the usual range of chemical engineering measurements, i.e., at N'_{Re} values of 1 and greater. Raimondi et al. used pulse injection of radioactive tracer in a 1.22-in.-diam column 35.4 in. high, with glass beads 0.0045, 0.0214 and 0.0256 in. in diameter.[21] Their data led to a P value of 1.45 ± 0.2 (or ϵP of 0.575 ± 0.07) over the range of N'_{Re} from 0.015 to 0.28. Although this Péclet number value is lower than the upper limit (or $P' = 0.75$), which might be caused by channeling, it is much higher than the lower limit ($P' \approx 0.2$). This one experimental finding is in favor of the idea that Taylor diffusion can cause a rise in the Péclet number for liquids at $N'_{Re} < 1$. The reason that P values seem not to exceed the values found by McHenry and Wilhelm may be that the local velocities are always much higher in the channels between the voids than within the voids. Within each void, both axial and transverse molecular diffusion occur at comparable rates, so that the void is reconverted to a near-perfect mixing cell.

At very low flowrates, molecular diffusion in the axial direction becomes predominant. This effect is indicated by the lines of constant N_{Sc} that fall off to the left in Fig. II-20. In this region, the axial-dispersion coefficient E must be multiplied by the porosity to

obtain the coefficient of static diffusion $\mathscr{D}$ in a porous medium.[6] In turn, $\mathscr{D}$ is related to the coefficient of molecular diffusion, in the absence of the porous medium, by the relation $\mathscr{D}/D \approx \epsilon/\sqrt{2}$; the factor $\sqrt{2}$ is commonly adopted to represent the tortuosity of a packed bed. Thus, for low flowrates, where the molecular diffusion becomes important, E will be replaced by $D/\sqrt{2}$ and the modified Péclet number P' will be given by

$$P' \left(= U_0 d_p/E \right) = \sqrt{2}\, U_0 d_p/D \,. \tag{10}$$

The same definitions for N'_{Re} and N_{Sc} as above give the relation

$$P' = 0.85\, N_{Sc}\, N'_{Re} \,. \tag{11}$$

The gas-phase data of Carberry and Bretton fall in the range of molecular-diffusion curves shown here.[5]

E. Conclusions

The experimental results from this investigation lead to the following conclusions:

(a) The data show separate constant values for the Péclet number in the laminar and in the turbulent region, and the existence of a fairly sharp transition curve between these two regions.

(b) The segmented laminar-flow model, derived to provide a physical model for laminar-flow conditions, was found to give a poorer fit to experimental data under such conditions than the random-walk model.

(c) Experiments using water-glycerol solutions indicate that viscosity has a large effect on axial dispersion over the range investigated. The Péclet numbers for pure water and for water-glycerol solutions are found to be equal for the same Reynolds number.

(d) Axial Péclet numbers may be correlated as a function of porosity and of Reynolds number. A plot of modified Péclet number (ϵ P) vs a modified Reynolds number $N_{Re}/(1-\epsilon)$, shown in Fig. II-17, applies to the whole range of experimental results.

(e) No effect of packing arrangement was observed in this study; regular and random packing give identical results for the same porosity.

(f) An elementary derivation shows that the difference between gas and liquid Péclet numbers (in laminar-flow conditions) can be explained by molecular diffusion in the packing void spaces. At quite low N_{Re}, axial molecular diffusion causes P to decrease.

F. Notation for Part II

a_p	Surface area per unit volume
c	Concentration
c_0	Concentration for perfect mixing
d_p	Particle diameter
$(d_p)_a$	Equivalent diameter [defined by Eq. (2)]
$(d_p)_h$	Equivalent hydraulic diameter
$(d_p)_v$	Equivalent spherical diameter [defined by Eq. (1)]
d_t	Tube diameter
D	Molecular diffusivity
$\mathscr{D}$	Effective diffusivity within a packed bed
E	Superficial dispersion coefficient
h	Height of bed
ℓ	Mixing length
N	Column Péclet number (h/ℓ)
N_{Sc}	Schmidt number
N_{Re}	Reynolds number
N'_{Re}	Modified Reynolds number $[N_{Re}/(1-\epsilon)]$
p	Periphery of packing
P	Packing Péclet number (d_p/ℓ)
P'	Modified Péclet number (ϵP)
s	Midpoint slope (based on Θ scale)
s'	Midpoint slope of breakthrough curve (based on t/t_{50} scale)
s''	Midpoint slope (equals $[N/(N+1)] \cdot s$)
t	Time
t_{50}	Time corresponding to X equals 0.5
T	Dimensionless time
U	Intersticial velocity or mean linear velocity
U_0	Superficial velocity, equals $U\epsilon$
X	Dimensionless concentration (c/c_0)

β	Correction factor to N calculation based on midpoint slope
ϵ	Bed void fraction
Θ	Dimensionless time T/N
ν	Kinematic viscosity
ψ	Sphericity

References for Part II

1. R. J. Blackwell, Laboratory Studies of Microscopic Dispersion Phenomena in Porous Media, preprint, A. I. Ch. E. Annual Meeting, 1959 (unpublished).
2. G. G. Brown and associates, Unit Operations, (John Wiley and Sons, Inc., New York 1950), 216.
3. E. J. Cairns and J. M. Prausnitz, Chem. Eng. Sci. 12, 20 (1960).
4. P. C. Carman, Trans. Inst. Chem. Engrs. (London) 15, 150 (1937).
5. J. J. Carberry and R. H. Bretton, A. I. Ch. E. J. 4, 367 (1958).
6. F. E. Crane and G. H. F. Gardner, Measurement of Transverse Dispersion in Granular Media, Technical Report from Gulf Research and Development Co., Pittsburgh Pa., April 18, 1960.
7. R. L. Chuoke, P. Van Meurs, and C. van der Pool, J. Petrol. Technol., Petroleum Trans. AIME 216, 188 (1959).
8. P. V. Danckwerts, Chem. Eng. Sci. 2, 1 (1953).
9. E. A. Ebach and R. R. White, A. I. Ch. E. J. 4, 161 (1958).
10. S. Ergun, Chem. Eng. Progr. 48, 89 (1952); Ind. Eng. Chem., 47, 1135 (1955).
11. L. C. Graton and H. J. Frazer, J. Geol. 43, 785, 910 (1935).
12. F. Helfferich, Chem.-Ing. Techn. 34, 275 (1962).
13. H. Hofmann, Chem. Eng. Sci. 14, 193 (1961).
14. G. L. Jacques, J. E. Cotter, and T. Vermeulen, University of California Lawrence Radiation Laboratory Report UCRL-8658, 1959 (unpublished).
15. H. Kramers and G. Alberta, Chem. Eng. Sci. 2, 173 (1953).
16. M. Leva, Tower Packing and Packed Tower Design, United States Stone Ware Co., Akron, Ohio (1951).
17. J. J. Martin, W. W. McCabe, and C. C. Monrad, Chem. Eng. Progr. 47, 91 (1951).
18. K. W. McHenry and R. H. Wilhelm, A. I. Ch. E. J. 3, 83 (1957).
19. J. H. Perry, Chemical Engineers' Handbook, 3rd ed., (McGraw-Hill Book Company, Inc., New York 1950), p. 394.

20. H. R. C. Pratt, Trans. Inst. Chem. Engrs. (London) 29, 195 (1951).

21. P. Raimondi, G. H. F. Gardner, and C. B. Petrick, Effect of Pore Structure and Molecular Diffusion on the Mixing of Miscible Liquids Flowing in Porous Media, Technical Report from Gulf Research and Development Co., Pittsburgh Pa., Aug. 31, 1960 (unpublished).

22. N. E. Rifai (with W. T. Kaufman and K. Todd), Ph. D. Thesis, University of California, Berkeley, 1956 (unpublished).

23. P. G. Saffman and G. I. Taylor, Proc. Roy. Soc. (London) A245, 312 (1959).

24. D. A. Strang and C. J. Geankoplis, Ind. Eng. Chem. 50, 1305 (1958).

25. G. I. Taylor, Proc. Roy. Soc. (London) A219, 186 (1953); A223, 446 (1954); A225, 473 (1954).

26. G. I. Taylor, Proc. Roy. Soc. (London) A201, 192 (1950).

Appendixes for Part II

II-1. Computation from Experimental Midpoint Slopes (Using the Random-Walk Model)

Once the applicability of the random-walk model has been ascertained for any given breakthrough curve by matching its entire shape to the shapes given by the model, the most convenient and often the most accurate method for evaluating the Péclet group is to measure the slope at a well defined point.

The random-walk model describes the breakthrough curves by the expression

$$X = \frac{c}{c_0} = \int_0^{T'} \exp(-N-T')\, I_0(2\sqrt{NT'})\, dT' \,. \tag{1}$$

Differentiating Eq. (1) with respect to a time scale T/N gives for the dimensionless slopes

$$s'' = \frac{\partial X}{\partial (T'/N)} = N\left(\frac{\partial X}{\partial T'}\right) \tag{2}$$

and

$$s'' = N\, \frac{I_0(2\sqrt{NT'})}{\exp(\sqrt{N}-\sqrt{T'})^2 \exp(2\sqrt{NT'})}\,; \tag{3}$$

a different slope can be defined as

$$s = \frac{\partial X}{\partial \Theta} = \frac{N+1}{N}\, s'' \,, \tag{4}$$

where $\Theta = T/N$. It is not possible to determine directly the T or T' for which $X = 0.5$. Trial-and-error determinations were therefore performed on the computer; the results are presented in Table I-IX of Part I. It is found empirically that the following relation holds between $(T')_{X=0.5}$ and N:

$$(T')_{X=0.5} = N + 0.50 \tag{5}$$

which can be used in subsequent calculations. A simple form for the slope at this T' can be obtained by using infinite-series expressions for the various terms in Eq. (3).

$$I_0(2/NT') = \frac{e^{2\sqrt{NT'}}}{2\sqrt{\pi}(NT')^{1/4}} \left(1 + \frac{1}{16(NT')^{1/2}} + \frac{9}{512(NT')} + \cdots\right) \tag{6}$$

From known algebraic expansions, using Eq. (5), it can be shown that

$$\left[\exp(\sqrt{N} - \sqrt{T'})^2\right]^{-1} = 1 - \frac{1}{16N} + \frac{9}{512\,N^2} - \cdots \tag{7}$$

and

$$(NT')^{-1/4} = N^{-1/2}\left(1 - \frac{1}{8N} + \frac{5}{128\,N^2} - \cdots\right) \tag{8}$$

Substitution in Eq. (3) leads to

$$s'' = \frac{\sqrt{N}}{2\sqrt{\pi}} \left(1 - \frac{1}{8N} + \frac{7}{128\,N^2} - \cdots\right). \tag{9}$$

As it is not possible to determine the location of the point $T' = N$ from the data without resorting to trial and error, it is convenient to measure a slope s' with reference to a time scale t/t_{50}:

$$s' = \frac{dX}{d(t/t_{50})} = \frac{T'(X=0.5)}{N}\, s'' \tag{10}$$

and

$$s' = \left(1 + \frac{1}{2N}\right)s'' = \frac{\sqrt{N}}{2\sqrt{\pi}}\left(1 + \frac{3}{8N} - \frac{1}{128\,N^2} + \cdots\right). \tag{11}$$

This last equation gives a simple relation for computing N from the slope s':

$$N = 4\pi(s')^2/\beta$$

with

$$\beta = \left(1 + \frac{3}{8N} - \frac{1}{128\,N^2} + \cdots\right)^2. \tag{12}$$

For convenience a plot of β-1 versus $4\pi(s')^2$ is given in Fig. II-21. A good approximation to the exact relations is given by

$$\begin{aligned} N &= 4\pi(s')^2 - \Delta \\ &\approx 4\pi(s')^2 - 0.80\,. \end{aligned} \tag{13}$$

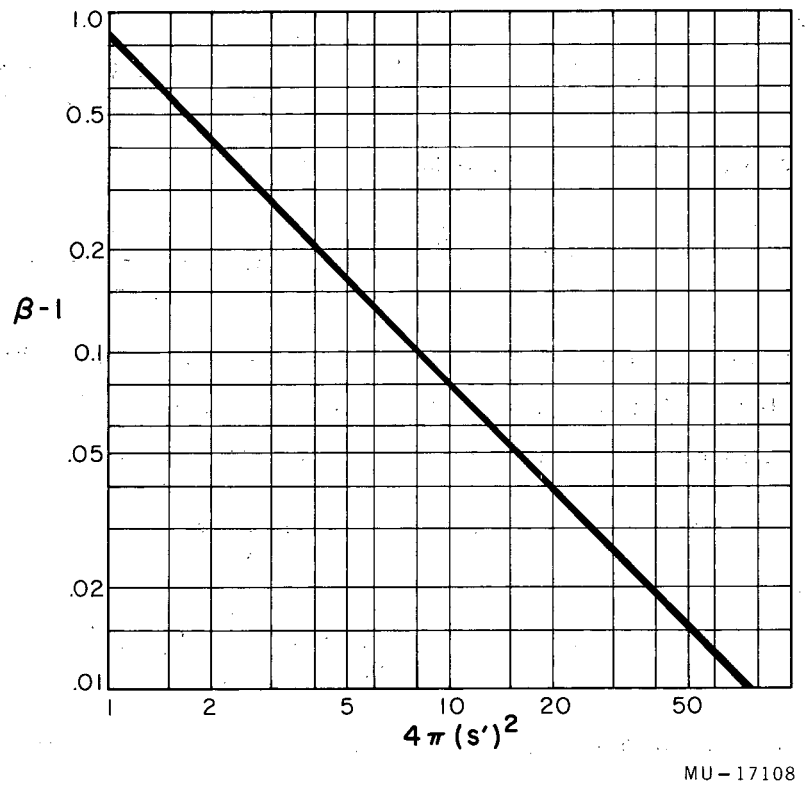

Fig. II-21. Midpoint-slope correction factor.

At $N = 1$, $\Delta = 0.869$; at $N = 5$, $\Delta = 0.778$; and in the upper limit $\Delta = 0.750$. Equation (13) is therefore quite useful in analyzing experimental breakthrough curves by the random-walk model.

II-2. Sample Calculation

The calculation method used will be demonstrated with the data from a run (Run 412) in Column 2 (3/4 in. spheres - orthorhombic-1; ϵ = 38%; flowrate 0.51 gal/min). The data from the recorder chart, and the calculations made on the breakthrough curve, are given in Table II-V. The calculations are made for both "salt-in" and "salt-out" breakthrough curves. A plot of the concentration (in percent) vs the ratio of the elapsed time to the time at the 50% concentration point is shown in Fig. II-22. From the slope (s'), taken at $t/t_{50} = 1$, the Péclet number is calculated by the relation

$$N_{RW} = 4\pi s'^2 \simeq 0.80$$

and

$$P_{RW} = \frac{d_p}{h} N_{RW},$$

where d_p is the packing diameter and h is the height of the bed (distance between the injection plane and the plane of measurement). For the represented run $s' = 1.41$, $N_{RW} = 24.3$ and $P_{RW} = 0.790$.

The analysis of the data by the segmented laminar-flow model is made on a modified semilog plot (X vs Θ); the advantage in this plot is that one can compare entire curves. Due to the nature of the logarithmic abscissa scale, the comparison can be made by sliding the experimental curve horizontally over master plots giving the breakthrough curves for the different models. A plot showing the experimental curve with the best match from the random-walk and the segmented-laminar-flow models, is given in Fig. II-16. For this particular run N_{SLF}=18.5 and P_{SLF}=0.602.

The experimental breakthrough curve is plotted on a t/t_{50} scale, and thus the theoretical stoichiometric point and the experimental stoichiometric points for the two models ($\Theta_{RW} = 1$ and Θ_{SLF}=1) occur beyond $t/t_{50} = 1$. For this column, the theoretical stoichiometric point, equal to the ratio of column void-volume (= cross section $\times$ height $\times$ porosity = 1.246 gal) to volumetric flowrate (0.51 gpm), is 2.44 min.

Table II-V. Sample calculations of an experimental breakthrough curve

Tracer in				Tracer out			
Recorder		breakthrough C		Recorder		breakthrough C	
C^a	$t_{(sec)}$	C/C_0(%)	t/t_{50}	C_0-C	$t_{(sec)}$	$\frac{C_0-C}{C_0}$ %	t/t_{50}
0	0	0	0	0	0	0	0
0.4	92.1	7.7	0.686	0.3	82.5	5.8	0.632
0.9	103.2	17.3	0.768	0.8	100.9	15.4	0.772
1.4	111.9	26.9	0.832	1.3	110.0	25.0	0.842
1.9	121.5	36.5	0.904	1.8	117.8	34.6	0.901
2.4	130.5	46.2	0.971	2.3	125.2	44.2	0.960
2.6	134.5	50.0	1.000	2.6	131.0	50.0	1.000
2.9	139.7	55.8	1.039	2.8	134.5	53.8	1.029
3.4	148.9	65.4	1.107	3.3	144.0	63.5	1.103
3.9	162.0	75.0	1.207	3.8	157.0	73.1	1.202
4.4	179.0	84.6	1.332	4.3	174.0	82.7	1.331
4.9	203.0	94.2	1.507	4.8	204.0	92.3	1.562
5.2	∞	100	∞	5.2	∞	100	∞

[a]Concentration given in recorder chart units.

Conditions:

Column 2, orthorhombic-2, ϵ = 38%.
Flowrate = 0.51 gal/min (N_{Re} = 31.4).
Injection at top of column.
Concentration of tracer = 0.05 N $NaNO_3$.
Amount of tracer = 2 volume %.

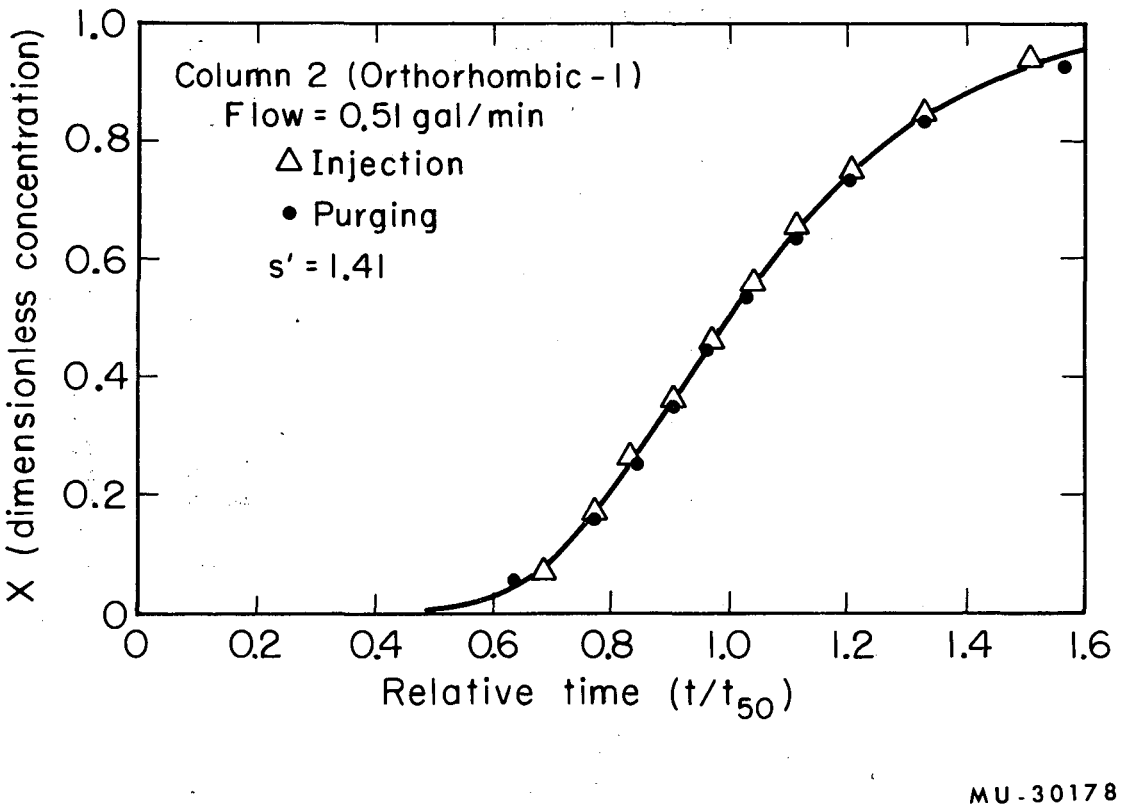

Fig. II-22. Dimensionless breakthrough curve.

II-3. Experimental Data

A. Column 1: 0.75-in. Spheres; Tetragonal Arrangement; Porosity 32%; Single-Phase, Water

Flow-rate (gal/min)	N_{Re}	$\frac{N_{Re}}{1-\epsilon}$	Slope	Random-walk			Segmented laminar flow			No. of measurements
				N	P	P'	N	P	P'	
0.1	6.2	9.2	1.29	19.6	0.620	0.205	11.2	0.354	0.117	8
0.2	12.3	18.4	1.28	19.7	0.629	0.209	11.3	0.360	0.119	8
0.3	18.4	27.6	1.48	27.8	0.890	0.297	21.0	0.666	0.220	10
0.51	31.4	46.8	1.59	30.7	0.976	0.322	22.0	0.697	0.230	10
1.0	61.5	91.8	1.78	38.9	1.240	0.411	37.0	1.180	0.391	10
2.0	123.0	183.5	2.04	51.3	1.631	0.544				6
3.0	184.5	275.3	2.24	62.1	1.980	0.653				6
4.86	298.8	446.0	2.22	60.9	1.935	0.639				6

B. Column 2: 0.75-in. Spheres; Orthorhombic Arrangement; Porosity 38%; Single-Phase, Water

Flow-rate (gal/min)	N_{Re}	$\frac{N_{Re}}{1-\epsilon}$	Slope	Random-walk N	Random-walk P	Random-walk P'	Segmented laminar flow N	Segmented laminar flow P	Segmented laminar flow P'	No. of measurements
0.1	6.2	9.9	1.15	16.0	0.520	0.198	9.0	0.293	0.112	7
0.2	12.3	19.8	1.19	16.9	0.550	0.209	9.7	0.315	0.120	9
0.3	18.4	29.7	1.24	18.6	0.606	0.231	11.2	0.364	0.138	8
0.51	31.4	50.6	1.41	24.3	0.790	0.301	18.5	0.602	0.229	6
1.0	61.5	99.2	1.68	34.8	1.135	0.431	33.0	1.074	0.608	6
2.0	123.0	198.3	1.85	42.2	1.380	0.525				6
3.0	184.5	297.5	2.03	51.20	1.665	0.631				6
4.86	298.8	481.9	2.08	53.8	1.755	0.668				6

C. Column 2: 0.75-in. Spheres; Orthorhombic Arrangement; Porosity 38%; Single-Phase, Water-Glycerol

Flow-rate (gal/min)	N_{Re}	$\frac{N_{Re}}{1-\epsilon}$	Slope	Random-walk			Segmented laminar flow			No. of measurements
				N	P	P'	N	P	P'	
0.31	3.2	5.2	1.17	16.3	0.532	0.202	9.0	0.294	0.111	6
0.55	5.6	9.0	1.17	16.3	0.532	0.202	9.0	0.294	0.111	8
1.0	10.3	16.6	1.18	16.5	0.546	0.207	9.2	0.300	0.114	6
1.43	14.7	23.8	1.22	17.8	0.580	0.220	10.6	0.346	0.131	6
1.93	19.8	32.0	1.31	20.8	0.680	0.258	13.0	0.425	0.162	6
2.85	29.0	46.9	1.55	29.1	0.915	0.348				6
4.7	48.3	78.0	1.63	32.5	1.120	0.425				4

D. Column 5: 0.75-in. Spheres; Random Arrangement; Porosity 41.2%; Single-Phase, Water

Flow-rate (gal/min)	N_{Re}	$\frac{N_{Re}}{1-\epsilon}$	Slope	Random-walk			Segmented laminar flow			No. of measurements
				N	P	P'	N	P	P'	
0.3	18.4	30.8	1.21	17.5	0.525	0.216	11.0	0.330	0.136	6
0.51	31.4	52.4	1.40	23.8	0.714	0.294	18.0	0.540	0.223	8
1.0	61.5	102.2	1.68	34.6	1.038	0.415	33.0	0.99	0.396	6
2.0	123.0	205.0	1.94	46.4	1.390	0.572				6
3.0	184.5	308.0	2.06	52.2	1.570	0.645				6

E. Column 5: 0.75-in. Spheres; Random Arrangements; Porosity 41.2%; Single-Phase, Water-Glycerol

Flow-rate (gal/min)	N_{Re}	$\frac{N_{Re}}{1-\epsilon}$	Slope	Random-walk N	Random-walk P	Random-walk P'	Segmented laminar flow N	Segmented laminar flow P	Segmented laminar flow P'	No. of measurements
1.0	10.2	17.0	1.21	17.0	0.510	0.210	9.5	0.284	0.117	6
2.85	29.1	48.5	1.42	24.4	0.730	0.306	18.8	0.56	0.231	4
4.7	47.9	80.0	1.65	33.2	0.993	0.398	28.1	0.840	0.346	4

F. Column 6: 0.75-in. Spheres; Orthorhombic-2 Arrangement; Porosity 39.5%; Single-Phase, Water

Flow-rate (gal/min)	N_{Re}	$\frac{N_{Re}}{1-\epsilon}$	Slope	Random-walk N	Random-walk P	Random-walk P'	Segmented laminar flow N	Segmented laminar flow P	Segmented laminar flow P'	No. of measurements
0.3	18.3	30.2	1.26	19.2	0.606	0.238	12.0	0.376	0.149	6
0.51	26.8	44.3	1.46	26.1	0.819	0.324	18.5	0.580	0.229	6
1.0	52.6	86.9	1.68	34.8	1.086	0.429	31.5	0.985	0.389	6

G. Column 7: 0.75-in. Raschig Rings;* Random Arrangement; Porosity 64.8%; Single-Phase, Water

Flow-rate (gal/min)	N_{Re}	$\frac{N_{Re}}{1-\epsilon}$	Slope	Random-walk N	Random-walk P	Random-walk P'	Segmented laminar flow N	Segmented laminar flow P	Segmented laminar flow P'	No. of measurements
0.3	16.5	46.8	1.19	16.1	0.487	0.316	10.1	0.275	0.178	8
0.51	28.1	76.6	1.32	20.9	0.603	0.392	15.3	0.416	0.269	14
1.0	55.0	156.1	1.50	27.50	0.792	0.514	25.2	0.685	0.445	10
2.0	110.0	312.1	1.65	33.4	0.961	0.622	32.0	0.870	0.564	8
3.0	165.1	468.2	1.71	35.91	1.032	0.671				6
4.86	267.4	758.5	1.76	38.10	1.100	0.710				6

*Equivalent-volume sphere diam , 0.68 in.

H. Column 7: 0.75-in. Raschig Rings;* Random Arrangement; Porosity 64.75%; Single-Phase, Water-Glycerol

Flow-rate (gal/min)	N_{Re}	$\frac{N_{Re}}{1-\epsilon}$	Slope	Random-walk N	Random-walk P	Random-walk P'	Segmented laminar flow N	Segmented laminar flow P	Segmented laminar flow P'	No. of measurements
0.32	2.9	8.2	1.02	11.5	0.313	0.202	6.0	0.163	0.106	6
0.54	5.0	14.2	1.02	11.5	0.313	0.202	6.0	0.163	0.106	6
1.0	9.2	26.1	1.15	15.6	0.450	0.292	8.4	0.228	0.148	8
1.93	17.8	50.5	1.20	17.3	0.499	0.324	11.0	0.299	0.195	8
2.85	26.2	74.4	1.31	20.2	0.574	0.379	15.3	0.418	0.272	4
4.7	43.2	122.8	1.414	24.3	0.701	0.455				4

*Equivalent-volume sphere diam , 0.68 in.

I. Column 9: 1-in. Berl Saddles;* Random Arrangement; Porosity 68.6%; Single-Phase, Water

Flow-rate (gal/min)	N_{Re}	$\frac{N_{Re}}{1-\epsilon}$	Slope	Random-walk N	Random-walk P	Random-walk P'	Segmented laminar flow N	Segmented laminar flow P	Segmented laminar flow P'	No. of measurements
0.3	18.4	58.8	1.22	17.7	0.537	0.368	11.2	0.340	0.233	10
0.51	31.4	99.9	1.36	22.2	0.675	0.463	17.3	0.525	0.360	6
1.0	61.5	195.8	1.52	28.2	0.858	0.588	25.0	0.758	0.521	8
2.0	123.0	391.7	1.62	32.4	0.985	0.676	30.1	0.945	0.646	4
3.0	184.5	587.5	1.70	35.7	1.085	0.744				4
4.86	299.9	951.7	1.73	36.5	1.111	0.764				4

*Equivalent-volume sphere diam , 0.76 in.

J. Column 10: 0.38-in. Spheres;* Random Arrangement; Porosity 42%; Single-Phase, Water

Flow-rate (gal/min)	N_{Re}	$\frac{N_{Re}}{1-\epsilon}$	Midpoint Slope	Random-walk N	Random-walk P	Random-walk P'	Segmented laminar flow N	Segmented laminar flow P	Segmented laminar flow P'	No. of measurements
				Column height; 23.7-in.						
0.3	9.6	16.6	1.72	36.20	0.595	0.252	34.9	0.576	0.240	6
0.51	16.3	28.1	1.73	36.3	0.605	0.254	35.0	0.579	0.243	6
1.0	32.0	55.3	1.94	46.3	0.774	0.325	(46.3)	(0.774)	(0.325)	6
2.0	64.0	110.5	2.22	61.0	1.020	0.428	(61.0)	(1.020)	(0.428)	6
				Column height; 12.0-in.						
0.3	9.6	16.6	1.14	15.5	0.526	0.221	8.5	0.288	0.121	8
0.51	16.3	28.1	1.20	17.3	0.586	0.246	10.0	0.339	0.142	6
1.0	32.0	55.3	1.39	23.4	0.794	0.333	17.3	0.585	0.244	6
2.0	64.0	110.5	1.60	31.4	1.040	0.437	29.0	0.980	0.410	8

*Equivalent-volume sphere diam , 0.76 in.

Summary of Jacques's Data for High Flow Rates

Column No.	Packing description	N_{Re}	$\frac{N_{Re}}{1-\epsilon}$	P	P'
1	Tetragonal (0.75-in. spheres) $\epsilon = 0.32$	646 1940	950 2853	2.442 2.448	0.781 0.783
2	Orthorhombic-1 (0.75-in. spheres) $\epsilon = 0.38$	646 1940	1042 3129	1.893 1.881	0.719 0.715
4	Random (0.25-in. polyethylene pellets) $\epsilon = 0.35$	528	812	2.082	0.729
5	Random (0.75-in. spheres) $\epsilon = 0.412$	646 1940	1099 3299	1.838 1.858	0.757 0.765
6	Orthorhombic-2 (0.75-in. spheres) $\epsilon = 0.395$	646 1940	1068 3207	1.885 1.903	0.745 0.752
7	Random (0.75-in Raschig rings) $\epsilon = 0.648$	560	1.591	0.909	0.589

PART III. LONGITUDINAL DISPERSION IN COUNTERCURRENT LIQUID FLOW

A. Introduction

The usual textbook method for designing a packed extraction column, as introduced by Colburn, involves computing the number of transfer units (NTU) required to bring about a given extraction, and multiplying this number by a height factor (the HTU) determined from direct or indirect experience.[1] For extraction columns, the HTU values vary widely with the physical properties of the two phases, the nature and amount of solute, and rates of flow, making it necessary to obtain very specific data for the contemplated design. Numerous experimental studies have been conducted to measure effective mass-transfer coefficients and HTU's in extraction columns; these have been reviewed by Elgin and Wynkoop[4] by Treybal,[13] and by Vermeulen et al.[17]

The mathematical definition of HTU is based upon a piston-flow model for each of the two counterflowing phases. The actual phases would appear to be far from homogeneous at any one cross-section, and the complex flow behavior within the packing would seem to produce considerable "back mixing" within each phase. For systems with still more evident internal mixing, such as multicompartment agitated reactors[18] and pulsed extraction columns,[16] longitudinal dispersion is known to control the performance.

The phenomenon of axial mixing or longitudinal dispersion arises from the fact that a molecular-scale "packet" of fluid does not move through a bed at a constant velocity, nor usually at the same local velocity as other packets passing a given point. These fluctuations appear to result from (a) separation of the flow into filaments taking different paths through the packing, and (b) eddy motion of the fluid. The former appears to be more characteristic of a laminar-flow regime, and the latter is probably more characteristic of turbulent flow, but the possibility also exists of the two effects occurring together.

Longitudinal dispersion in an extraction column has the effect of reducing the driving potential for mass-transfer substantially, so

that a longer column (for any given mass-transfer coefficient) is required to produce the same overall separation. It thus becomes evident that any design correlation of mass-transfer coefficients or HTU values should account separately for longitudinal dispersion rather than submerge its effect into apparent mass-transfer behavior. Mathematical relations have been developed for this purpose which are described below. Therefore, the present investigation was conducted to measure the longitudinal-dispersion coefficients in counterflowing liquid-liquid systems (in the absence of actual extraction), in order to provide the numerical parameters needed for both interpretation and design of steady-state extraction operations in packed beds. Measurements have been made for both the continuous and the dispersed phase, with separate results for the latter in the cases where it does or does not wet the packing material.

1. Mathematical Treatment

A diffusion model for describing the influence of longitudinal dispersion in countercurrent systems undergoing mass transfer between the phases has been developed by Miyauchi[10] and Sleicher.[12] The dispersion effect for each phase is described by an effective longitudinal diffusivity E_i. The basic equations obtained by material balance in a differential slice of the column, for the X phase and Y phase respectively, are

$$d^2C_x/dZ^2 - P_xB\, dC_x/dZ - N_{ox}P_xB(C_x - mC_y) = 0 \quad (1)$$

and

$$d^2C_y/dZ^2 + P_yB\, dC_y/dZ + N_{oy}P_yB(C_x - mC_y) = 0 \quad (2)$$

with the boundary conditions:

at $Z = 0$, $dC_x/dZ = P_xB(1 - C_{xo})$

and $dC_y/dZ = 0$;

at $Z = 1$, $dC_y/dZ = 0$

and $dC_y/dZ = P_yB(C_{y1} - C_y^1)$;

where:

P_i = $U_i d_p / E_i$, Péclet number of ith phase,

B = h/d_p = dimensionless length,

h = column height,

d_p = particle diameter,

Z = dimensionless length variable, ranging from zero at the X-feed end to unity at the Y-feed end of the column,

C_i = dimensionless concentration in the i phase measured at a point Z expressed relative to X-feed concentration. The number accompanying C, if a subscript, is the Z value inside the column; if it is a superscript (0 or 1), it is the Z value in the feed or product stream outside the column,

m = slope of equilibrium curve, dC^*_x/dC_y,

N_{oi} = True overall number of transfer units for the ith phase,

N_{oy} = ΛN_{ox},

Λ = $\dfrac{m(U_0)_x}{(U_0)_y}$ = extraction factor,

U_i = mean linear velocity of the ith phase,

and

$(U_0)_i$ = superficial velocity of the ith phase.

Equations (1) and (2) are differential equations of the second order with constant coefficients. Their solution, obtained by differentiation and subsequent integration of a single fourth-order equation, gives the concentration of any point inside the column.[10] Figure III-1 shows representative behavior of the concentration profiles in an extractor, for piston flow (broken lines) and for axial dispersion (solid lines). The decrease in driving force due to axial mixing is shown by the arrows. Graphical and tabular results corresponding to the solution of Eqs. (1) and (2) have been provided by McMullen, Miyauchi and Vermeulen.[8, 9] The solutions are obtained in the form

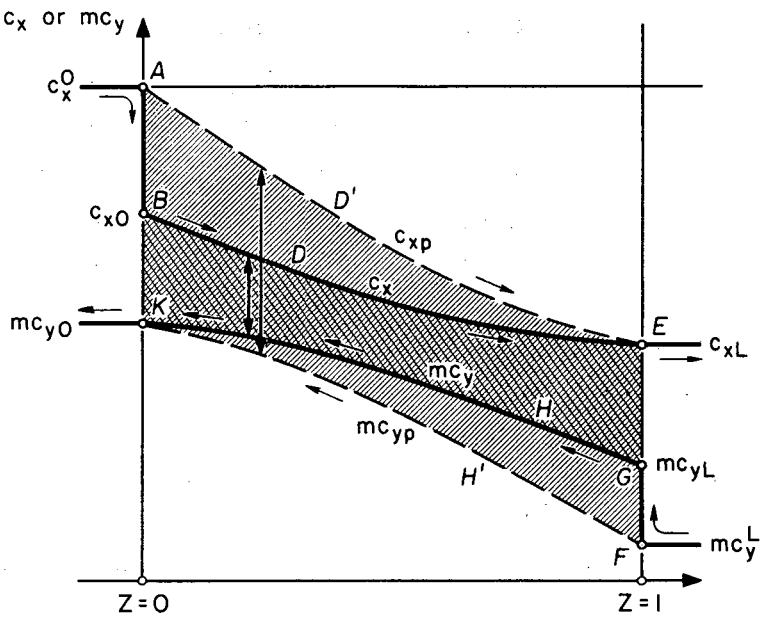

Fig. III-1. Concentration profile in a typical extraction.

$$X = X(N_{ox}, A, P_xB, B_yB, Z) \tag{3}$$

and

$$Y = Y(N_{ox}, A, P_xB, P_yB, Z) . \tag{4}$$

The outlet concentrations are, at $Z = 1$,

$$X_1 = \frac{C_{x1} - (Q + mC_y^1)}{1 - (Q + mC_y^1)}, \tag{5}$$

and, at $Z = 0$,

$$Y_o = \frac{m\left(C_{yo} - C_y^1\right)}{1 - (Q + mC_y^1)} . \tag{6}$$

Here Q is the intercept of a linear-equilibrium plot,

$$C_x^* = Q + mC_y . \tag{7}$$

Ideally one should be able to establish the value of any one parameter from a knowledge of the other parameters. The practical use of Eqs. (3) and (4) has been facilitated by the derivation of several empirical relations between the different parameters.[9] An apparent NTU, as given from Underwood's result,[14] has been defined as

$$N_{oxP} = \frac{1}{1 - A} \ln\left[\frac{1 - A(1-X_1)}{X_1}\right]. \tag{8}$$

The subscript P indicates that the definition stems from a "piston-flow" model. The true NTU can be related to the apparent NTU by a difference in reciprocals:

$$\frac{1}{N_{oxP}} - \frac{1}{N_{ox}} = \frac{1}{N_{oxD}} . \tag{9}$$

Here N_{oxD} is related to P_xB and P_yB by an approximate empirical equation

$$\frac{1}{N_{oxD} - \ln A/(A-1)} = \frac{A}{f_x P_x B} + \frac{1}{f_y P_y B}, \tag{10}$$

where f_x and f_y are weighting factors which are functions of N_{ox} and A.[9] At $A = 1$, the term $(\ln A)/(A-1)$ reduces to unity, and $f_x = f_y = 1$. By the use of these relations, it should be possible to carry out any of the following calculations:

(1) From an experimental X_1, and experimental P_xB and P_yB, to determine the true N_{ox}.

(2) From an experimental X_1, and a correlational N_{ox}, to determine an experimental N_{oxD}.

(3) From experimental or correlational P_xB, P_yB, and N_{ox} values, to predict the X_1 value for a column to be designed or operated.

2. Analysis of Experimental Data

The column Péclet-number values (P_iB) for the individual phases can be determined independently of any extraction operation by use of tracer techniques for unsteady-state flow. Such methods involve the injection of a tracer into one phase, the tracer being insoluble in the other phase. Similarly to the "one-phase" study, a step input of salt solution was used as a tracer and a breakthrough curve was obtained by conductivity measurements. The resulting breakthrough curve is related to the dispersion coefficient by a suitable mathematical model. Van de Vusse has shown that the diffusion model is applicable to both continuous and discontinuous phases.[15] For convenience we analyzed our data by the random-walk model, which as we have shown (Part I) is equivalent to the diffusion model with finite boundaries. An alternate model, that of segmented laminar flow, was not used because it was found to fit more poorly than random walk or diffusion in the single-phase studies (Part II).

Based on the random-walk model, Péclet numbers were obtained by comparing the experimental curve with theoretical ones on semilog coordinates, or by applying the simple relation

$$N = 4\pi(s')^2 - 0.80, \qquad (11)$$

where s' is the midpoint slope measured on a t/t_{50} time scale (see Part II).

B. Apparatus and Procedure

1. Columns

Nine different columns were used for the investigations, three with ordered packings and octagonal or hexagonal cross-sections and six with random packings and circular or octagonal cross-sections. The column dimensions are given in Table III-I and described in more detail in Part II.

2. Conductivity Cells

Conductivity was used to determine the breakthrough curve for the aqueous phase. When water is the continuous phase, the conductivity cells were the same as those used for single phase experiments; they were constructed of two spherical sections of 3.4-in. Bakelite spheres, connected by a pair of rhodium-plated pins. When the aqueous phase was the dispersed one, the breakthrough curves were recorded by a special conductivity cell used by Dunn et al.[3] in their study of gas-absorption columns. A photograph of the cell used is shown in Fig. III-2, and a cross-sectional drawing in Fig. III-3. The conducting discontinuous phase entered the sampler through the funnel-shaped top and left through the post in the side. The probe was fixed just under the packed column in the expanded column head. The conductance of the solution between the pins was determined by the same electronic equipment as the one that is used in the continuous-phase and single-phase work (see Part II).

3. Feed Nozzle

Special consideration was given to the nozzle through which the discontinuous phase is introduced. Uniform drop size was desired in order to achieve uniform drop rise or fall with minimum of coalescence of the drops. According to Johnson and Bliss,[7] velocity at the hole has to be maintained between 1000 and 1500 ft/hr and a hole diameter of 0.10-in. seems to be the optimum. Consequently the distribution nozzle was designed with a set of six removable plates, varying in number of holes (from 37 to 169) to provide the wide range of flow rates required.

Table III-I. Discussions and packing of experimental columns

Column number	Packing	d_{eff}	$(d_p)_v$ (in.)	Arrangement	Fraction of voids (%)	Sphericity	Height for continuous phase runs	Height for dispersed phase runs	Cross-sectional area ($in.^2$)
1[a]	Spheres	0.75	0.75	Tetragonal	32.0	1.0	23.6	24.0	30.3
2[a]	Spheres	0.75	0.75	Orthorhombic-1	38.0	1.0	23.0	24.1	30.3
5[a]	Spheres	0.75	0.75	Random	41.2	1.0	25.0	24.0	30.7
6[a]	Spheres	0.75	0.75	Orthorhombic-2	39.5	1.0	24.0	25.2	30.6
7[a]	Ceramic rings	0.75	0.65	Random	64.8	0.42	23.6	24.0	30.7
9	Berl saddles	1.0	0.76	Random	68.6	0.33	25.0	25.0	30.7
10[b]	Spheres	0.38	0.38	Random	42.0	0.95	25.0	24.0	30.7
11[b]	Ceramic rings	0.50	0.48	Random	62.0	0.54	24.0	24.0	30.7
12	Carbon rings	0.75	0.72	Random	67.0	0.40	23.6	24.0	30.7

[a] Packing used by Jacques[5]

[b] Packing used by Cotter[6]

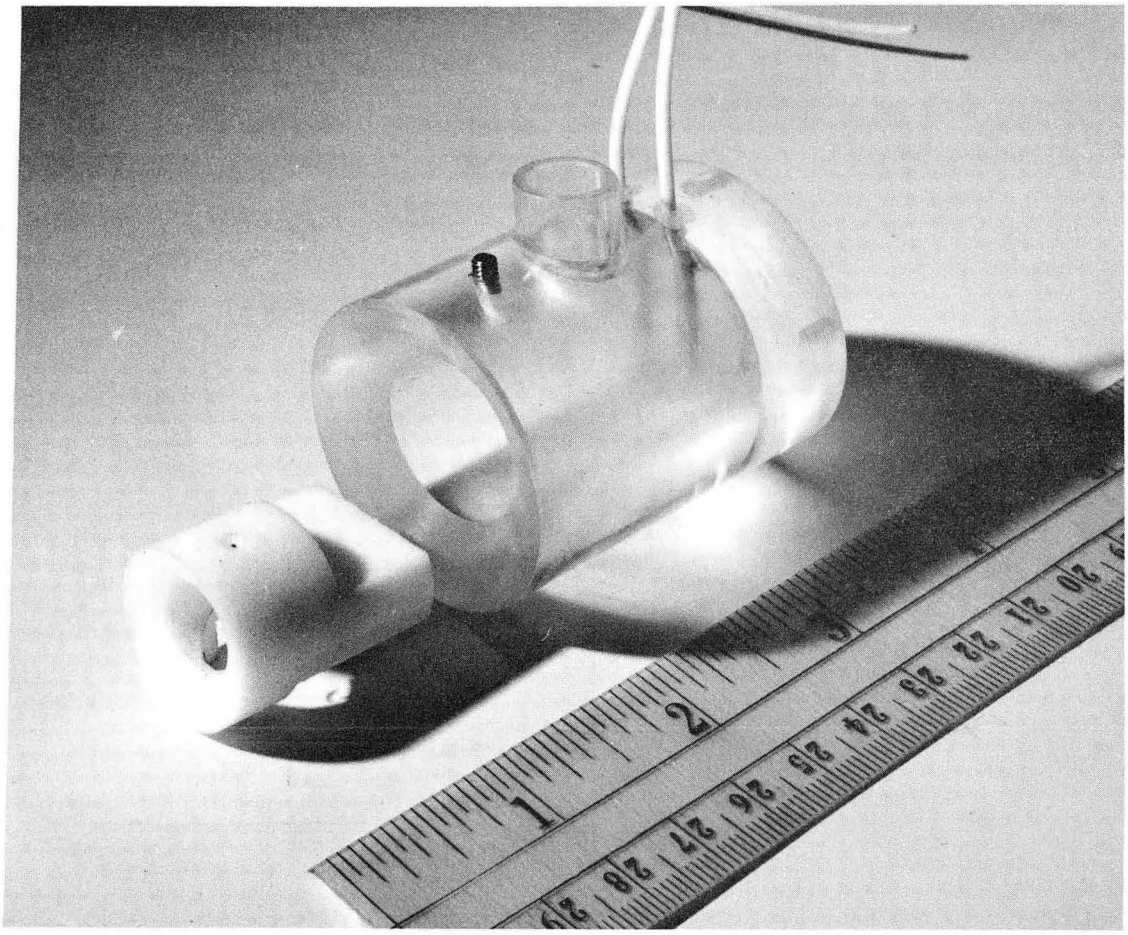

ZN-2876

Fig. III-2. Liquid conductivity cell.

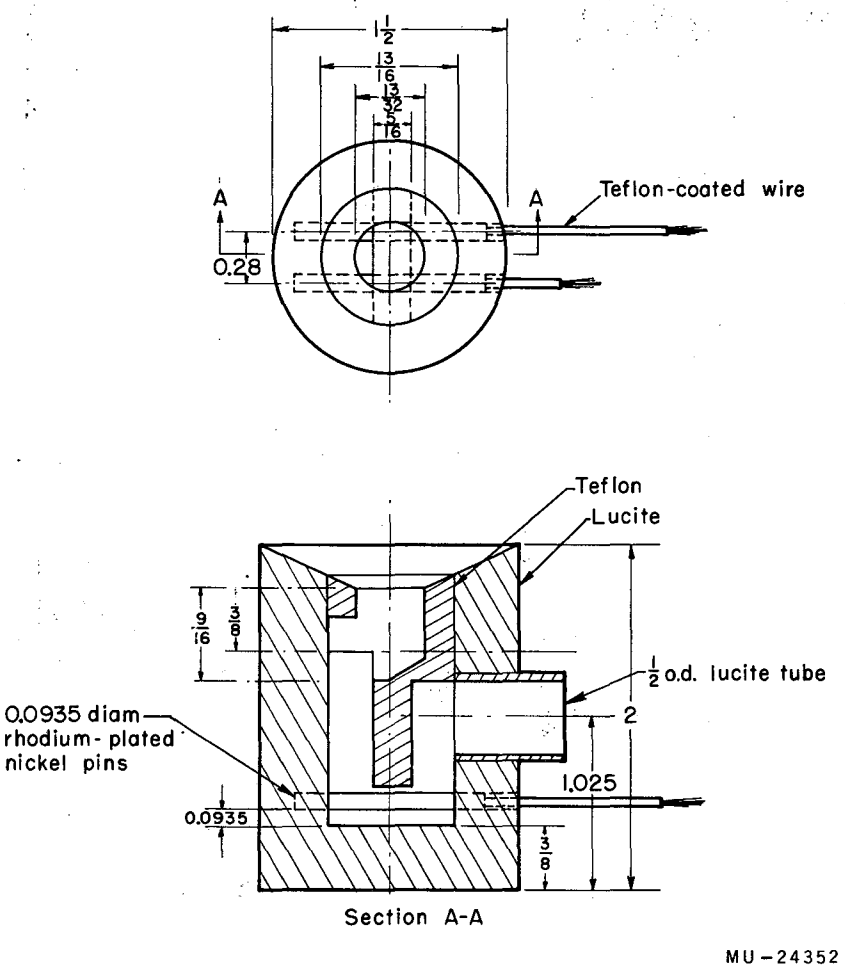

Fig. III-3. Cross-sectional drawing of a liquid-conductivity cell.

Five of these had 0.10-in.-diam holes, while the sixth, for high flowrates, had 0.15-in. holes to avoid too great a drop in pressure.

4. Liquid-Level Control

The interface could be maintained at the top or bottom of the packing, depending on whether the water phase was continuous or dispersed. Two Teflon-covered nickel-rod probes were mounted in each head section for this purpose. These probes were slightly staggered in level to provide a neutral zone. Originally, they were connected to a solenoidal valve or to the outlet water line, which was bypassed by a manually adjustable gate valve. Later, a single-speed floating control was adapted, with all probes connected to a motorized-valve controller, and the column grounded to complete the circuit. With this system, a probe would conduct when immersed in the water phase. The outlet water valve opened when both probes conducted and closed when neither did.

5. Piping Arrangement

The organic phase (kerosene) and tracer solution were piped from storage tanks with centrifugal pumps. Water was supplied from a constant-head tank, about 25 ft above the column, under gravity flow. The incoming flows were manifolded and valved, so as to meter each of them through the appropriate unit in a bank of six rotameters. The organic phase was returned to the supply tanks through an overhead line, and the water was drained to the sewer.

6. Start-Up

At the beginning of a run, continuous phase was allowed to fill the column, and flow of the dispersed phase was then started. Experimental measurements were made only when the interface was made stationary by close adjustment of the outlet flow rates. This precaution was essential for the following reasons. First, if the interface changes, the flowrates in the column are different from those indicated by the rotameters. Second, due to the level change, the outlet valve closes, causing an abrupt change in the continuous-phase flowrate, which affects the dispersion rates in both phases.

7. Conductivity Measurements

a. Water as the continuous phase. When steady-state flow was reached for both phases, a solution of sodium nitrate (0.1N) was injected in an amount from 0.25 to 2.0 volume-percent of the water stream. The starting time was noted by a pip on the strip-chart recorder. When the breakthrough curve leveled off to a steady-state value, injection was stopped, and a second strip-chart record was taken to measure the purging of the tracer solution. The breakthrough curves recorded were not as smooth as in single-phase experiments because of the interference of droplets of the discontinuous organic phase in the conductance path; these fluctuations were averaged out for Péclet-number computation.

b. Water discontinuous. For water dispersed, the breakthrough curves were again measured by conductivity, using the special probe described above. The same steps already outlined were taken to establish steady-state flow in the column, to set the liquid level below the new conductivity probe, to inject the tracer, and to record the breakthrough curves. As the organic phase was excluded from the interior of this probe, the curves were as smooth as in single-phase experiments.

All runs were made at an ambient temperature of 68 ± 2°F. At this temperature, the kerosene used had a viscosity of 2.46 cP and a density of 0.820 g/cm^3.

C. Results and Discussion

1. Continuous Phase

The results of measurements of longitudinal dispersion in the continuous phase, using the methods just described, are shown in Appendix III-1. Related data taken by Jacques[5] and Cotter,[6] which will be used to obtain a generalized correlation, are also given in Appendix III-1. These tables report both the packing Péclet number P_c itself and the product ϵP_c, which will be used in the correlation to account for the effect of void space available to the continuous phase. In each system studied, the modified Péclet number for the continuous phase ϵP_c was

found to increase with increasing superficial velocity of the continuous phase, and to decrease with increasing superficial velocity of the dispersed phase.

One would also expect Péclet numbers to be functions of the type of channels encountered by the flowing fluid. Some measurable variables that affect the channel shapes are the size (d_p), sphericity (ψ), and porosity (ϵ) of the packing material. The particle sphericity is defined as the ratio A_s/A_p, where A_s is the surface area of a sphere having the same particle volume, and A_p is the surface area of the particle. The data from Appendix III have been correlated in terms of these variables. The runs available are insufficient to distinguish between the effects of sphericity and void-fraction. A linear regression based on the four factors U_{c0}, U_{d0}, d_0, and ψ showed a 98% correlation coefficient for a dependence of ϵP upon the terms

$$\frac{\psi^{0.53}\, U_{d0}^{0.46}}{d_p^{0.29}\, U_{c0}^{0.76}} \,. \tag{12}$$

In using this correlating function we assumed a straight-line relation between logarithms, whereas, in fact ϵP should converge asymptotically upon the single phase value as U_d decreases. Nevertheless, the regression was of major assistance in determining a suitable plotting function.

It also appeared that "backmixing" in the continuous phase is produced by entrainment of that phase by the dispersed-phase droplets. This effect would increase with the kinematic viscosity; introduction of a viscosity term would render the correlating group dimensionless. With some further trial of the effects of different exponents, the following correlation was tentatively adopted:

$$\epsilon P_c = \text{fn}\left[\left(\frac{\psi \nu}{d_p U_{c0}}\right)^{1/2}\left(\frac{U_{d0}}{U_{c0}}\right)\right]. \tag{13}$$

A dimensional correlating factor of somewhat different form, $d_p U_{d0}/\psi U_{c0}^2$, was suggested by Cotter,[6] based on a smaller number of

run conditions. In his calculations, the runs at smaller d_p and high ψ were weighted differently by a preponderence of low U_{c0} values. Unlike his correlating factor, the one now adopted does provide the prospect of accounting for a possible viscosity effect, in an entirely dimensionless form. Another correlational possibility that has not yet been explored, but should await further experimental data, is the use of $P_c P_o$ as the ordinate, where P_o is the Péclet number for single-phase flow in the same packing. (The same superficial velocity and the same mean linear velocity should both be tried as possible bases.) Jacques[5] and Cotter[6] both appear to have used P_c/P_o, but their P_o was always taken as the limiting laminar-flow value, thus giving an ordinate really proportional to our ordinate ϵP_c.

Figure III-4 shows the data of Appendix III-1, plotted on the coordinates indicated by Eq. (13). This figure indicates the different asymptotes for different continuous-phase Reynolds numbers.

2. Dispersed Phase

The results of a few dispersed-phase measurements are shown in Appendix III-2 and in Fig. III-5. The different packings used were: (Column 7) 3/4-in. ceramic Raschig rings; (Column 9) 1-in. Berl saddles; and (Column 12) 3/4-in. carbon Raschig rings.

For the carbon packing (nonwetting phase discontinuous), the Péclet number remains practically constant over the full range of U_{c0} and U_{d0} values studied; whereas, for ceramic Raschig rings, P decreases slightly with increasing U_{d0}, although it increases slightly with increasing U_{c0}.

In previous studies[5,6] with kerosene dispersed in water, and with the breakthrough curves (for a step input of dye) obtained by photoelectric measurement, the dispersed-phase Péclet numbers were much smaller than those found here. It is possible, in the earlier measurements, that additional mixing occurred in the measuring region, thus leading to unduly low Péclet-number values. It appears to be simpler and more accurate to monitor the continuous phase in the presence of

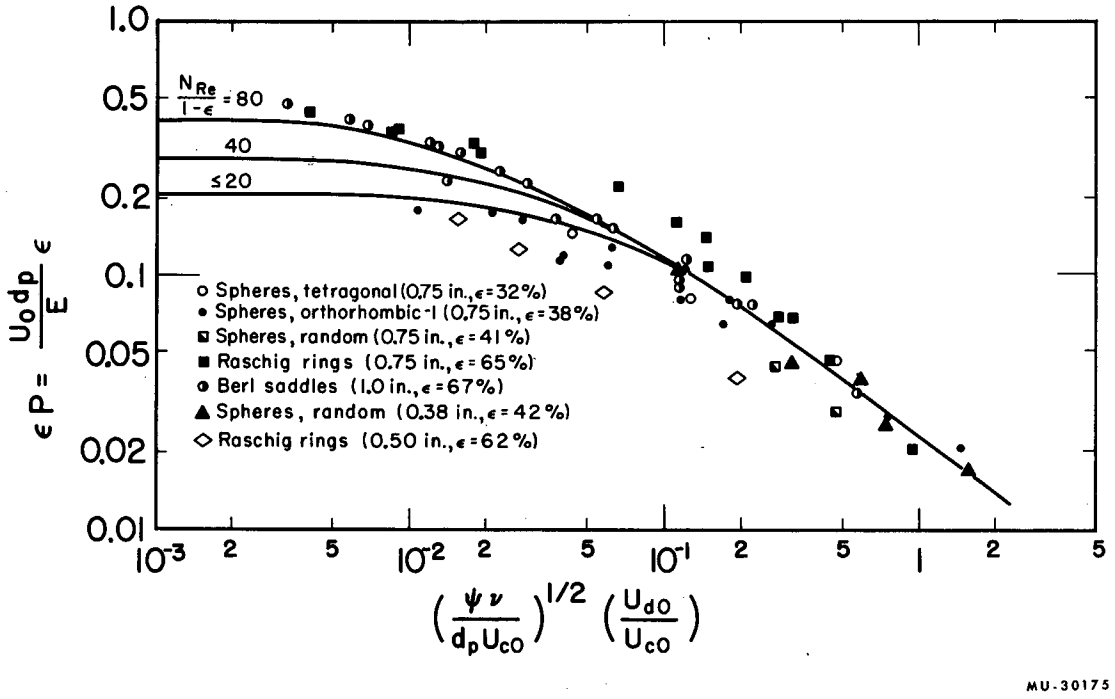

Fig. III-4. Dimensionless correlation for continuous-phase Péclet number.

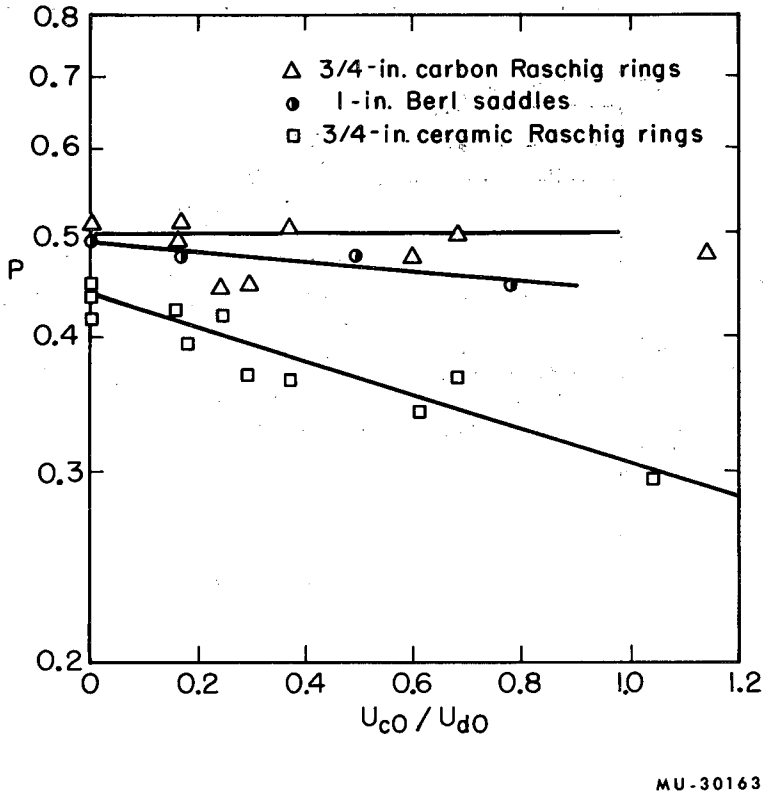

Fig. III-5. Discontinous-phase Péclet number.

dispersed phase than the reverse. In general it is necessary to collect an appreciable quantity of dispersed phase in order to measure its properties. It is essential to do this collecting under piston flow conditions, and then a correction must be made for the time lag involved. (In the present study, this time lag is estimated at 2 to 5% of the total time elapsed at the point of measurement.)

Since the present measurements are higher than previous values,[6] they show the need for much more data before correlation can be attempted.

D. Application to Packed-Column Extraction

The experimental Péclet-number values obtained should be of direct use, in conjunction with experimental extraction data from an operating column, to determine the true mass-transfer rates in such a column. To illustrate the calculation, and also to determine the typical magnitude of the correction from apparent to actual rates, data from Colburn and Welsh[2] have been selected, in which the transfer resistances lie almost entirely in a single phase.

The method outlined previously [Eqs. (8) to (10)] does not give precise results when applied to this limiting case. However, since no appreciable change in concentration (or activity) occurs in the "inactive" phase which does not offer a transfer resistance (to water or to isobutanol) a separate algebraic result by Miyauchi can be applied.[10] Complete mixing of the inactive phase can be assumed, indicated by $P_y B = 0$. The applicable relation is then

$$N_{oxP} = \ell n \frac{N_{ox}\left(e^{-\lambda_2} - e^{-\lambda_1}\right) + \lambda_1 e^{-\lambda_2} - \lambda_2 e^{-\lambda_1}}{P_x B (1 + 4r)^{1/2}}, \qquad (14)$$

where

$$\lambda_1 = (P_x B/2)\left[1 + (1 + 4r)^{1/2}\right], \qquad (15)$$

$$\lambda_2 = (P_x B/2)\left[1 - (1 + 4r)^{1/2}\right], \qquad (16)$$

and

$$r = N_{ox}/P_x B. \qquad (17)$$

This relation is illustrated graphically in Fig. III-6 where N_{oxP} is plotted against N_{ox} for several values of P_xB. A simple empirical relation, equivalent to Eq. (14) but explicit in N_{ox}, has been developed by Moon:[11]

$$N_{ox} - N_{oxP} = \frac{0.96(N_{oxP})^2}{P_xB + 0.63} . \qquad (18)$$

Smoothed values for the apparent HTU were taken from Colburn and Welsh's work, at superficial velocity values (G_x) of 1000 lb/hr-ft^2 for the "active" phase. The steps involved in estimating the actual HTU values are given in Table III-II, and the resulting values are compared with the apparent HTU in Fig. III-7 for the continuous phase only. In this particular system, the ratio H_{cP}/H_c is seen to vary from 1.1 to 1.8 for the continuous phase.

If the higher P values found for the dispersed phase are confirmed for further studies, then the ratio H_{dP}/H_d will be much nearer to 1.0 probably in the range 1.10 to 1.20 for usual operating conditions.

Although the example chosen was a somewhat simplified case, where transfer resistance lies only in one phase, the conclusion drawn should apply even more to cases where dispersion occurs in both phases. The exact calculations for the general case are quite complicated but can be substituted for by rapid approximate methods.[9]

From the values obtained, it is seen that for cases where simultaneously the dispersed-phase flowrate is large and the continuous-phase flowrate is small, the dispersion effect may dominate the effective HTU. For small dispersed-phase flowrates with large continuous-phase flows, mass transfer will often provide the principal resistance; however, in scaling-up to larger packings, both effects should still be considered. Thus, it can be concluded that the longitudinal dispersion will often have a substantial influence on the efficiency of an extraction column.

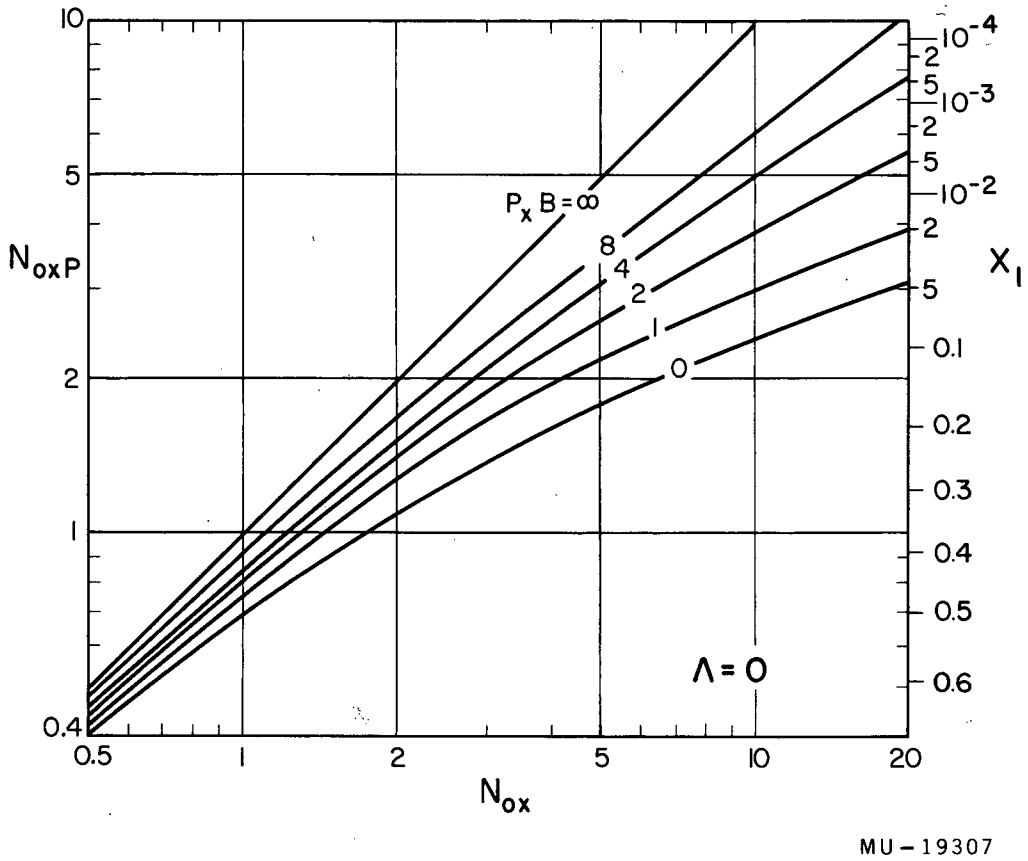

Fig. III-6. N_{oxp} as a function of N_{ox} and $P_x B$ with $\Lambda = 0$.

Table III-II. Single-phase extraction studies of water-isobutanol system[a] (G_x = 1000 lb/hr ft^2; Column height, 1.75 ft)

G_y	H_{xp}	N_{xp}	ϵP_c	$P_x B$	N_x	N_{xp}/N_x	H_x
Continuous phase: water							
250	3.50	0.50	0.125	6.12	0.536	0.931	3.264
500	1.50	1.17	0.095	4.29	1.437	0.814	1.218
750	0.87	2.01	0.075	3.39	2.975	0.676	0.588
1000	0.64	2.74	0.065	2.94	4.760	0.575	0.367
Continuous phase: isobutanol							
500	3.50	0.50	0.086	3.90	0.553	0.904	3.160
750	2.60	0.68	0.065	2.94	0.804	0.846	2.177
1000	2.00	0.88	0.052	2.34	1.130	0.779	1.549

[a] From Ref. 2.

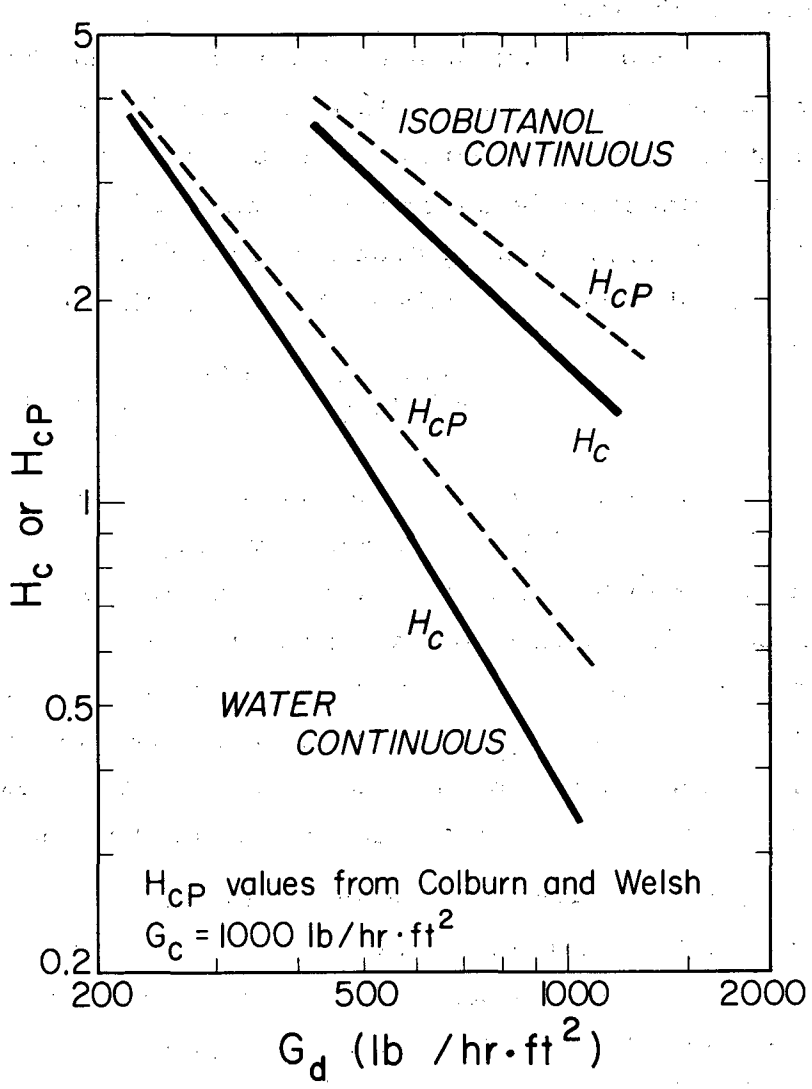

Fig. III-7. N_c and N_{cp} for isobutanol-water system.

E. Conclusions

Analysis of the results obtained in this study of axial dispersion in two-phase countercurrent flow through packed beds leads to the following conclusions:

(1) The axial Péclet number of the continuous phase increases with increasing continuous-phase flow rate and decreases with increasing discontinuous-phase flowrate. It is believed that the decrease relative to the single-phase behavior may be caused by intermittent entrainment of the continuous phase by droplets of the dispersed phase. The modified Péclet number (ϵP) is believed to be a function of the dimensionless parameter

$$\psi^{1/2}\left(\frac{\nu}{d_p U_{co}}\right)^{1/2}\left(\frac{U_{co}}{U_{do}}\right);$$

the effect of viscosity, only, has not yet been confirmed quantitatively.

(2) The axial Péclet number of a wetting discontinuous-phase decreases somewhat with decreasing continuous-phase flowrate and with increasing discontinuous-phase flowrate. For a nonwetting dispersed phase, the Péclet number remains practically constant over the full range of U_{co} and U_{do} values studied. Previous invetigations[6] gave Péclet values much smaller than obtained in the present study; this appears to be a result of the experimental methods used.

(3) True mass-transfer rates were computed from experimental extraction data,[2] using the measured continuous-phase axial-dispersion coefficients. For the particular system used it is seen that the true H_x is from 10 to 80% smaller than the piston flow H_{xP}. Although only a simplified example, for which the mass-transfer resistance lies in one phase, was investigated, its result should apply to the general case where approximate methods of solution are available.[9]

F. Notation for Part III

A	Surface area of packing particle.
B	Dimensionless height, h/d_p
C	Dimensionless concentration, c/c_x^0
c	Concentration
d_p	Particle diameter
E	Superficial dispersion coefficient
f	Weighting factor in correlation, Eq. (10)
G	Superficial mass velocity
H_{ox}	Overall height of transfer unit, relative to X phase
h	Total height of packed section of column
k	Mass-transfer coefficient
m	Partition ratio; c_x/c_y at equilibrium
N_i	Péclet number for the column; hU/E
N_{ox}	Overall number of transfer units, relative to X phase
N_{Re}	Reynolds number; $d_p(U_0)_c/\nu$
P	Péclet number for the packing; N_{Pe}
s	Dimensionless midpoint slope of breakthrough curve (based on t/t_{50} scale)
t	Time
U	Mean interstitial velocity
Z	Dimensionless height, z/h
z	Height within column
ϵ	Void-fraction or porosity
Λ	Extraction factor; $m(U_0)_x/(U_0)_y$
ν	Kinematic viscosity
ψ	Sphericity of the packing; (area of a sphere having the particle volume)/(actual area of particle)

Superscripts

0	Feed end of column, outside the column
1	Solvent-entering end of column, outside the column

Subscripts

c	Continuous phase
D	Dispersion unit
d	Dispersed phase
f	Final
i	For the "i" phase; as yet undesignated
o	Overall
o,0	Initial
0	Superficial
P	Exterior apparent value, conforming to piston-flow model
x	For the X phase (usually the feed or raffinate)
y	For the Y phase (usually the solvent extract)
0	Feed end of column, inside the column
1	Solvent-entering end of column, inside the column

References for Part III

1. A. P. Colburn, Trans. Am. Inst. Chem. Engr. 29, 174 (1939); Ind. Eng. Chem. 33, 459 (1941).
2. A. P. Colburn, and D. G. Welsh, Trans. Am. Inst. Chem. Engrs. 38, 179 (1942).
3. W. E. Dunn, T. Vermeulen, C. R. Wilke, and T. T. Word, Lawrence Radiation Laboratory Report UCRL-10394 (1962).
4. J. C. Elgin, and R. Wynkopp, in J. H. Perry, Chemical Engineers' Handbook, 3rd ed. (McGraw-Hill Book Company, Inc., New York, 1950).
5. G. L. Jacques, and T. Vermeulen, University of California Radiation Laboratory Report UCRL-8029, 1957 (unpublished).
6. G. L. Jacques, J. E. Cotter, and T. Vermeulen, Lawrence Radiation Laboratory Report UCRL-8658, 1959 (unpublished).
7. H. F. Johnson, and H. Bliss, Trans. Am. Inst. Chem. Engrs. 42, 331 (1946).
8. A. K. McMullen, T. Miyauchi, and T. Vermeulen, University of California Radiation Laboratory Report UCRL-3911-Suppl., 1958 (unpublished).
9. T. Miyauchi, and T. Vermeulen, Ind. Eng. Chem. Fundamentals 2, (May 1963).
10. T. Miyauchi, University of California Radiation Laboratory Report UCRL-3911, 1957 (unpublished).
11. J. S. Moon, (Lawrence Radiation Laboratory) private communication.
12. C. A. Sleicher, A. I. Ch. E. J. 5, 145 (1959).
13. R. E. Treybal, Liquid Extraction (McGraw-Hill Book Company, New York, 1962).
14. A. J. W. Underwood, Ind. Chemist 10, 129 (1934).
15. J. G. Van de Vusse, Chem. Eng. Sci. 10, 229 (1959).
16. T. Vermeulen, A. L. Lane, H. R. Lehman, and B. Rubin, University of California Radiation Laboratory Report UCRL-718, 1950, and UCRL-2983, 1955 (unpublished), revision in progress.

17. T. Vermeulen, N. N. Li, J. S. Moon, and T. Miyauchi, paper presented at A. I. Ch. E. Meeting, New Orleans (1961).
18. S. Yagi, and T. Miyauchi, Chem. Eng. (Japan) 17, 382 (1953); ibid 507 (1955).

Appendix for Part III

III-1. Experimental Data

A. Continuous-Phase Péclet Numbers for Kerosene in Water, 1-in. Berl Saddles

F_c (gal/min)	U_{co} (ft/hr)	F_d (gal/min)	U_{do} (ft/hr)	U_{do}/U_{co}	$\left(\frac{\nu\psi}{d_p U_{co}}\right)^{1/2} \frac{U_{do}}{U_{co}}$	N_c	P_c	ϵP_c	No. of measurements
2.21	83.2	0.15	5.6	0.0673	0.0033	22.80	0.693	0.478	6
		0.31	11.7	0.1406	0.0069	18.90	0.574	0.396	6
		0.58	21.8	0.2620	0.0129	15.60	0.474	0.327	4
		0.71	26.7	0.3209	0.0158	14.60	0.443	0.306	6
1.53	57.6	0.15	5.6	0.0972	0.0058	19.5	0.593	0.409	6
		0.31	11.7	0.2031	0.0120	16.2	0.492	0.339	6
		0.58	21.8	0.3785	0.0224	12.3	0.373	0.257	4
		0.97	36.5	0.6337	0.0375	8.0	0.243	0.168	6
0.85	32	0.15	5.6	0.1750	0.0139	11.3	0.343	0.237	8
		0.31	11.7	0.3656	0.0290	11.0	0.334	0.230	6
		0.58	21.8	0.6813	0.0540	8.0	0.243	0.168	6
		1.23	46.5	1.450	0.1152	4.20	0.128	0.0883	6
0.5	19.2	0.31	11.7	0.6094	0.0624	7.24	0.220	0.152	6
		0.58	21.8	1.1354	0.1162	4.5	0.137	0.0945	6
		0.97	36.5	1.9010	0.1946	3.20	0.097	0.0669	6
0.33	12.4	0.31	11.7	0.9435	0.1202	5.43	0.165	0.1138	6
		0.58	21.8	1.7581	0.2239	3.20	0.097	0.0669	6
		1.50	56.4	4.5484	0.5793	1.66	0.050	0.0345	8

B. Continuous-Phase Péclet Numbers for Kerosene in water, 0.75-in. Raschig Rings

F_c (gal/min)	U_{co} (ft/hr)	F_d (gal/min)	U_{do} (ft/hr)	U_{do}/U_{co}	$\left(\frac{\nu\psi}{d_p U_{co}}\right)^{1/2} \frac{U_{do}}{U_{co}}$	N_c	P_c	ϵP_c	No. of measurements
2.21	83.2	0.15	5.6	0.0673	0.00404	25.2	0.685	0.445	6
		0.31	11.7	0.1406	0.00845	21.3	0.579	0.376	6
		0.44	16.6	0.1995	0.0120	19.1	0.519	0.337	6
		0.66	24.8	0.2981	0.0179	18.8	0.511	0.332	6
1.3	48.9	0.15	5.6	0.1145	0.00896	21.9	0.596	0.387	6
		0.31	11.7	0.2393	0.0187	17.2	0.468	0.304	6
		0.58	21.8	0.4458	0.1104	12.7	0.345	0.224	6
0.85	32	0.31	11.7	0.3656	0.0659	13.40	0.364	0.237	6
		0.71	26.7	0.8344	0.1495	7.90	0.215	0.140	6
		0.97	36.5	1.1406	0.2044	5.6	0.152	0.099	6
		1.50	56.4	1.7625	0.3160	3.8	0.104	0.0676	6
0.51	19.2	0.31	11.7	0.6094	0.0761	8.49	0.231	0.150	6
		0.58	21.8	1.1354	0.14181	5.60	0.152	0.0988	6
		1.50	56.4	2.9375	0.3669	2.86	0.077	0.0501	6
0.33	12.4	0.15	5.6	0.4516	0.0702	9.0	0.246	0.160	6
		0.31	11.7	0.9435	0.1466	6.12	0.166	0.108	6
		0.58	21.8	1.7581	0.2732	3.88	0.106	0.0689	6
		0.97	36.5	2.9435	0.4560	2.46	0.070	0.0455	6

C. Continuous-Phase Péclet Numbers for Kerosene in Water, 0.75-in. Spheres, Tetragonal (Jacques)

F_c (gal/min)	U_{co} (ft/hr)	F_d (gal/min)	U_{do} (ft/hr)	U_{do}/U_{co}	$\left(\frac{\nu\psi}{d_p U_{co}}\right)^{1/2} \frac{U_{do}}{U_{co}}$	N_c	P_c	ϵP_c	No of measurements
0.6	22.6	0.16	5.95	0.264	0.0436	14.44	0.454	0.145	5
0.3	11.3	0.16	5.95	0.526	0.1232	7.95	0.250	0.080	4
0.3	11.3	0.61	22.6	2.00	0.4681	4.45	0.142	0.046	5

D. Continuous-Phase Péclet Numbers for Kerosene in Water, 0.75-in. Spheres, Random (Jacques)

F_c (gal/min)	U_{co} (ft/hr)	F_d (gal/min)	U_{do} (ft/hr)	U_{do}/U_{co}	$\left(\frac{\nu\psi}{d_p U_{co}}\right)^{1/2} \frac{U_{do}}{U_{co}}$	N_c	P_c	ϵP_c	No. of measurements
0.6	22.6	0.98	36.6	1.63	0.2680	3.37	0.105	0.043	5
0.3	11.3	0.61	22.6	2.00	0.4710	2.21	0.069	0.028	5
0.3	11.3	1.21	45.5	4.01	0.9421	1.57	0.049	0.020	5

E. Continuous-Phase Péclet Numbers for Kerosene in Water, 0.75-in. Spheres, Orthorhombic-2 (Jacques)

F_c (gal/min)	U_{co} (ft/hr)	F_d (gal/min)	U_{do} (ft/hr)	U_{do}/U_{co}	$\left(\frac{\nu\psi}{d_p U_{co}}\right)^{1/2} \frac{U_{do}}{U_{co}}$	N_c	P_c	ϵP_c	No. of measurements
1.0	37.6	0.95	35.8	0.95	0.1221	8.73	0.270	0.107	5
0.3	11.3	0.95	35.8	3.17	0.7414	2.20	0.068	0.026	4

F. Continuous-Phase Péclet Numbers for Kerosene in Water, 0.75-in. Spheres, Orthorhombic-1 (Jacques)

F_c (gal/min)	U_{co} (ft/hr)	F_d (gal/min)	U_{do} (ft/hr)	U_{do}/U_{co}	$\left(\frac{\nu\psi}{d_p U_{co}}\right)^{1/2} \frac{U_{do}}{U_{co}}$	N_c	P_c	ϵP_c	No. of measurements
2.0	76.0	0.23	8.7	0.114	0.0103	14.54	0.474	0.180	4
		0.46	17.5	0.230	0.0208	14.45	0.471	0.179	4
1.0	38.0	0.16	6.0	0.158	0.0201	15.28	0.498	0.189	4
		0.22	8.3	0.218	0.0279	13.01	0.424	0.161	6
		0.49	18.5	0.486	0.0621	10.31	0.336	0.128	10
		0.95	36.1	0.950	0.1212	8.44	0.275	0.104	14
0.8	30.4	0.22	8.3	0.273	0.0390	8.53	0.278	0.106	5
		1.00	38.0	1.250	0.1788	6.38	0.208	0.079	5
0.6	22.8	0.16	6.0	0.264	0.0433	9.48	0.309	0.117	6
		0.22	8.3	0.364	0.0600	8.71	0.284	0.108	6
		0.43	16.2	0.710	0.1171	5.52	0.180	0.068	6
		0.95	36.1	1.590	0.2608	4.26	0.139	0.053	5
0.3	11.4	0.22	8.3	0.730	0.1698	5.15	0.168	0.064	5
		0.95	36.1	3.200	0.7378	2.21	0.072	0.027	4
		1.82	69.0	6.050	1.4120	1.66	0.054	0.021	5

G. Continuous-Phase Péclet Numbers for Kerosene in Water, 0.50-in. Raschig Rings (Cotter)

F_c (gal/min)	U_{co} (ft/hr)	F_d (gal/min)	U_{do} (ft/hr)	U_{do}/U_{co}	$\left(\frac{\nu\psi}{d_p U_{co}}\right)^{1/2} \frac{U_{do}}{U_{co}}$	N_c	P_c	ϵP_c	No. of measurements
0.850	31.80	0.100	3.74	0.118	0.0151	13.0	0.271	0.168	3
0.578	21.60	0.100	3.74	0.173	0.0269	9.8	0.204	0.126	3
0.351	13.10	0.100	3.74	0.285	0.0570	6.6	0.137	0.085	3
0.154	5.76	0.100	3.74	0.649	0.1941	3.1	0.063	0.039	3

H. Continuous-Phase Péclet Numbers for Kerosene in Water, 0.38-in. Spheres (Cotter)

F_c (gal/min)	U_{co} (ft/hr)	F_d (gal/min)	U_{do} (ft/hr)	U_{do}/U_{co}	$\left(\frac{\nu\psi}{d_p U_{co}}\right)^{1/2} \frac{U_{do}}{U_{co}}$	N_c	P_c	ϵP_c	No. of measurements
0.10	3.73	0.056	2.09	0.560	0.3127	6.9	0.107	0.045	3
0.10	3.73	0.105	3.90	1.045	0.5836	5.9	0.092	0.039	3
0.05	1.86	0.100	3.73	2.000	1.5850	2.6	0.040	0.017	3

I. Dispersed-Phase Péclet Numbers for Water Dispersed in Kerosene; 0.75-in. Ceramic Raschig Rings

F_d (gal/min)	U_{do} (ft/hr)	F_c (gal/min)	U_{co} (ft/hr)	U_{co}/U_{do}	N	P	No. of measurements
1.30	48.9	0.0	0.0	0.000	16.6	0.452	10
		0.15	5.6	0.116	15.6	0.424	10
		0.31	11.7	0.238	15.6	0.424	10
0.85	32	0.0	0.0	0.0	16.3	0.442	10
		0.15	5.6	0.176	14.5	0.394	10
		0.31	11.7	0.364	13.1	0.362	10
		0.58	21.8	0.684	13.2	0.368	10
0.51	19.2	0.0	0.0	0.0	15.1	0.416	10
		0.15	5.6	0.293	13.3	0.368	10
		0.31	11.7	0.606	12.3	0.340	10
		0.58	21.8	1.140	10.8	0.295	10
		0.87	32.73	1.705	6.7	0.184	10

J. Dispersed-Phase Péclet Numbers for Water Dispersed in Kerosene; 1.0-in. Ceramic Berl Saddles

F_d (gal/min)	U_{do} (ft/hr)	F_c (gal/min)	U_{co} (ft/hr)	U_{co}/U_{do}	N	P	No. of measurements
0.85	32	0.0	0.0	0.0	16.3	0.492	12
		0.15	5.6	0.176	15.8	0.476	10
		0.42	15.8	0.494	15.8	0.476	6
		0.68	24.8	0.774	14.8	0.446	6

K. Dispersed-Phase Péclet Numbers for Water Dispersed in Kerosene; 0.75-in. Carbon Raschig Rings

F_d (gal/min)	U_{do} (ft/hr)	F_c (gal/min)	U_{co} (ft/hr)	U_{co}/U_{do}	N	P	No. of measurements
1.3	48.9	0.0	0.0	0.0	18.7	0.510	10
		0.15	5.6	0.116	18.2	0.494	10
		0.31	11.7	0.238	16.4	0.445	10
0.85	32	0.0	0.0	0.0	17.7	0.480	8
		0.15	5.6	0.176	18.9	0.515	6
		0.31	11.7	0.364	18.6	0.505	6
		0.58	21.8	0.684	18.4	0.500	8
0.51	19.2	0.0	0.0	0.0	18.0	0.490	6
		0.15	5.6	0.293	16.4	0.445	8
		0.31	11.7	0.606	17.5	0.475	8
		0.58	21.8	1.140	17.6	0.478	8

ACKNOWLEDGMENT

Appreciation is expressed to H. A. Einstein, Irving Fatt, D. R. Olander, and J. M. Prausnitz for helpful discussion, to R. B. Waite and R. C. Gilmore for their part in construction of the experimental equipment, to F. E. Vogelsberg for design and installation of the electronic instrumentation, and to J. E. Cotter, N. N. Li, and J. S. Moon for participation in the experimental program.

The work reputed was done in the Lawrence Radiation Laboratory under the auspices of the U. S. Atomic Energy Commission.